

# Highly Integrated MEMS Resonators for CO<sub>2</sub> Gas Sensing

By

Alberto PRUD HOMME BUELNA

MANUSCRIPT-BASED THESIS PRESENTED TO ÉCOLE DE  
TECHNOLOGIE SUPÉRIEURE IN PARTIAL FULFILLMENT FOR A  
MASTER'S DEGREE WITH THESIS IN ELECTRICAL ENGINEERING  
M.A.Sc.

MONTREAL, JUNE 15, 2020

ÉCOLE DE TECHNOLOGIE SUPÉRIEURE  
UNIVERSITÉ DU QUÉBEC



Alberto Prud homme Buelna, 2020



This Creative Commons license allows readers to download this work and share it with others as long as the author is credited. The content of this work can't be modified in any way or used commercially.

**BOARD OF EXAMINERS (THESIS M.Sc.A.)**  
**THIS THESIS HAS BEEN EVALUATED**  
**BY THE FOLLOWING BOARD OF EXAMINERS**

Mr. Frederic Nabki, Thesis Supervisor  
Department of Electrical Engineering, École de technologie supérieure

Mr. Ricardo Izquierdo, President of the Board of Examiners  
Department of Electrical Engineering, École de technologie supérieure

Mr. Dominic Deslandes, Member of the jury  
Department of Electrical Engineering, École de technologie supérieure

**THIS THESIS WAS PRESENTED AND DEFENDED**  
**IN THE PRESENCE OF A BOARD OF EXAMINERS AND PUBLIC**  
**MAY 29, 2020**  
**AT ÉCOLE DE TECHNOLOGIE SUPÉRIEURE**



# RÉSONATEUR MEMS HAUTEMENT INTÉGRÉ POUR LA DÉTECTION DU CO<sub>2</sub>

Alberto PRUD HOMME BUELNA

## RÉSUMÉ

Les capteurs de gaz sont une technologie largement utilisée pour de nombreuses applications, faisant de la crise climatique actuelle un déclencheur pour le développement de ces technologies pour mesurer les gaz à effet de serre, principalement le CO<sub>2</sub>.

Avec le développement de nouveaux processus de microfabrication, il a été possible de produire des micro-résonateurs pour de multiples applications, telles que les capteurs de gaz, offrant de multiples avantages par rapport aux capteurs commerciaux, grâce au fait qu'ils utilisent moins d'énergie, sont plus petits et plus économiques à produire.

Bien que les différentes parties qui intégreraient les micro-résonateurs devant être utilisés comme capteurs aient fait l'objet de recherches pendant des années, la possibilité de créer un capteur MEMS entièrement intégré comme capteur de gaz n'a pas été suffisamment explorée.

Il est donc nécessaire de déterminer s'il est possible de créer un capteur MEMS entièrement intégré basé sur les micro-résonateurs, qui soit fonctionnel et présente une compétitivité sur le marché actuel des capteurs de gaz.

Ce projet est axé sur la création d'un prototype de capteur MEMS CO<sub>2</sub> entièrement fonctionnel dont la variable de mesure est la variation de la fréquence de résonance du micro-résonateur intégré, pour lequel ils ont été caractérisés par de multiples revêtements à base d'amines polymères.

Avec la mise au point réussie d'un capteur MEMS pour le CO<sub>2</sub>, il est possible de réaliser une solution entièrement intégrée en utilisant des micro-résonateurs et qui peut être compétitive avec les capteurs existants sur le marché, cependant, en raison de l'impact de variables externes telles que la pression, la température et l'humidité sur la performance du capteur, il est nécessaire de réaliser des éléments de compensation qui garantissent la fiabilité et la précision de ces capteurs.

**Mots-clés:** résonateur MEMS, Polyéthylèneimine; Micro-résonateur; Capteur de CO<sub>2</sub>; Capteur de gaz; Capteur d'humidité; Oxyde de graphène réduit; Revêtements; Capteur de masse, capteur régénératif, adsorbant CO<sub>2</sub>.



# HIGHLY INTEGRATED MEMS RESONATORS FOR CO<sub>2</sub> GAS SENSING

Alberto PRUD HOMME BUELNA

## ABSTRACT

Gas sensors are a technology widely used for many applications and purposes. Notably, the current climate crisis is a motivation for the development of sensors to measure greenhouse gases, mainly CO<sub>2</sub>. With the development of new microfabrication processes it has been possible to produce micro-resonators for multiple applications, such as gas sensors, offering multiple advantages over commercial sensors, thanks to the fact that they use less energy, are smaller, and are more economical to produce.

While the different parts of an integrated micro-resonator sensor have been researched for years, the possibility of creating a fully integrated gas sensor using a micro-resonator has not been sufficiently explored. This has created the need to examine whether it is possible to create a fully integrated microelectromechanical system (MEMS) CO<sub>2</sub> sensor based on micro-resonators, which is functional and competitive with the current gas sensor market.

This master's thesis is focused on the creation of a fully functional CO<sub>2</sub> MEMS sensor prototype whose measurement variable is the variation of the resonance frequency of the integrated micro-resonator in the presence of a CO<sub>2</sub> concentration in air. For this purpose, multiple adsorbance coatings based on polymeric amines are characterized.

Afterward, a fully integrated MEMS CO<sub>2</sub> sensor is implemented, including both electronics and micro-resonator with its adsorbent coating. It is shown that the sensor can be competitive with commercial optical CO<sub>2</sub> sensors. However, due to the impact of external variables such as pressure, temperature and humidity on the performance of the sensor, it is necessary to perform compensation to guarantee the reliability and accuracy of the measurements.

**Keywords:** MEMS resonator, Polyethylenimine; Micro-resonator; CO<sub>2</sub> Sensor; Gas Sensor; Humidity Sensor; Reduced Graphene Oxide; Coatings; Mass Sensor, Regenerative sensor, CO<sub>2</sub> adsorbent.



## TABLE OF CONTENTS

|  | Page |
|--|------|
| INTRODUCTION .....   | 1    |
| CHAPTER 1 LITERATURE REVIEW .....  | 9    |
| 1.1 Main parameters of gas sensors .....   | 9    |
| 1.2 Gas sensing techniques .....   | 10   |
| 1.2.1 Methods based on impedance variation .....   | 11   |
| 1.2.2 Methods based on other kinds of variations .....   | 15   |
| 1.2.3 Comparative of CO <sub>2</sub> sensor (ranges and precision) .....   | 19   |
| 1.2.4 Conclusion .....   | 21   |
| 1.3 Microelectromechanical system (MEMS) .....   | 21   |
| 1.3.1 MEMS resonators .....  | 23   |
| 1.3.2 MEMS mass sensing for gas concentration measurement .....  | 29   |
| 1.4 Material adsorbent coatings .....  | 46   |
| 1.4.1 Selectivity .....  | 46   |
| 1.4.2 Interaction with other gases .....   | 47   |
| 1.4.3 External influences .....  | 47   |
| 1.4.4 Deposition technique .....   | 47   |
| 1.4.5 Reversibility .....  | 47   |
| 1.4.6 Sensitivity .....  | 48   |
| 1.4.7 Partition coefficient .....  | 48   |
| 1.4.8 Regeneration of coatings .....   | 49   |
| 1.5 Conclusion .....   | 52   |
| CHAPTER 2 COMPARISON BETWEEN LINEAR AND BRANCHED<br>POLYETHYLENIMINE AND REDUCED GRAPHENE OXIDE<br>COATINGS AS A CAPTURE LAYER FOR MICRO RESONANT<br>CO <sub>2</sub> GAS CONCENTRATION SENSORS ..... | 55   |
| 2.1 Introduction .....   | 56   |
| 2.2 Materials and Methods .....  | 59   |
| 2.2.1 Coating Preparation .....  | 60   |
| 2.2.2 Test Setup .....   | 65   |
| 2.2.3 Micro-resonator Characteristics .....  | 67   |
| 2.3 Results .....  | 68   |
| 2.3.1 Linear and Branched Polyethylenimine Coatings Characterization .....   | 69   |
| 2.3.2 Linear Polyethylenimine with reduced Graphene Oxide Coating<br>Characterization .....  | 71   |
| 2.3.3 Performance Comparison between the Coatings .....  | 73   |
| 2.3.4 Micro-resonator CO <sub>2</sub> sensor Proof-of-concept .....  | 77   |
| 2.4 Discussion .....   | 79   |
| 2.5 Conclusion .....   | 82   |

|           |   |     |
|-----------|---|-----|
| CHAPTER 3 | AN 8 MW FULLY INTEGRATED REGENERATIVE RESONANT MEMS CO <sub>2</sub> SENSOR USING LINEAR POLYETHYLENIMINE AS A CAPTURE LAYER ..... | 85  |
| 3.1       | Introduction.....   | 86  |
| 3.2       | System Integration .....  | 88  |
|           | 3.2.1 MEMS micro-resonator fabrication and characterization.....  | 88  |
|           | 3.2.2 Adsorption coating deposition .....   | 90  |
|           | 3.2.3 CO <sub>2</sub> sensor characterization setup .....   | 92  |
|           | 3.2.4 MEMS CO <sub>2</sub> integration.....   | 93  |
| 3.3       | Measurement Results .....   | 96  |
|           | 3.3.1 Response to CO <sub>2</sub> concentrations .....  | 97  |
|           | 3.3.2 Impact of ambient conditions.....   | 101 |
|           | 3.3.3 Long term stability .....   | 102 |
| 3.4       | Discussion .....  | 104 |
| 3.5       | Conclusions.....  | 106 |
|           | CONCLUSION AND DISCUSSION.....  | 108 |
|           | BIBLIOGRAPHY.....   | 113 |

## LIST OF TABLES

|           |  | Page |
|-----------|--|------|
| Table 1.1 | Sensors performance comparison .....   | 20   |
| Table 1.2 | Main published micro-resonators for gas sensing .....  | 34   |
| Table 1.3 | Excitation methods in resonators .....   | 37   |
| Table 1.4 | PolyMUMPS fabrication parameters .....   | 42   |
| Table 1.5 | PiezoMUMPS fabrication parameters .....  | 45   |
| Table 1.6 | Most common adsorbent coating for gas sensors .....  | 51   |
| Table 2.1 | Frequency shift of each coating at different concentration of CO <sub>2</sub> .....              | 74   |
| Table 2.2 | Linearized coefficient of the frequency shift by ppm of CO <sub>2</sub> .....                    | 74   |
| Table 2.3 | Adsorption time for each coating.....  | 75   |
| Table 2.4 | Recovery time for each coating .....   | 76   |
| Table 2.5 | Frequency shift of the micro-resonator at different CO <sub>2</sub><br>concentrations .....      | 79   |
| Table 2.6 | Comparison of the studied CO <sub>2</sub> adsorbing coatings with<br>other published works ..... | 80   |
| Table 3.1 | Comparison of the studied CO <sub>2</sub> MEMS sensor with other<br>published works .....        | 105  |



## LIST OF FIGURES

|             |  | Page |
|-------------|--|------|
| Figure 0.1  | CO <sub>2</sub> generation sources.....                    | 1    |
| Figure 0.2  | Global CO <sub>2</sub> concentration level .....           | 2    |
| Figure 0.3  | Main elements of a resonant MEMS resonant gas sensor ..... | 4    |
| Figure 1.1  | Gas Sensing methods .....                                  | 11   |
| Figure 1.2  | Recovery time of gas sensors.....                          | 11   |
| Figure 1.3  | Metal Oxide sensor diagram .....                           | 12   |
| Figure 1.4  | Polymer sensor diagram.....                                | 14   |
| Figure 1.5  | Carbon Nanotubes sensors.....                              | 14   |
| Figure 1.6  | Optical Sensors .....                                      | 16   |
| Figure 1.7  | Calorimetric sensors.....                                  | 17   |
| Figure 1.8  | Gas Chromatography Sensors.....                            | 17   |
| Figure 1.9  | Piezoelectric sensors .....                                | 18   |
| Figure 1.10 | Undamped system diagram.....                               | 24   |
| Figure 1.11 | Damped system diagram.....                                 | 25   |
| Figure 1.12 | Trace of system with different level of damping .....      | 26   |
| Figure 1.13 | Amplitude of resonance by damping .....                    | 27   |
| Figure 1.14 | Q factor diagram .....                                     | 28   |
| Figure 1.15 | Frequency deviation diagram.....                           | 30   |
| Figure 1.16 | Resonant modes of MEMS bridge.....                         | 31   |
| Figure 1.17 | Cantilever micro-resonator .....                           | 32   |
| Figure 1.18 | Bridge micro-resonator .....                               | 32   |
| Figure 1.19 | Free-Free beam micro-resonator.....                        | 33   |

|             |  |    |
|-------------|--|----|
| Figure 1.20 | Disc micro-resonator.....  | 33 |
| Figure 1.21 | Piezoelectric actuation in resonator .....   | 35 |
| Figure 1.22 | Electrostatic cantilever.....  | 35 |
| Figure 1.23 | Electro-thermal micro-resonator.....   | 36 |
| Figure 1.24 | Electrostatic MEMS resonator operation.....  | 40 |
| Figure 1.25 | PolyMUMPS lateral cut representation .....   | 41 |
| Figure 1.26 | Piezoelectric MEMS resonator operation.....  | 43 |
| Figure 1.27 | PiezoMUMPS lateral cut representation.....   | 44 |
| Figure 1.28 | Coating regeneration diagram.....  | 50 |
| Figure 2.1  | (a) Branched Polyethylenimine Molecule, and (b) Lineal Polyethylenimine Molecule .....   | 60 |
| Figure 2.2  | Coating deposition technique, (a) Spin coater for the Quartz Crystal used for initial coating tests, (b) Micro-drop deposition by piezo probe used for the micro-resonator .....       | 62 |
| Figure 2.3  | Reduced Graphene Oxide by Microwave reduction.....   | 63 |
| Figure 2.4  | SEM image of the quartz crystal coated with the (a) Branched PEI layer, (b) Linear PEI layer and (c) rGO with Linear PEI layer.....  | 64 |
| Figure 2.5  | IR absorption spectroscopy result for the three deposited coatings on the quartz crystals .....  | 65 |
| Figure 2.6  | Diagram of the characterization setup .....  | 65 |
| Figure 2.7  | (a) Setup for the quartz crystals and the resonator characterization, (b) Close-up of the micro-resonator during the characterization with the laser from the vibrometer visible ..... | 66 |
| Figure 2.8  | Cross-section of the micro-resonator with oxide as sacrificial layer.....  | 67 |
| Figure 2.9  | (a) 3D view of the real micro-resonator obtained by the Olympus LEXT OLS4000 Confocal microscope, (b) Eigenfrequency FEM COMSOL simulation.....  | 68 |
| Figure 2.10 | Quartz crystal frequency shift in response to different CO <sub>2</sub> concentration cycles for (a) Branched PEI coated crystal, and (b) Linear PEI coated crystal .....              | 70 |

|             |   |    |
|-------------|---|----|
| Figure 2.11 | Branched PEI and Linear PEI coated crystals .....   | 71 |
| Figure 2.12 | Frequency shift of the quartz crystal with LPEI+rGO.....  | 72 |
| Figure 2.13 | Response of the three different coatings at CO <sub>2</sub> concentrations<br>of (a) 0.1%, (b) 0.5%, and (c) 1%.....  | 73 |
| Figure 2.14 | Frequency shift of each coating from 0.05% to 1% of CO <sub>2</sub> .....   | 75 |
| Figure 2.15 | (a) Adsorption time for each coating at different CO <sub>2</sub> concentrations,<br>(b) Recovery time for each coating at different CO <sub>2</sub> level .....                                  | 75 |
| Figure 2.16 | Frequency shift at different range of air humidity from 15<br>to 75 %RH.....  | 76 |
| Figure 2.17 | Response of the coated micro-resonator to a 0.8% CO <sub>2</sub> concentration<br>variation .....   | 77 |
| Figure 2.18 | Behavior of the micro-resonator over time at different concentrations<br>of CO <sub>2</sub> .....   | 78 |
| Figure 3.1  | Cross-section of the MEMS resonator based on a cantilever structure. ....   | 89 |
| Figure 3.2  | Uncoated micro-resonator (a) SEM micrograph, and (b) 3D<br>view obtained by confocal microscope.....  | 89 |
| Figure 3.3  | Micro-resonator resonance frequency at (a) mode 1, (b) mode 2,<br>(c) mode 3; (d) Vibrometer resonant frequency measurement of<br>the three modes of the micro-resonator .....                    | 90 |
| Figure 3.4  | Setup used for the deposition of the LPEI coating using the two-axis<br>piezo actuator .....  | 91 |
| Figure 3.5  | Vibrometer measurement after the LPEI coating deposited .....   | 92 |
| Figure 3.6  | (a) Diagram of the characterization setup, (b) Setup for the CO <sub>2</sub> gas<br>sensor characterization.....  | 93 |
| Figure 3.7  | MEMS CO <sub>2</sub> sensor block diagram.....  | 94 |
| Figure 3.8  | Measured CO <sub>2</sub> MEMS sensor signal waveforms at the different points<br>labelled in Fig. 3.7 steady-state at (a) P1 and (b) P2, and (c) startup<br>transient of the resonator at P3..... | 95 |
| Figure 3.9  | Fully integrated sensor, (b) Sensor integrated with protector casing.....   | 96 |
| Figure 3.10 | MEMS and optical sensor response to different CO <sub>2</sub> concentrations.....   | 97 |

|             |   |     |
|-------------|---|-----|
| Figure 3.11 | Adsorption and Recovery times based in the CO <sub>2</sub> concentration .....                                  | 99  |
| Figure 3.12 | MEMS sensor frequency deviation by CO <sub>2</sub> concentration .....  | 100 |
| Figure 3.13 | Response of the MEMS sensor to variations in (a) humidity,<br>(b) temperature and (c) atmospheric pressure..... | 101 |
| Figure 3.14 | Long term test of the CO <sub>2</sub> MEMS sensor .....   | 103 |

## LIST OF ABBREVIATIONS

|                 |  |
|-----------------|--|
| AlN             | Aluminum Nitride                       |
| BPEI            | Branched Polyethylenimine              |
| CAGR            | Compound Annual Growth Rate Calculator |
| CO <sub>2</sub> | Carbon Dioxide                         |
| GO              | Graphene Oxide                         |
| LPEI            | Linear Polyethylenimine                |
| MEMS            | Microelectromechanical systems         |
| NDIR            | Nondispersive Infrared Detector        |
| NO <sub>x</sub> | Nitrogen Oxide                         |
| O               | Oxygen                                 |
| PCB             | Printed Circuit Board                  |
| PEI             | Polyethylenimine                       |
| PPM             | Parts per Million                      |
| QCM             | Quartz Crystal Microbalance            |
| Q-Factor        | Quality Factor                         |
| rGO             | Reduced Graphene Oxide                 |
| SAW             | Surface Acoustic Wave                  |
| SEM             | Scanning Electron Microscopy           |
| VNA             | Vector Network Analyzer                |
| % RH            | Relative Humidity                      |



## LIST OF SYMBOLS

|            |                          |
|------------|--------------------------|
| $\zeta$    | Damping ratio            |
| Y          | Young's modulus          |
| $\rho$     | Material density         |
| $\omega_n$ | Natural frequency        |
| m          | Mass                     |
| k          | Spring constant          |
| $\tau$     | Period                   |
| $F_n$      | Natural frequency        |
| Cc         | Damping coefficient      |
| $\omega_d$ | Damped natural frequency |
| Q          | Q-factor                 |
| $F_{max}$  | Resonance Frequency      |
| K          | Partition Coefficient    |



## INTRODUCTION

### Motivation

The concentration of greenhouse gases in air have increased in recent years, and the consequences have begun to be visible in our environment. The source of these gases is mainly based on industrial processes, combustion engines in the transport system, electricity production, among others (EPA, 2017). The main CO<sub>2</sub> sources are summarized in Figure 0.1.

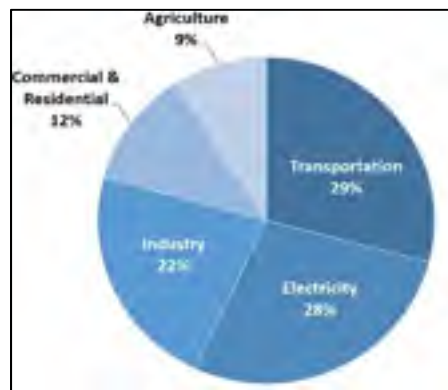


Figure 0.1 CO<sub>2</sub> generation sources  
Adapted from EPA (2017)

Concentration levels of gases harmful to humans have become a metric that requires constant supervision for open areas or enclosed spaces (Arshak, 2004; Kumar, Kim, & Hancke, 2013; Mahyuddin & Awbi, 2012). The common effects presented in humans are shown in Table 0.1

Table 0.1 Effects of different levels of CO<sub>2</sub> concentration in humans  
Taken from Satish et al. (2012)

| CO <sub>2</sub> concentration | Effects in humans  |
|-------------------------------|--|
| 250-400 ppm                   | Normal outdoor ambient air   |
| 400-1,000 ppm                 | Concentrations typical of occupied indoor spaces   |
| 1,000-2,000 ppm               | Complaints of drowsiness and poor air  |
| 2,000-5,000 ppm               | Headaches, sleepiness and stagnant, stale, stuffy air.   |
| >40,000 ppm                   | Exposure may lead to serious oxygen deprivation resulting in permanent brain damage, coma, even death. |

The global CO<sub>2</sub> concentration level in the atmosphere has been steadily increasing over the last decades. The measurements made indicate that the global CO<sub>2</sub> level of 400 ppm has been exceeded in 2018, being a drastic change in a short period of time from 340 ppm in only a period of 20 years (ESRL, 2020). The change of CO<sub>2</sub> levels during the last years is show in Figure 0.2.

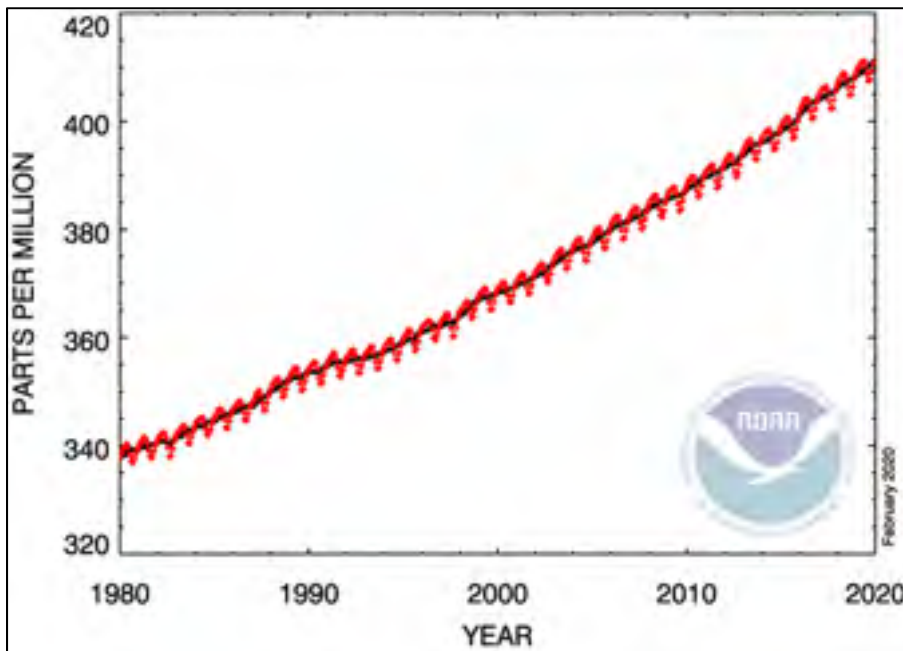


Figure 0.2 Global CO<sub>2</sub> concentration level  
Adapted from ESRL (2020)

The constant need to monitor the concentration of gases such as CO<sub>2</sub> in open spaces or areas of common use among people, has encouraged the development of economical, reduced and low power consumption gas sensors. Notably, the sensors with the greatest expansion potential are Oxygen (O), Carbon Dioxide (CO<sub>2</sub>), and Nitrogen Oxide (NOX) sensors. This has led to the market for gas sensors being valued at more than USD 2 billion since 2018 with a Compound Annual Growth Rate Calculator (CAGR) of 7.8% to reach in 2025. ("Gas Sensor Market Size, Share & Trends Analysis Report By Product (CO<sub>2</sub>, NO<sub>x</sub>, CO, O<sub>2</sub> Sensors), By Technology (Semiconductor, Infrared), By End Use (Building Automation & Domestic Appliance, Industrial), And Segment Forecasts, 2019 - 2025," 2019).

## Research problem

The sensors for measuring the concentration of gases in the air has been a subject of research and development both academically and industrially, due to their wide range of applications, especially for measuring the concentration of toxic gases or for gas control in chemical processes that require precision in the concentration of the elements in reaction. The measurement of the concentration of CO<sub>2</sub> in the air has now become very important due to its impact on both human health and the climatic effects that develop because of the high concentrations present in the air (Aleixandre & Gerboles, 2012).

Different techniques are used in a sensor to measure the concentration of gases (Nazemi, Joseph, Park, & Emadi, 2019). Certain are resistive, which are formed by a metal oxide that changes its resistance or conductivity when exposed to different ambient gases (Dey, 2018; C.-H. Yu, Huang, & Tan, 2012). Another common method used in gas sensors is electrochemical reactions that happen between the gas and the an electrolyte producing a current that depends on the gas concentrations (J. Zhang et al., 2019). Infrared Gas Absorption is one of the most common technology for CO<sub>2</sub> sensors. These sensors pass infrared light through the gas and the asymmetric molecules presented in the gas adsorb the radiation at determined bands of adsorption characteristic of each molecule (Bogue, 2015).

L. M. Roylance in 1979 (Muro, 2013) pioneered MEMS resonant gas sensors which have become an innovative method of gas measurement, and are based on the mechanical properties of microstructures. Every mechanical structure has a resonance mode, whose frequency is given by the dimensions, geometry and material of which it is made. Microfabrication has allowed creating structures so small that they are susceptible to the weight of a few gas molecules, which adhere to the microstructure by means of an adsorbent material that is a function of the type of gas of interest (Subhashini & Juliet, 2012; Zribi, Knobloch, Tian, & Goodwin, 2005).

MEMS gas sensors have been shown to have the potential to measure concentrations in the range of parts per billion in volume requiring a much smaller volume and a very low current consumption compared to traditional systems (Lv, Xu, Yu, Xu, & Li, 2018). These sensors have two elements that define their sensitivity and operating capabilities. The first is the coating that will adsorb the molecules of the gas to be monitored by increasing the mass of the micro-resonator, whereby the resonance frequency will decrease depending on the concentration of the gas. The second element is the microstructure which will resonate at a certain frequency based on its dimensions and geometry (R. Abdolvand, B. Bahreyni, J. E.-Y. Lee, & F. Nabki, 2016).

Multiple parameters define the gas sensors performance but the most relevant are their selectivity to the target gas, reaction and recovery times, and lifetime. In the MEMS gas sensors these characteristics depend mostly on the adsorbent coating, the gas selectivity being the most critical and complex of the parameters (Smulko Janusz, 2015). Figure 0. shows the main elements required to implement a MEMS resonant gas sensor.

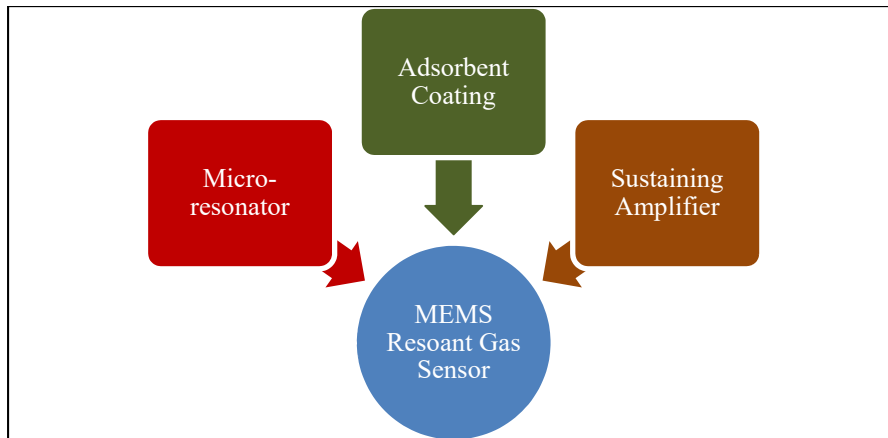


Figure 0.3 Main elements of a resonant MEMS resonant gas sensor

The micro-resonator requires a transducer to keep the micro-structure in resonance, transducing electrical energy to mechanical energy. This can be done through piezoelectric materials, electrostatic actuation, thermal actuation, etc. In addition to the transducer, a closed loop control system is normally developed to maintain the micro-resonator in constant

resonance. Its design is a function of the characteristics of the micro-resonator and its application, this control system is known as a sustaining amplifier. Its main function is to amplify, condition, and feedback the signal generated by the micro-resonator to achieve a stable oscillator equilibrium based on the resonance frequency of the micro-resonator. This oscillation can in turn be monitored in order to capture resonant frequency changes in the micro-resonator due to the adsorbent coating in the presence of gas molecules.

### **Research Objectives**

The goal of this thesis is the development of a fully integrated and operational CO<sub>2</sub> MEMS sensor that has similar capabilities to commercial sensors with regard to measurement range. Size and low power consumption of the sensor are also important parameters to minimize to make it suitable for highly integrated systems.

The specific objectives are:

- the design of a micro-resonator for the measurement of gas concentration by applying a commercial MEMS fabrication process, as well as existing simulation and modeling techniques;
- the analysis of CO<sub>2</sub> adsorbent materials for use with the micro-resonator in order to enable good CO<sub>2</sub> adsorption and recovery performance;
- the design of a sustaining amplifier co-designed to support oscillation of the micro-resonator;
- the integration of the micro-resonator, adsorbent coating and sustaining amplifier and characterization of the resulting sensor.

Ultimately, the micro-resonator was designed, fabricated and coated with a adsorbent coating, and the electronics were designed and integrated with the micro-resonator to achieve an integrated CO<sub>2</sub> sensor. Characterization of the sensor and its comparison to a commercial CO<sub>2</sub> sensor were carried out in order to define the strengths and areas of opportunity for improvement of the proposed sensor.

## **Contributions**

The main contribution of this work is the development of a fully integrated CO<sub>2</sub> MEMS sensor that can show the capabilities and limitations of this kind of technology applied as mass sensors for gas sensing. The design, fabrication and integration are presented during the next chapters. The contributions of each element previously mentioned that were necessary to integrate the solution are:

### **1. Evaluation of the geometries and excitation method for micro-resonators for gas sensing**

During the development of this work, two micro-resonator chips were manufactured using different manufacturing and excitation techniques in order to ascertain the optimal micro-resonator geometry for the targeted application. The first chip was manufactured using the PolyMUMPS commercial process, which uses electrostatic excitation and has three layers of Polysilicon available. The second chip was manufactured using the commercial process of PiezoMUMPS, which uses a layer of piezoelectric material for the micro-resonator's excitation. Different geometries were manufactured in the two chips and were analyzed to be applied in the CO<sub>2</sub> MEMS sensor.

### **2. Comparison between multiple adsorbent materials for CO<sub>2</sub>**

For the selection of the adsorbent material, three options based on Polyethylenimine (PEI) were analyzed, in which its properties and performance were analyzed under different conditions allowing the best of them to be selected for use with the micro-resonator.

### **3. Fully integrated CO<sub>2</sub> MEMS sensor demonstration**

The micro-resonator, adsorbent coating and sustaining amplifier were integrated to demonstrate a complete integrated CO<sub>2</sub> sensor. Once the sensor was integrated, a complete

characterization was carried out showing the capabilities and limitations of this type of solutions for the measurement of CO<sub>2</sub> concentration, as well as its advantages over commercial sensors.

#### **4. Adsorbent material disposition method and gas chamber test setup**

A deposition method to deposit a droplet of adsorbent material on a released micro-resonator after its micro-fabrication was devised.

A custom gas chamber test setup was designed and implemented to characterize the proposed sensor and allow its optical characterization using a vibrometer.

#### **Thesis Outline**

This is a manuscript-based thesis. Hence, chapters 2 and 3 present one journal paper each. The thesis is organized as follows:

**Chapter 1** covers the literature review on gas sensing techniques of multiple sensors focussing on the advantages and disadvantages of each one. Also the operation principle of the MEMS resonators for the mass sensors is described, with a general introduction to the adsorption materials used in this kind of sensors.

**Chapter 2** presents a comparison between the Linear and Branched Polyethylenimine to be applied as adsorption coating. Also, includes the evaluation of Linear Polyethylenimine with reduced graphene oxide. For the coating's characterization, quartz crystals were used. Once the best coating was selected, an electrostatic MEMS resonator was tested as a proof-of-concept.

**Chapter 3** includes the complete integration of the MEMS CO<sub>2</sub> sensor. The design and simulations of the micro-resonator, as well as its response to different conditions are presented.

The coating used was Linear Polyethylenimine which was the one that provided the best results in Chapter 2. The sustaining amplifier and its integration with the micro-resonator is shown. Characterization of the resulting sensor to different CO<sub>2</sub> levels, atmospheric pressure, humidity and temperature are presented, and it is compared to a commercial CO<sub>2</sub> sensor.

In the last chapter, the conclusions and discussion of this thesis are presented, including recommendations for future research and improvements.

## CHAPTER 1

### LITERATURE REVIEW

This chapter will discuss the most common techniques to measure the concentration of gases in environment atmosphere. A comparison of the advantages and disadvantages of each one will be made. The targeted gas will be CO<sub>2</sub> as it is the focus of this thesis.

#### 1.1 Main parameters of gas sensors

The measurement of the gas concentration in a specific space is of high relevance for many sectors, i.e. industrial production, mining, automotive, medical applications, environment conditions, indoor air quality, etc.

Each sector has specific requirements based in the conditions and applications of the sensor; this requirement will define the sensing technique to be used and the performance will be delimited by this technique.

Amongst the main characteristics that a sensor needs to satisfy, we find the sensibility of detection of the target gas, this means the minimum value of concentration that the sensor is capable of measuring with precision.

The repeatability of the measurements within the same conditions is a basic value that establishes the reliability of the sensor to be applied. The selectivity of the target gas is a crucial parameter in special at environment atmosphere, where the mixture and concentration of different gases change constantly, and the sensor needs to separate the target gas and obtain a reliable measure of it in comparison with the rest of the gas mixture.

Reaction time can be an important parameter for specific application, where the reaction of a subsystem depends of the measurement of the target gas in real time, or in systems where the

concentration of the gas changes drastically in a short period and it is necessary to follow this change with precision.

The concentration range of the gas that the sensor can operate is defined by the measure range. This limitation could be paramount when the process to be evaluated changes to a much wider range. The sensors with a wide concentration range usually have very low precision.

Once the sensor takes the measurement it is important that the system readapts to the current condition, this is known as reversibility. The sensing technique that uses a non-reversible chemical process, shortens the life span of the product, or alters its performance with the passing of time, also affected by the damage caused by the same reaction.

As a commercial consideration the fabrication cost will be an important parameter that defines whether the technology is competitive with other technologies. In the same way the power consumption will be a definitive parameter, specially for portable sensing equipment where the energy is provided by internal batteries (Arshak, Moore, Lyons, Harris, & Clifford, 2004; D. D. Lee, 2001; X. Liu et al., 2012).

## **1.2 Gas sensing techniques**

As a general classification of the techniques used in the main gas sensor, it is possible to consider two main blocks, an electrical resistance variation based in the presence of the target gas and a second group of techniques that uses physics behaviors, like photons absorption, sound waves absorption or mass additional that change mechanical properties of the sensor.

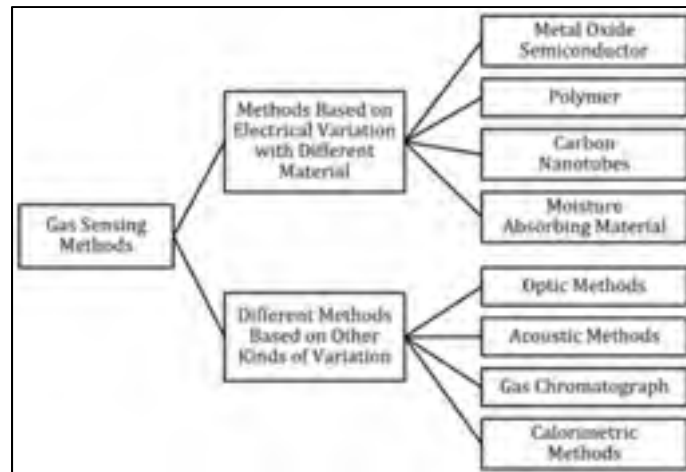


Figure 1.1 Gas Sensing methods  
Taken from X. Liu et al. (2012)

### 1.2.1 Methods based on impedance variation

This method of measurement is based in the variation of the electrical properties of the material that conforms the sensor that will react proportionally to the concentration of the target gas in contact with the sensing material. For this technique, different materials and measurements can be used, these are the most used.

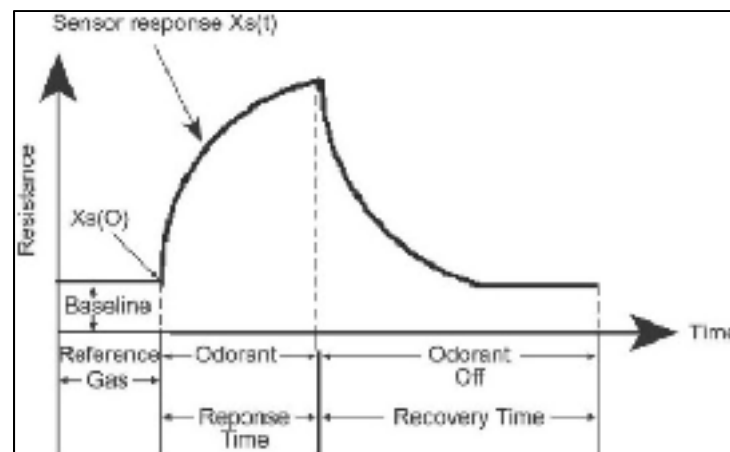


Figure 1.2 Recovery time of gas sensors  
Taken from Arshak et al. (2004)

### 1.2.1.1 Metal Oxide Semiconductor

The metal oxide semiconductor sensors are based in the reaction of oxidation or reduction when the target gas gets in contact with the metal oxide surface. These reactions will cause a proportional change in the electrical resistance of the semiconductor in relation to the concentration of the gas present in the atmosphere (Arshak et al., 2004).

The metal oxide semiconductor sensor is very used for the detection of the inflammable gases and certain toxic gases. This kind of sensor usually includes a high temperature surface that will increase the performance of detection, a consequence of the nature of operation (D. D. Lee, 2001).

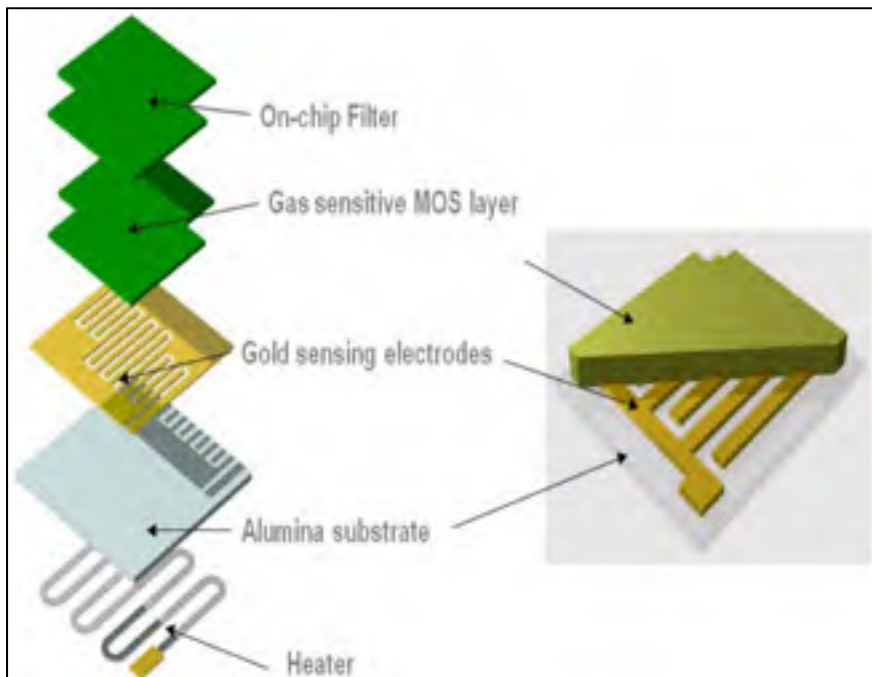


Figure 1.3 Metal Oxide sensor diagram  
Taken from Binions et Naik (2013)

This kind of sensors usually require a working temperature between 25°C to 600°C and the selectivity of the gases can be affected because if the temperature deviates too much from the optimal value, other gas components may be more reactive towards (X. Liu et al., 2012).

Because the principle of operation, this kind of sensors present a high sensibility and a very good recovery time and stability. The required space for this kind of sensor is equivalent to others that use different techniques and can be integrated directly with the control circuit.

The main disadvantage of this technology is the high consumption of energy in comparison with other sensors as consequence of the necessity of work at high temperature, that represents an energy loss in case of portable sensors (Dey, 2018).

#### **1.2.1.2 Polymer**

While the gas sensor based in metal oxide semiconductor has a high sensibility especially for inorganic gases and some organic compounds, the polymer sensor can be applied for the detection of inorganic gases as CO<sub>2</sub> and H<sub>2</sub>O with better sensibility and stability (D. D. Lee, 2001).

In the case of the polymers as gas concentration sensors, it can be applied in two ways, as a conductive polymer and as a non-conductive polymer. As a conductive polymer the electrical resistance of the polymer will be affected linearly to the concentration of the target gas with a similar behavior of the metal oxide semiconductor.

In the case of the non-conductive polymer the target gas will be absorbed changing the mass of the polymer, this change can be applied in sensing systems like Quartz Crystal Microbalances, Surface acoustic wave, resonators, etc.

This kind of sensor will be evaluated in the next chapters. The selective factor of this kind of sensors depends on the physisorption mechanisms of the polymer used in the sensors. Polymer base sensors have the advantage of being capable of operating at room temperature, this represents a good alternative to the metal oxide sensor because of the reduction of the energy required to operate with portable sensors powered by batteries. Another quality of this kind of sensor is the low cost of production and the simple principle of operation.

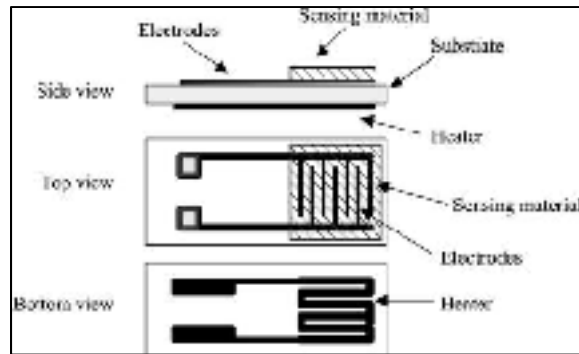


Figure 1.4 Polymer sensor diagram  
Taken from D. D. Lee (2001)

The polymer sensors provide a high linear response to concentration for various analyses and good repeatability after a long number of exposures. Also, it has a high discrimination with a fast response and good recovery. This kind of material have high sensitivity to humidity and the sensor response can drift with time.

### 1.2.1.3 Carbon Nanotubes

The carbon nanotubes as gas sensing material uses the same principle of measurement of the polymers but with a bigger area to capture the gas, it can have a higher sensibility. The main difference with the metal oxide is the same as the polymers, it can work at ambient temperature, so it has a low power consumption.

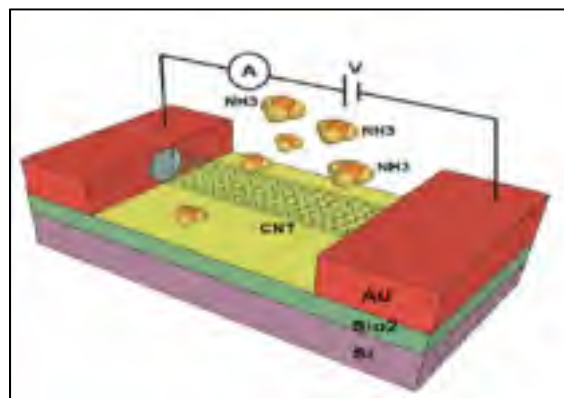


Figure 1.5 Carbon Nanotubes sensors  
Taken from Akbari et al. (2014)

By having a high sensibility, it can measure the concentration of the gas without a preconcentration of the target gas, this facilitates the integration with the controller, reducing weight and production costs.

The nanotubes can be categorized in single-walled carbon nanotubes (SWCNTs) and multiwall carbon nanotubes (MWCNTs). MWCNTs are usually used for remote detection of carbon dioxide (CO<sub>2</sub>), oxygen (O<sub>2</sub>), and ammonia (NH<sub>3</sub>) depending on the measured changes in MWCN's permittivity and conductivity. The measure of CO<sub>2</sub> and O<sub>2</sub> shows that the response is both linear and reversible, which means that the operation process only involves physisorption (Akbari et al., 2014).

### **1.2.2 Methods based on other kinds of variations**

As it is possible to observe in the sensors with variation in the electrical resistance, the principle of operation is basically the same, only with the difference of the necessity of operating at high temperature but the signal to be evaluated will be the same.

Other methods to measure the concentration of gas can include techniques that use physics behaviors, like photons absorption, sound waves absorption or resonance systems that change the mechanical properties of the sensor proportionally to the concentration of the gas.

#### **1.2.2.1 Optical measurement**

The measurement of the gas concentration by optical system applies the spectroscopy principle, which is based in the molar absorptivity of the photon at specific wavelengths by the molecules of the gas, that will define the kind of gas and the concentration of it in the volume analyzed.

Based in the principle that this kind of sensors do not operate by contact of the gas with some reactive, the sensor will not be deteriorated and will offer a higher sensibility, a good selectivity and a better stability in comparison with the non-optical sensors (X. Liu et al., 2012).

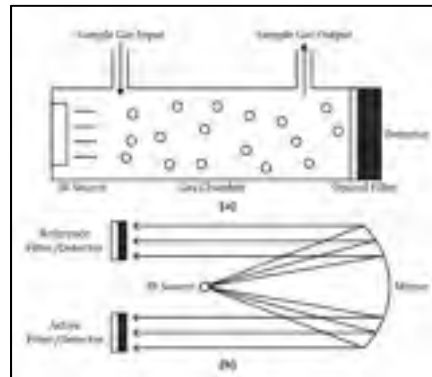


Figure 1.6 Optical Sensors  
Taken from X. Liu et al. (2012)

The molecules of CO<sub>2</sub> and CO have a unique spectrum at 4.25 and 4.7m in the IR region, and the volume of photons absorbed will be in linear relation to the concentration of the gas.

Considering the capabilities and advantages of this kind of sensors it can be considered an excellent option, but at the same time, it is seriously restricted for the general applications due to miniaturization and high cost. Only a few commercial gas sensors are based on optical principles (Arshak et al., 2004; D. D. Lee, 2001).

### 1.2.2.2 Calorimetric

The calorimetric gas sensors use the thermal transmission coefficient of the gases to measure the concentration of the target gas in the volume. Usually this kind of sensors are used to detect gases with a significant difference in the thermal conductivity in relation with the air or combustible gases.

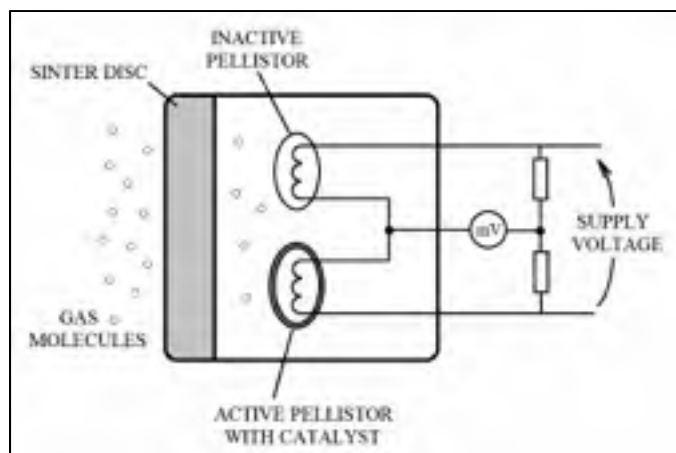


Figure 1.7 Calorimetric sensors  
Taken from X. Liu et al. (2012)

The main disadvantage of this kind of techniques for gas measurement is the low selectivity caused by the nature of the physical basis of the operation. In the same way the energy consumption is an important point to be considered in this technique (Spinelle et al., 2017).

### 1.2.2.3 Gas Chromatography

The gas chromatography is one of the most precise methods for gas sensing but usually it is focused for laboratory applications, a consequence of the kind of equipment, the complexity of the process and the interpretation of the results.

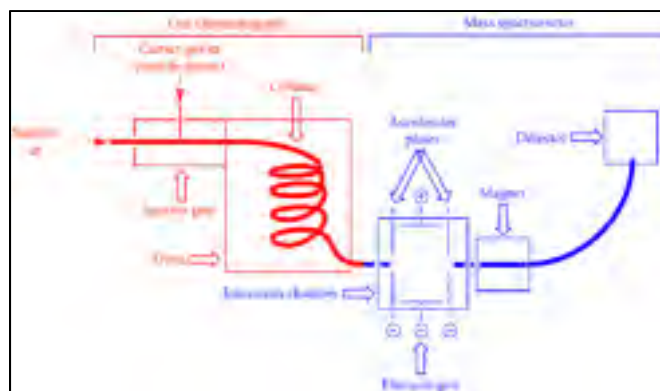


Figure 1.8 Gas Chromatography Sensors  
Taken from Jimenez, Riu, et Rius (2007)

The cost of this kind of equipment is very elevated in comparison with any other kind of gas sensing and the miniaturization for a portable version represents a high technology development, which represents a non-viable application for commercial sensors (Jimenez et al., 2007).

#### 1.2.2.4 Piezoelectric sensors

The piezoelectric sensor uses the combination of the absorption material properties for specific gases and the addition of mass for a resonant structure. In this kind of systems, the sensor can be confirmed by a surface acoustic wave (SAW) device and the quartz crystal microbalance (QCM). The SAW device produces a surface wave that travels along the surface of the sensor while the QCM produces a wave that travels through the bulk of the sensor (Arshak et al., 2004; D. D. Lee, 2001).

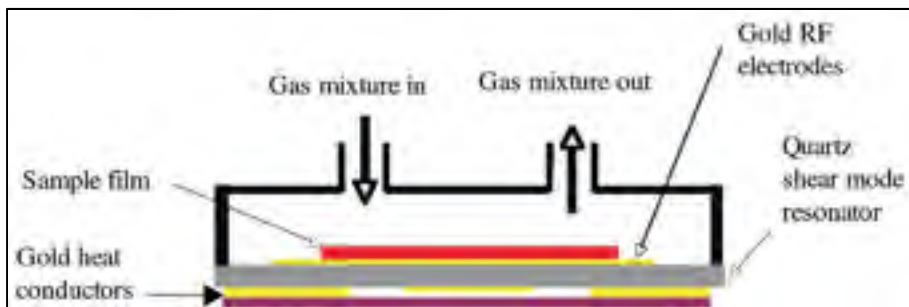


Figure 1.9 Piezoelectric sensors

Taken from Smith (2007)

The resonance frequency of the quartz will shift proportionally to the addition of the mass into the coating that can be a polymer or any other substance that absorbs the target gas. The most critical element for the selectivity of the gas is the coating, this will determine the sensibility and operation range in the concentration of the gas.

This kind of sensor has a good response time and the recovery time will depend on the coating; in some cases it is necessary to include a heat generation element to facilitate the desorption of the gas absorbed.

The disadvantage of this sensor is the complexity of the circuitry and the interpretation of the results in comparison with the polymers or the oxide metal sensors, which change the resistance linearly. In this case it is necessary to measure the frequency shift with high precision, ignoring the noise generated by the natural variations of the system. The same principle of measurement can be applied for different resonant structures, as cantilever, bridges, etc. This will be the case of analysis of this project.

### **1.2.3 Comparative of CO<sub>2</sub> sensor (ranges and precision)**

Table 1.1 shows the analysis of how the market for sensors designed for the measurement of CO<sub>2</sub> in the air is mainly covered by NDIR technology, due to the great advantage mentioned above.

Also, the range covered by most of the available sensors is 300 to 10000 ppm, given the industrial applications it is necessary to be able to make such high measurements in the concentration of CO<sub>2</sub>. On the other hand, it is not common to find sensors that guarantee the linearity of their signal below 300 ppm, because as aforementioned, the average concentration in the atmosphere is around 350 ppm, so it will not be common to find environments smaller than this concentration.

As far as accuracy is concerned, there is a wide range that will obviously depend on the quality of the sensor and the requirements of the application, however, it is possible to find acoustic or resonant sensors that reach a sensitivity of fractions of ppm (Chuang, Wu, Lu, & Lin, 2017; Gomes, Duarte, & Oliveira, 1995).

The response time also varies drastically from model to model and between technologies, however, the average time is between 10 and 15 seconds, being useful for most applications, and even measuring atmospheric conditions can be extended to minutes with no major impact on the process.

Table 1.1 Sensors performance comparison

| <b>Model/Paper</b> | <b>Technique</b> | <b>Range (ppm)</b> | <b>Accuracy (ppm)</b> | <b>Response time (s)</b> |
|--------------------|------------------|--------------------|-----------------------|--------------------------|
| K30                | NDIR             | 0-2000             | 30                    | 30                       |
| S100               | NDIR             | 0-5000             | 30                    | 20                       |
| AN100              | NDIR             | 0-5000             | 30                    | 60                       |
| T6615              | NDIR             | 0-5000             | 200                   | 30                       |
| MT30               | NDIR             | 0-5000             | 75                    | 120                      |
| K30-FR             | NDIR             | 10000              | 30                    | 2                        |
| H30-ER             | NDIR             | 1000               | 30                    | 0.5                      |
| K33-ICB            | NDIR             | 10000              | 30                    | 2                        |
| K33-ELG            | NDIR             | 30000              | 200                   | 2                        |
| K33-BLG            | NDIR             | 100                | 30                    | 15                       |
| LP8                | NDIR             | 30000              | 200                   | 15                       |
| S8                 | NDIR             | 10000              | 50                    | 16                       |
| Sprint-WR          | NDIR             | 500                | 20                    | 2                        |
| COZIR-WR           | Led-NDIR         | 10000              | 70                    | 0.05                     |
| COZIR-AMB          | Led-NDIR         | 10000              | 50                    | 0.25                     |
| COZIR-RM           | Led-NDIR         | 10000              | 50                    | 1                        |
| MISIR              | Led-NDIR         | 10000              | 50                    | 1                        |
| MiniR              | Led-NDIR         | 5000               | 50                    | 0.5                      |
| Win-0005           | Led-NDIR         | 10000              | 70                    | 30                       |
| J.A Theile         | Acoustic         | 1000               | 100                   | N.R                      |
| A. Z Sadek         | Acoustic         | 1000               | 70                    | N.R                      |
| A. Z Sadek         | Acoustic         | 1500               | 80                    | N.R                      |
| Chunbae            | Capacitive       | 2000               | 21.2                  | N.R                      |

#### **1.2.4 Conclusion**

After a brief collection of information on the existing sensors in the market and the main technologies they use, as well as their main advantages and areas of opportunity, it is possible to conclude that the measurement system to be developed should be able to cover the same requirements as the existing sensors, improving the range and accuracy that have been obtained, as well as providing a different option in measurement technique.

Among the main improvements that should be included is the ability to make measurements with an adequate linearity in a concentration range from 0 to 10000 ppm, which would give an important advantage. Also, to obtain a higher sensitivity that is in the tenth of a part per million ppm.

Finally, the energy consumption should be as low as possible, in order to give an energy advantage and cover areas where optical-based sensors have not been able to reach, as well as hot-plate sensors or any resistive techniques, which have a relatively high energy consumption. The stability on thermal changes and compensation on the humidity level must be a critical factor in the operation and precision of the system to be developed, otherwise it would be very limited to the operation in real situations.

### **1.3 Microelectromechanical system (MEMS)**

MEMS are typically defined as small devices composed of microfabricated active and passive elements that perform different functions such as perception, data processing, communication and environmental performance. The types of MEMS devices can range from relatively simple structures that have no moving parts, to very complex electromechanical systems in which multiple elements move under the control of integrated electronics.

Thanks to advances in the field of semiconductors, MEMS is a technology that can be applied using a wide variety of materials and manufacturing techniques; the choice will depend on the type of device to be manufactured and the commercial sector in which you wish to operate.

This vision of MEMS, where microsensors, micro actuators, microelectronics and other technologies can be integrated into a microchip, is expected to be one of the most important advances of the future.

MEMS generally vary in size from one micrometer (one millionth of a meter) to one millimeter (one thousandth of a meter). At this level of size scale, the constructs of classical physics are not always true. Due to the large surface area in relation to the volume of MEMS, surface effects such as electrostatics and viscosity dominate volume effects such as inertia or thermal mass. Therefore, the design and characterization stage of the microsystems will be essential for the analysis and development of new applications (Layton, 2010).

MEMS can be classified into six different types:

- **Sensors:** MEMS devices designed to measure changes in the environment. These microsystems include chemical, motion, inertial, thermal, and optical sensors.
- **Actuators:** are a group of devices designed to provide a stimulus to other components or MEMS devices. In microsystems the actuators are operated electrostatically or thermally.
- **RF MEMS:** are a class of devices used to transmit radio frequency signals. Typical devices include switches, capacitors, antennas, etc.
- **MOEMS (Micro-Opto-Electro-Mechanical Systems):** are devices designed to direct, reflect, filter, and/or amplify light. These components include optical switches and reflectors.
- **Microfluidic MEMS:** they are designed to interact and work with fluids. Devices such as micro-pumps and micro-valves are designed to handle small volumes of fluid.
- **Bio MEMS:** devices that, like many MEMS for microfluids, are designed to specifically interact with biological samples. Devices such as these are made to interact with proteins, biological cells, medical reagents, etc. and can be used to provide medication or other medical tests on site (Layton, 2010).

### **1.3.1 MEMS resonators**

As mentioned, there are several methods for measuring the concentration of gases. In the field of MEMS technology, it is possible to apply these techniques for the manufacture of sensors, however, in this work only the measurement of gas concentration by means of mass measurement is studied.

This type of measurement is normally performed by means of Quartz crystals, which can detect extremely low changes in mass, detection is performed by means of variation in the oscillation frequency. Applying the same property of a vibrating body, a resonant sensor will be manufactured which, by absorbing the gas molecules, will make a displacement in the natural frequency; the difference will lie in the geometry and materials to be used (Stephen Beeby, 2004).

#### **1.3.1.1 Vibrations**

It is a cyclic movement of a system with determined frequency, amplitude and direction, which depends of the geometry, mechanical properties and external forces acting in the system that occurs about an equilibrium point.

#### **1.3.1.2 Simple Harmonic Motion**

The simple harmonic movement is a periodic, vibratory movement in the absence of friction, produced by the action of a recuperating force that is directly proportional to the position, and which is described as a function of time by a trigonometric function (sine or cosine).

### 1.3.1.3 Undamped system

An undamped system is a theoretical system whose existence is not possible, because it is not characterized by mechanical nor frictional losses, but it allows to establish the basic equations of the movement of a harmonic system, which will be initiated to complete the system.

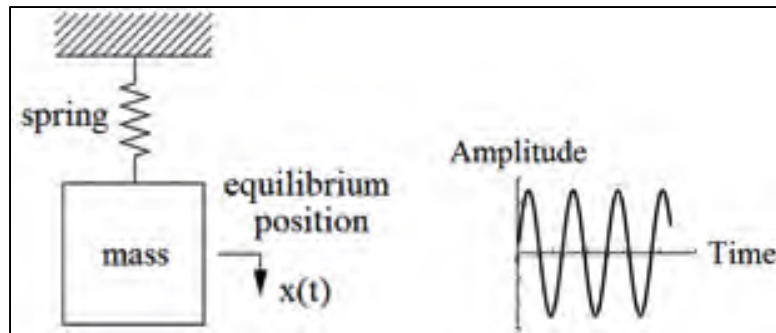


Figure 1.10 Undamped system diagram  
Adapted from Layton (2010)

Newton's equation for the mass  $m$  where the force  $m\ddot{x}$  generated by the mass on the spring is equal and contrary to the force  $kx$  applied by the spring on the mass:

$$m\ddot{x} + kx = 0 \quad (1.1)$$

where  $x = 0$  characterizes the initial point of the displacement.

$$w_n = \sqrt{\frac{k}{m}} \quad (\text{rad/sec}) \quad (1.2)$$

Where  $w_n$  represents the natural frequency.

The sinusoidal oscillation runs continuously, and the time interval to complete the cycle is called period:

$$\tau = \frac{2\pi}{w_n} \quad (1.3)$$

The reciprocal of the period is the natural frequency:

$$f_n = \frac{1}{\tau} = \frac{1}{2\pi} \sqrt{\frac{k}{m}} = \frac{\omega_n}{2\pi} \quad (1.4)$$

#### 1.3.1.4 Damped system

All real oscillators are subjected to some friction. Friction forces are dissipative and the work they do is transformed into heat that is dissipated outside the system. As a result, movement is damped, unless some external force maintains it. If the damping is greater than a certain critical value, the system does not oscillate, but returns to the equilibrium position. The speed with which this return occurs depends on the magnitude of the damping, and two different cases may occur: over damping and critically damped movement.

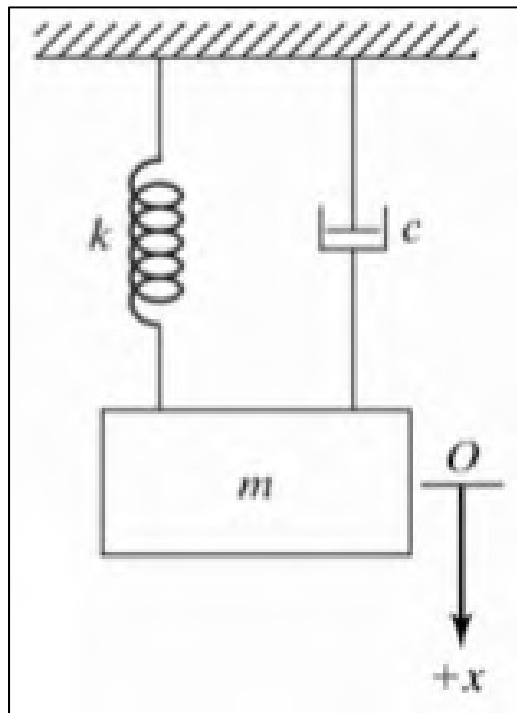


Figure 1.11 Damped system diagram  
Adapted from Layton (2010)

When the damping does not exceed this critical value, the system performs a slightly damped movement, like the simple harmonic movement, but with an amplitude that decreases exponentially over time.

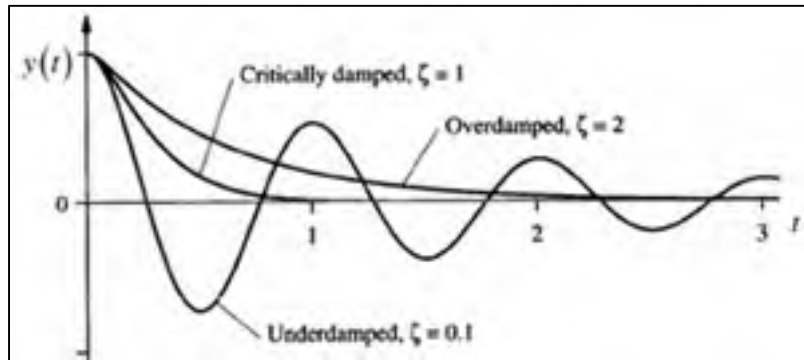


Figure 1.12 Trace of system with different level of damping  
Adapted from Mahajan (2006)

The differential equation of motion of mass  $m$  for the undamped system is:

$$m\ddot{x} + c\dot{x} + kx = 0_n \quad (1.5)$$

The critical damping coefficient  $c_c$  is defined as:

$$c_c = 2\sqrt{km} = 2mw_n \quad (1.6)$$

The ratio  $\zeta$  is defined as the fraction of critical damping:

$$\zeta = c/c_c \quad (1.7)$$

The damped natural frequency is related to the undamped natural frequency by the equation:

$$w_d = w_n(1 - \zeta^2)^{\frac{1}{2}} \quad (rad/sec) \quad (1.8)$$

### 1.3.1.5 Forced vibration damped system

Unlike the free damped system, the forced vibration system has an external force that excites the system at a specific frequency as well as a defined amplitude. When this frequency is equal to the value of the system's natural frequency, the amplitude of the vibrating element will peak, and is considered the most efficient value in the system.

This frequency is usually avoided in engineering as it puts at risk the integrity of the structures, however, in this case it requires the highest efficiency and sensitivity of the system, so it is constantly sought to obtain such value.

### 1.3.1.6 Resonance

Resonance is the characteristic of all bodies to vibrate at a specific frequency given its physical characteristics, this value is also known as natural frequency, and will be the key point of analysis of this system.

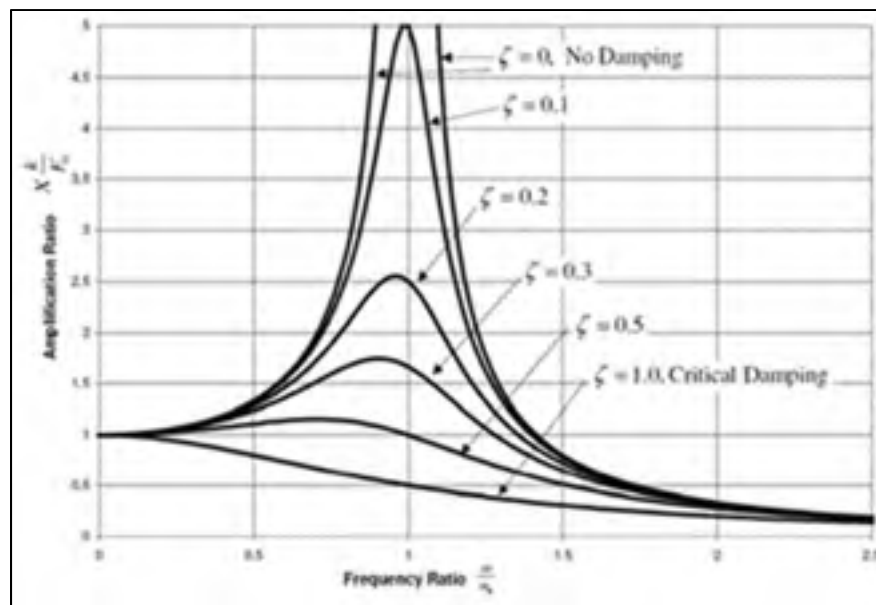


Figure 1.13 Amplitude of resonance by damping  
Adapted from Mahajan (2006)

### 1.3.1.7 Q Factor

The Q factor, also called the quality factor or selectivity factor, is a parameter that measures the ratio between the reactive energy it stores and the energy it dissipates over a complete signal cycle. A high Q factor indicates a low rate of energy loss relative to the energy stored by the resonator.

For the estimation of the Q value the properties of the system must be known, however, it can become very complex, so a technique known as -3 dB bandwidth method is applied, which, based on the amplitude curve and the resonant frequency, allows us to obtain the Q factor easily, as shown below:

$$Q = \frac{F_{max}}{\Delta f} \rightarrow \Delta f = 0.707 * f_{max} \quad (1.9)$$

$$Q = \frac{\sqrt{km}}{c} \quad (1.10)$$

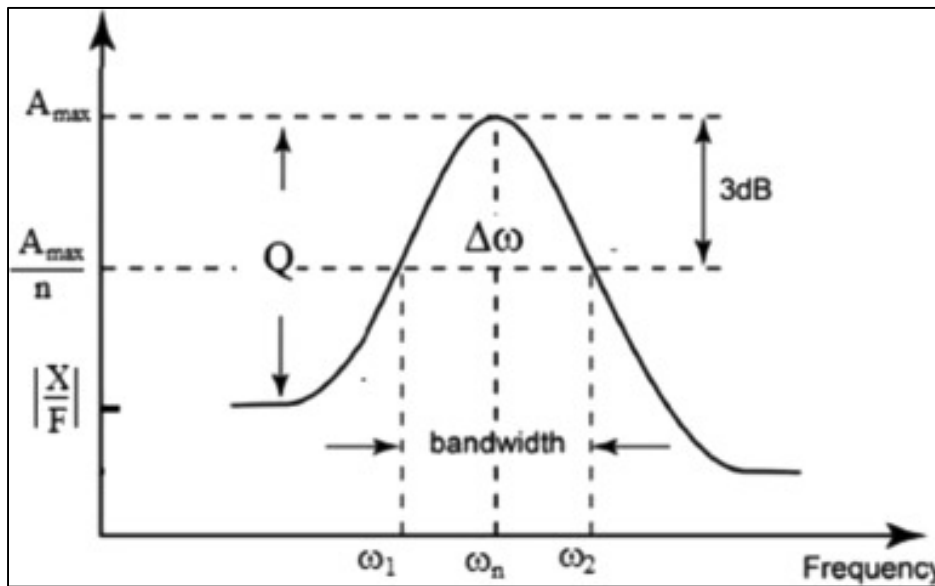


Figure 1.14 Q factor diagram  
Adapted from Mahajan (2006)

Damping in a system can be defined by noting the maximum response. This is defined by the Q-factor sometimes and defined with respect to mechanical vibration as:

$$Q = \frac{1}{2} \zeta \quad (1.11)$$

The damping is also indicated by the width of the resultant curve in the resonance frequency  $w_n$  defined by:

$$\frac{\Delta w}{w_n} = \frac{1}{Q} = 2\zeta \quad (1.12)$$

### 1.3.2 MEMS mass sensing for gas concentration measurement

As discussed at the beginning of this paper, it is possible to detect gas concentration by means of various techniques, however, all of them have a limitation mainly in the cost-dimensions-sensitivity relationship.

To try to provide a solution to this situation, mass sensors are available as an option by measuring the resonant frequency of a structure, which by means of a film of absorbent material will be able to capture the gas in the environment and measure its concentration.

#### 1.3.2.1 Principle of Operation

As can be concluded from the previous module where the relationship between the natural frequency of a mechanical system, the mass and the damping coefficient is established, it is possible to define that the greater the mass, the lower the resonance frequency will tend to decrease.

By applying this principle, it is possible to create a resonant system which, by absorbing the target gas molecules, will cause an increase in the mass of the resonant body and since its damping coefficient will not vary, the resonant frequency will suffer a decrease proportional to the amount of the absorbed mass, this effect can be seen in the following figure.

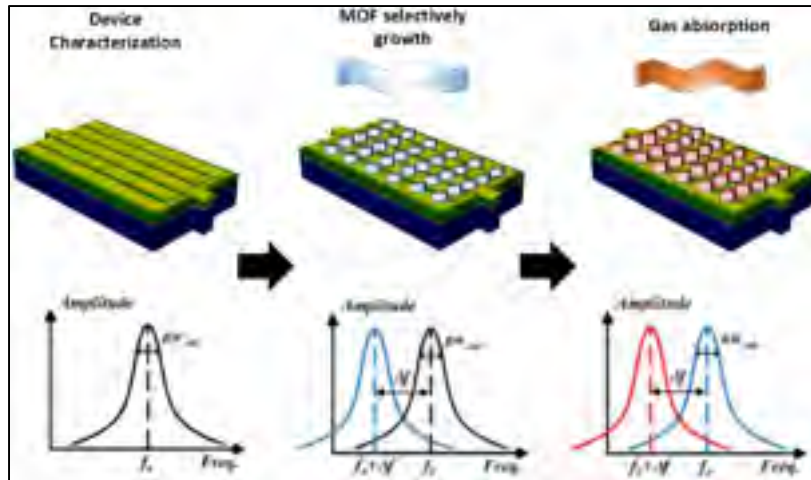


Figure 1.15 Frequency deviation diagram  
Adapted from MIT (2016)

The relationship between the aggregate mass and the resonance frequency offset will depend on the dimensions, geometries and materials of the resonators. This topic has been extensively studied to obtain the best possible result.

### 1.3.2.2 Geometries and resonant modes

The resonators made by MEMS technology can be manufactured with different geometries, materials and manufacturing processes. The possible geometries of these resonators have been a subject of study for several decades, given that the efficiency of the resonator, as well as the sensitivity that will be obtained, is directly related to the dimensions and shape of the resonant system.

One of the properties of resonators are the modes to which they vibrate, this depends on the mechanical properties of the system and the frequency to which it is subjected. The most

common method to use in gas concentration sensors is mode 1, where the lowest resonance frequency is used, this is because it is the simplest to measure and because the application is sought to be as stable as possible (Stephen Beeby, 2004).

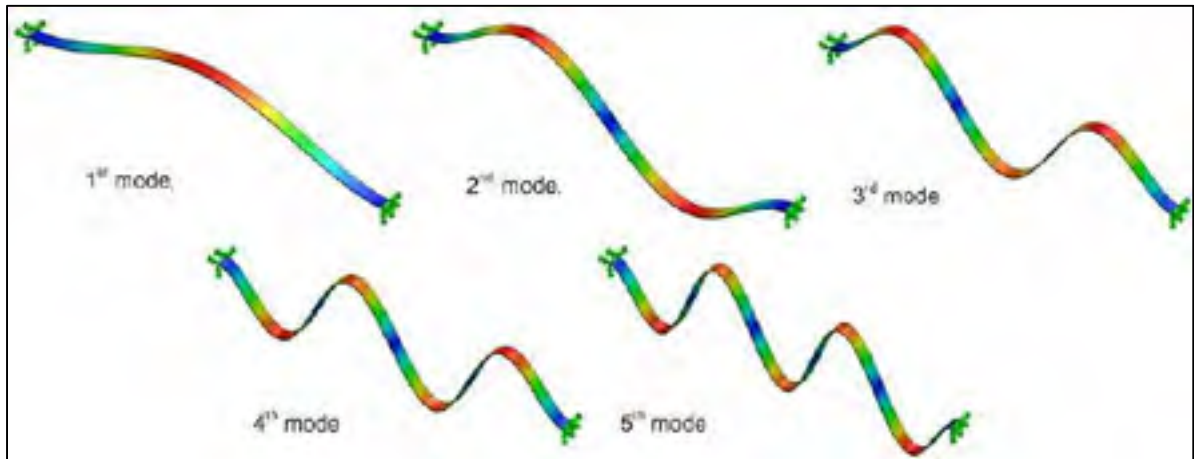


Figure 1.16 Resonant modes of MEMS bridge  
Adapted from Zaman et al. (2014)

As mentioned above, there is a possibility of creating a resonant system based on any desired geometry, each one of them presenting its advantages, which will depend on the mechanical properties already mentioned.

The resonators that have been widely used are based on beams, and these can be either with a fixed cantilever end, with both fixed bridge ends, among others. On the other hand, plates or discs held by small arms with low mechanical resistance have been used, reducing the intervention in their frequency of oscillation.

An important factor that has defined the type of geometry is the manufacturing processes, which have limited the ability to create complex geometries, this is due to the dimensions and tolerances existing in these systems, which have forced to create standardized manufacturing systems to obtain considerable repeatability (R. Abdolvand, B. Bahreyni, J. E. Y. Lee, & F. Nabki, 2016).

### 1.3.2.3 Resonator Geometries for mass sensing

Multiple geometry options are potentially applicable as sensors, however, in order to have a gas sensor it is necessary to have a high sensitivity, this will allow to obtain a detectable and low noise response with the addition of a minimum amount of mass.

One of the most commonly used geometries is the fixed beam at one end, also known as a cantilever. This structure offers great sensitivity due to the amplitude of its resonant frequency and its alteration with increasing mass.

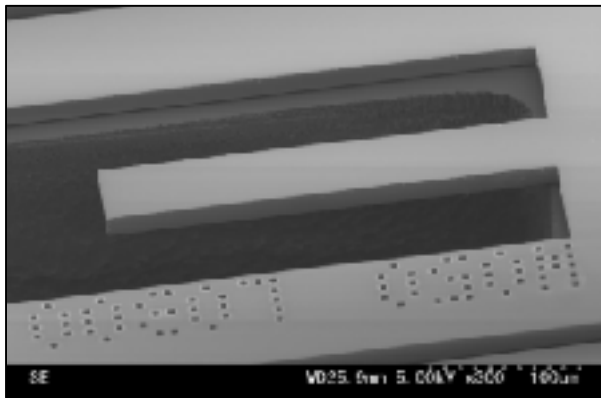


Figure 1.17 Cantilever micro-resonator  
Adapted from R. Abdolvand et al. (2016)

Another commonly used structure is a beam but attached at both ends known as a bridge. This structure has less sensitivity; however, it also shows greater stability and noise reduction.

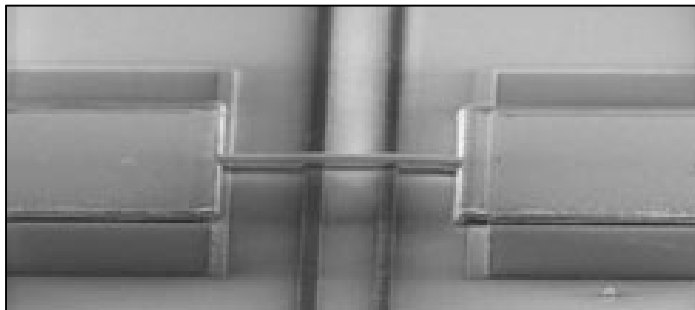


Figure 1.18 Bridge micro-resonator  
Adapted from R. Abdolvand et al. (2016)

This type of structure tends to have the highest sensitivity to a lower absorbed mass, which makes it the best choice for this type of sensor.

Other not so common structures are free-free beam resonators, which have a greater freedom of movement, but their stability and sensitivity do not give them a competitive advantage among other geometries, in addition to having a much higher noise level than other structures.

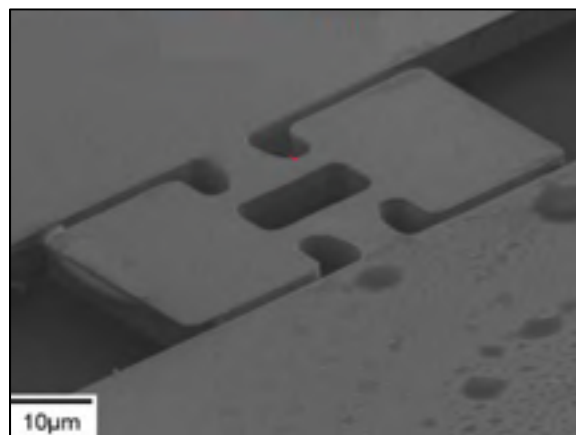


Figure 1.19 Free-Free beam micro-resonator  
Adapted from Hajjam et Pourkamali (2012)

The plates or discs have been analyzed; however, they have not shown an advantage to the beams despite having a larger area and greater capacity to place a larger volume of absorption film.

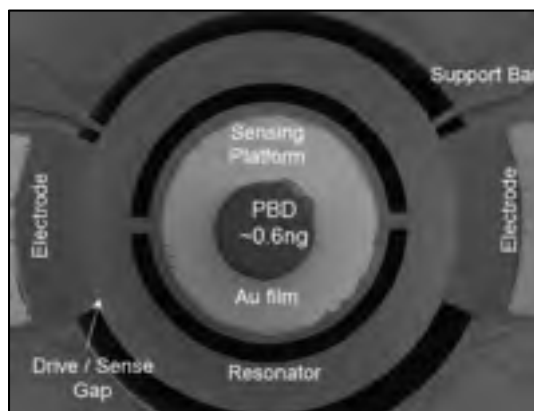


Figure 1.20 Disc micro-resonator  
Adapted from Konno et al. (2011)

These are the sensors that have been most documented for airborne gas concentration measurement systems under the principle of absorption of target gas molecules. Among the most commonly used are the cantilever type, below you can find a comparison of the documented as well as their characteristics.

Table 1.2 Main published micro-resonators for gas sensing  
Adapted from Fanget et al. (2011)

| Shape      | Length (um) | Width (um) | Thickness (um) | Sensibility     | Gas             |
|------------|-------------|------------|----------------|-----------------|-----------------|
| Cantilever | 1000        | 324        | 45             | 3.18Hz /100ppm  | CO <sub>2</sub> |
| Cantilever | 1000        | 300        | 45             | 16mHz/ppm       | CO <sub>2</sub> |
| Cantilever | 1000        | 400        | 6              | 0.04Hz/ppm      | Ethanol         |
| Cantilever | 150         | 90         | 10             | 0.12Hz /ppm     | CO <sub>2</sub> |
| Cantilever | 200         | 50         | 3.5            | 0.5Hz / 100ppm  | CO              |
| Bridge     | 1100        | 300        | 40             | 3.2Hz / ng      | CO <sub>2</sub> |
| Disc       | 200         | 100        | 12             | 0.04Hz / 100ppm | CO <sub>2</sub> |
| Cantilever | 100         | 30         | 5              | 2.1 fg/Hz       | CO <sub>2</sub> |
| Cantilever | 200         | 20         | 15             | 0.025Hz / ppm   | CO <sub>2</sub> |

The table above shows some of the main gas sensors that apply the focused technique to this project. It can be concluded that most of the sensors use cantilever geometries due to the advantages mentioned above.

Another important factor to define is the means of action for these resonators, i.e. as mentioned above a system that operates in resonance, operates under an external force at a specific amplitude and frequency.

#### 1.3.2.4 Actuation methods

For the excitation of the resonators, different methods can be used from piezoelectric effect, electrostatic attraction, heat expansion or magnetic actuation. In the case of the magnetic

actuation, there are many inconvenients in the use of this technique, like the size, the power, the interference with other elements inside the chip, etc.

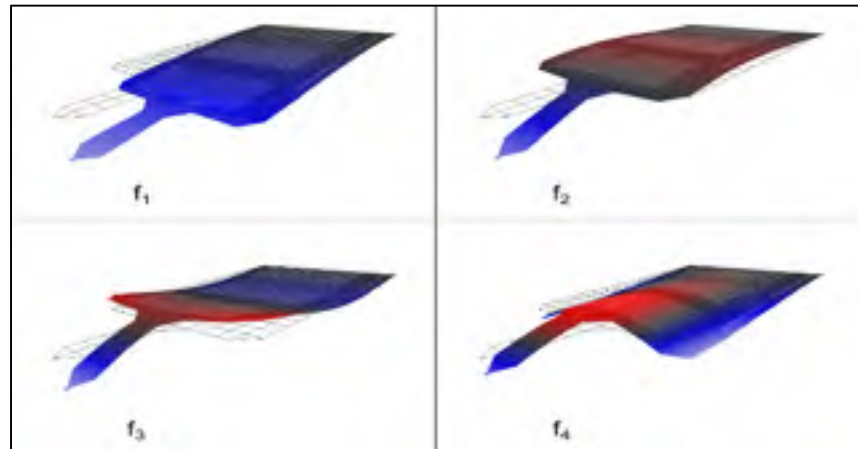


Figure 1.21 Piezoelectric actuation in resonator  
Adapted from Fowler, Bulut Coskun, et Reza Moheimani (2017)

One of the most commonly used systems for excitation of resonators is shown in the figure above: piezoelectric actuators, which allow impulse in both directions, are easily adaptable to the geometry of the resonator; the potential and current used are considerably low, which gives it a great advantage over other systems (Fowler et al., 2017; Mahdavi, Mehdizadeh, & Pourkamali, 2018).

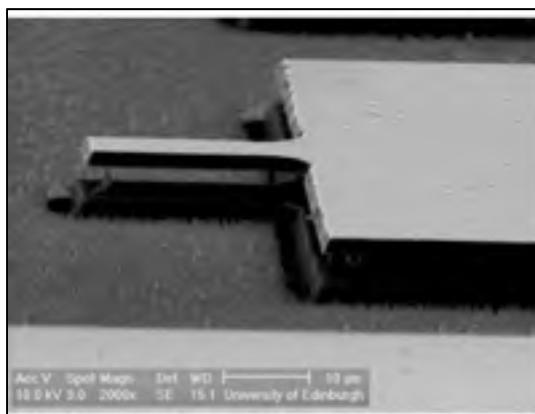


Figure 1.22 Electrostatic cantilever  
Adapted from Han et al. (2018)

The figure above shows one of the most commonly used systems for excitation of resonators: the piezoelectric actuators, which allow impulse in both directions, are easily adaptable to the geometry of the resonator; the potential and current used are considerably low, which gives it a great advantage over other systems (R. Abdolvand et al., 2016; Wood, Svilicic, Mastropaolo, & Cheung, 2016).

Both the activation by means of piezoelectric actuators and electrostatic charges are devices that, in addition to generating the impulse for the resonator, provide feedback for the control of the exciter circuit, which facilitates the integration of the control system with the resonators (Stephen Beeby, 2004).

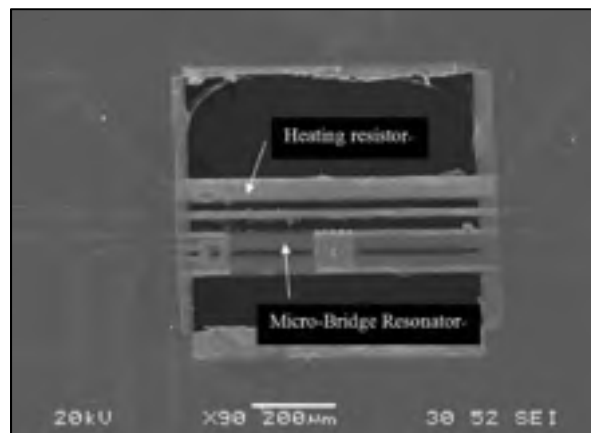


Figure 1.23 Electro-thermal micro-resonator  
Adapted from (Han et al., 2018)

One method of excitation with a different principle is that of thermo-expanding resonators, which use the flow of current in a conductor that tends to increase its temperature, expanding and generating a displacement. It is a very efficient and widely used system, however, it has the great disadvantage of the current consumption, the precision that the control system must have to avoid variations in the vibrations by a variation of the expansion factor between cycles. On the other hand, there are temperature sensitive coatings, which can be affected by the resonator temperature (Han et al., 2018).

Table 1.3 Excitation methods in resonators  
Adapted from Fanget et al. (2011)

| Shape      | Length (um) | Width (um) | Thickness (um) | Sensibility    | Gas             | Excitation    |
|------------|-------------|------------|----------------|----------------|-----------------|---------------|
| Cantilever | 1000        | 324        | 45             | 3.18Hz/100ppm  | CO <sub>2</sub> | Electrostatic |
| Cantilever | 1000        | 300        | 45             | 16mHz/ppm      | CO <sub>2</sub> | Electrostatic |
| Cantilever | 1000        | 400        | 6              | 0.04Hz/ppm     | Ethanol         | Piezoelectric |
| Cantilever | 150         | 90         | 10             | 0.12Hz /ppm    | CO <sub>2</sub> | Piezoelectric |
| Cantilever | 200         | 50         | 3,5            | 0.5Hz / 100ppm | CO              | Piezoelectric |
| Bridge     | 1100        | 300        | 40             | 3.2Hz / ng     | CO <sub>2</sub> | Piezoelectric |
| Semi-Disc  | 200         | 100        | 12             | 0.04Hz/100ppm  | CO <sub>2</sub> | Thermal       |
| Cantilever | 100         | 30         | 5              | 2.1 fg/Hz      | CO <sub>2</sub> | Piezoelectric |
| Cantilever | 200         | 20         | 15             | 0.025Hz / ppm  | CO <sub>2</sub> | Piezoelectric |

The table above compares the same resonators that have been analyzed, and the distribution between piezoelectric and electrostatic systems are the most used due to their simplicity, low current consumption and reliability.

#### 1.3.2.5 Materials used in resonators

It would be possible to use any type of material used for traditional mechanics to manufacture the resonators from the operational point of view, however, the manufacturing processes and the compatibility of the materials currently used by the CMO's manufacturing processes have limited to a few options.

Polysilicon is the most commonly used material in these resonators, since its mechanical properties are exceptional and very efficient in micro-mechanical systems, the coefficients of thermal expansion are low, which gives it an advantage in processes that require stability at various temperatures. The electrical properties of the doped material give it good conductivity

values, which has made it the most widely used option for this type of system (R. Abdolvand et al., 2016; Gargiulo, Pepe, & Caputo, 2014).

Despite these qualities, several models have been developed using different materials such as Anodic alumina, ZrO<sub>2</sub>/Y<sub>2</sub>O<sub>3</sub>, Borosilicate glass, among others. These materials are promising in processes that require a temperature close to 1000°C, or processes with very low electrical resistance, processes in which polysilicon can hardly meet the requirements (Vasiliev et al., 2016).

#### **1.3.2.6 MEMS resonators fabrication process**

The fabrication of micro-resonators presents a technological challenge and very advanced methodologies due to the small dimensions and tolerances that these devices require to obtain the necessary resolution, repeatability and quality.

There are several standardized microfabrication processes that have been developed, which allow to create devices of great quality and with good repeatability. This is important when micro-devices are fabricated in order to ensure batch fabrication and uniform performance metrics between devices.

As previously mentioned, one of the most common methods of excitation of the micro-resonators is by means of a piezoelectric layer which will allow to generate the mechanical excitation to the micro-resonator but at the same time it will generate the necessary current to use it as a sensing element. A commercial process for manufacturing piezoelectric micro-resonators is PiezoMUMPS, which is offered by the company MEMSCAP.

Another type of micro-resonator that is common in this type of application is the electrostatic type, which basically uses the attraction force between two parallel plates to create the mechanical excitation to the device. This requires an DC voltage to be applied between the plates to accumulate charge onto them. This allows, in turn, for a current to be generated as the

micro-resonator's capacitance varies during its motion, and allows for it to operate as a sensing element. These types of micro-resonators can be manufactured using the commercial process known as PolyMUMPS offered too by MEMSCAP, and also by the PiezoMUMPs process.

These two types of micro-resonators will be analysed in more detail to consider their advantages in the context of this thesis.

### **Electrostatic Micro-resonators**

The electrostatic micro-resonators use the principle of attraction between two plates in which there is an electrical potential. The force depends on the area, distance between plates and bias electrical potential. This type of micro-resonator uses a fixed plate and another movable plate separated by a gap. If the excitation signal supplied to the micro-resonator has a sinusoidal shape the micro-resonator will vibrate at the same frequency increasing its amplitude as it approaches its resonance frequency. A typical diagram of a micro-resonator is shown in figure 1.24.

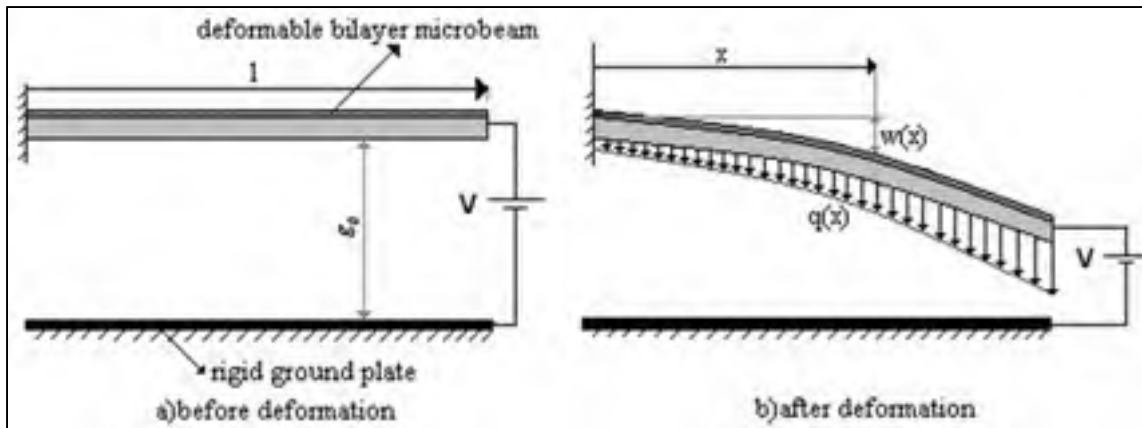


Figure 1.24 Electrostatic MEMS resonator operation  
 Taken from Pashapur, Pesteii, Rezazadeh, et kouravand (2009)

Figure 1.24 shows an example of a cantilever-type micro-resonator, where the end of the beam has a greater attraction due to the fact that as it deforms, the gap between the electrodes decreases and the attraction force is greater. The distance between the plates is a critical factor for the operation of these micro-resonators, which will depend on the micro-manufacturing process.

#### Electrostatic MEMS resonators fabrication process using PolyMUMPs

PolyMUMPs is a three-layer polysilicon surface micromachining process. The process starts with n-type silicon wafers. The surface of the wafer is doped with phosphorus using a phosphate glass sacrifice layer (PSG) as the doping source. Then, after removal of the PSG film, a 600 nm low-voltage silicon nitride layer is deposited as an insulation layer. In figure 1.25 the lateral cut of the layers used in the PolyMUMPS are shown.

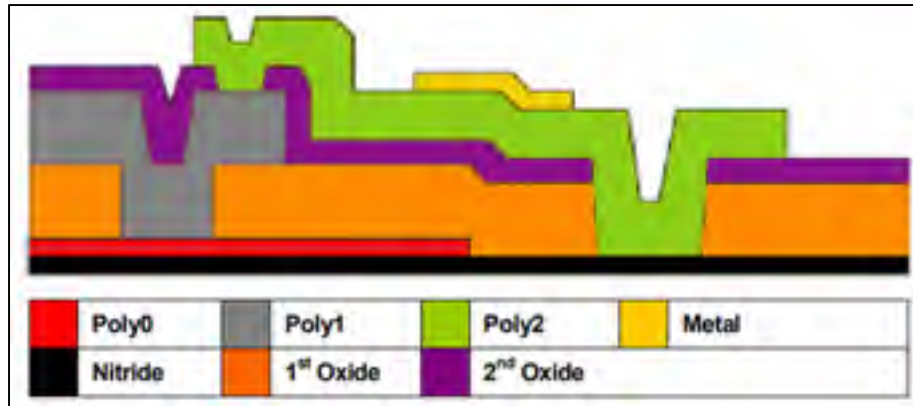


Figure 1.25 PolyMUMPS lateral cut representation  
Taken from (MEMSCAP, 2011).

A 500 nm LPCVD polysilicon film is deposited and modelled by photolithography. After creating the photoresist pattern, it is etched into a plasma system. A sacrificial layer of 2.0  $\mu\text{m}$  phosphosilicate glass (PSG) is then deposited by LPCVD and annealed at 1050°C for 1 hour in an argon atmosphere.

The sacrificial layer is patterned with the dimples mask and are transferred to the PSG sacrificial layer using an RIE (Reactive Ion Etch) system. The Poly0 layer is patterned using a RIE. Subsequently, the first structural polysilicon layer (Poly1) is deposited with a thickness of 2.0  $\mu\text{m}$ . A thin layer (200 nm) of PSG is deposited on the polysilicon and the wafer is annealed at 1050°C for 1 hour. The polysilicon is annealed with the phosphorus of the PSG layers.

The PSG layer is etched to produce a hard mask for subsequent polysilicon etching. After etching the polysilicon, the photoresist is removed and the remaining hard oxide mask is removed by the RIE. After etching the first layer of polysilicon, a second layer of sacrificial PSG is deposited with a 750 nm thickness.

The second structural layer of polysilicon (Poly2) is deposited and patterned by RIE, having a thickness of 1.5  $\mu\text{m}$ . The wafer is then annealed for one hour at 1050 °C in order to dope the polysilicon and render it conductive.

The last layer deposited in the PolyMUMPs process is a 0.5  $\mu\text{m}$  metal (gold) layer. The metal is patterned via liftoff. Finally the sacrificial layers are removed to release the structures using a wet HF etch.

Table 1.4 PolyMUMPS fabrication parameters  
Taken from (MEMSCAP, 2011).

| Material Layer | Thickness ( $\mu\text{m}$ ) | CD Tolerances  | Lithography Level Name     |
|----------------|-----------------------------|--|----------------------------|
| Nitride        | 0.6                         | —  | —                          |
| Poly 0         | 0.5                         | 1.800 to 2.200 $\mu\text{m}$ Lines   | POLY0 (HOLE0)              |
| First Choke    | 2.0                         | 1.800 to 2.300 $\mu\text{m}$ Spaces<br>1.700 to 2.300 $\mu\text{m}$ Spaces | DIMPLE<br>ANCHOR1          |
| Poly 1         | 2.0                         | 1.750 to 2.250 $\mu\text{m}$ Lines   | POLY1 (HOLE1)              |
| Second Choke   | 0.75                        | 1.750 to 2.250 $\mu\text{m}$ Spaces<br>1.750 to 2.250 $\mu\text{m}$ Spaces | POLY1 POLY2 VIA<br>ANCHOR2 |
| Poly 2         | 1.5                         | 1.700 to 2.300 $\mu\text{m}$ Lines   | POLY2 (HOLE2)              |
| Metal          | 0.5                         | 2.500 to 3.500 $\mu\text{m}$ Lines   | METAL (HOLEM)              |

The manufacturing process offered in the PolyMUMPS methodology has multiple limitations due to geometric tolerances, thickness of each layer and order of assembly. This is a critical factor and one of the limitations of this type of technology. Table 1.4 shows the manufacturing parameters and critical dimensions (CD) of each layer that make up the electrostatic devices manufactured with this technology.

### Piezoelectric MEMS Resonators

As mentioned previously, piezoelectric micro-resonators have a thin layer of piezoelectric material deposited onto the surface which allows it to function as an excitation method but can also be used as a sensing element. The simplicity of its manufacturing process and lack of requirement of a bias DC voltage makes it a common resonator type.

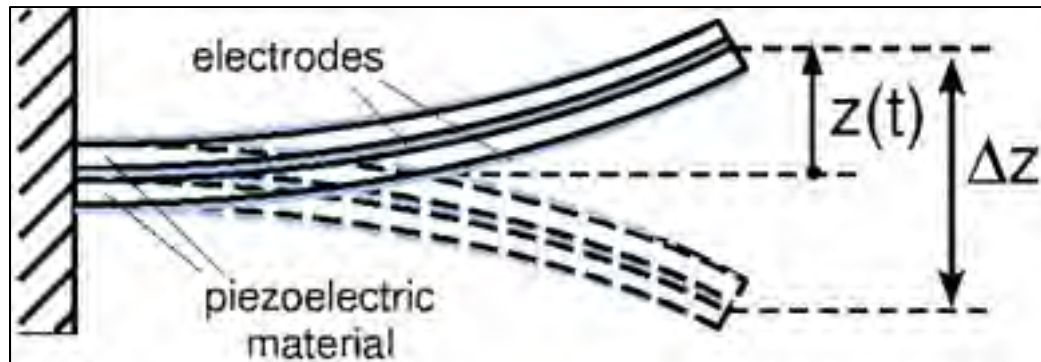


Figure 1.26 Piezoelectric MEMS resonator operation  
 Taken from Romani, Sangiorgi, Tartagni, et Paganelli (2011)

Figure 1.26 shows a scheme of a cantilever type resonator that when excited by a sinusoidal voltage, exhibits the expansion and compression of the piezoelectric material to generate a deformation of the resonator structure that depends on the resonant properties of the device.

#### Piezoelectric materials used in MEMS resonators

The piezoelectric effect describes the relationship between a mechanical voltage and an electrical voltage in solids. It is the ability of certain materials to produce an electrical charge in response to an applied mechanical stress. The reverse effect can also be observed, in which piezoelectric materials are deformed by the application of an electrical potential.

In the direct piezoelectric effect, the compression and expansion of a material generates opposite electrical charges on the respective faces of the sample. In the reverse piezoelectric effect, the application of a voltage to a piezoelectric material produces a certain amount of deformation.

Piezoceramic materials, such as aluminum nitride (AlN), have the property of being rigid and ductile, so they are good candidates for use as actuators, due to their high modulus of elasticity, which facilitates mechanical coupling to the structure. On the other hand, piezopolymers, such as PTFE, are better suited to act as sensors because they add a minimum rigidity to the structure

due to their flexibility and are also easy to fabricate. They are most commonly used as contact sensors and thin-film acoustic transducers.

### Piezoelectric MEMS resonators using the PiezoMUMPs fabrication process

PiezoMUMPS has a cross-section shown in figure 1.27. It is based on a silicon on insulator (SOI) wafer.

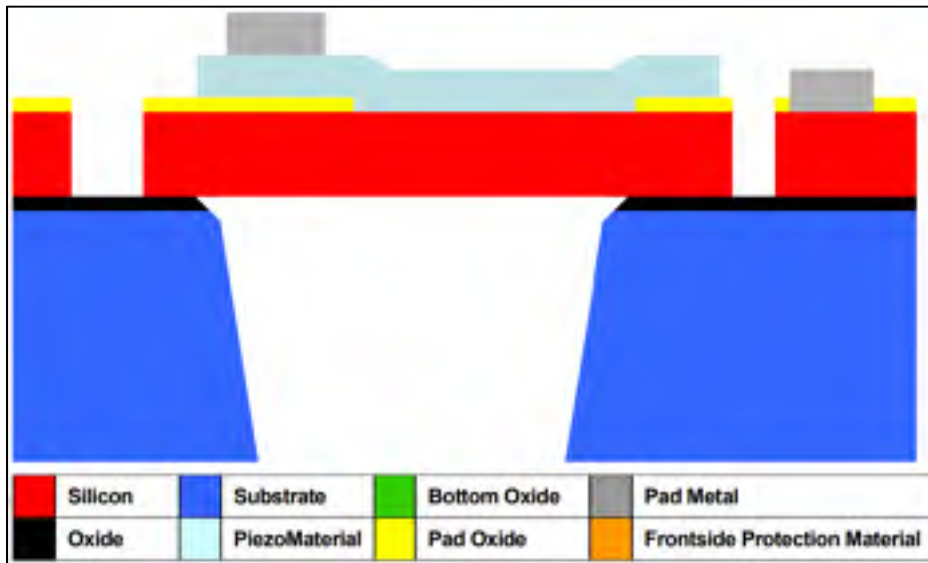


Figure 1.27 PiezoMUMPS cross-section  
Taken from (MEMSCAP Inc., 2014).

PiezoMUMPS consists of 5 levels as shown in figure 1.27 where the layer of piezoelectric material is AlN.

The first step starts with a 150 mm n-type polished SOI wafer where the top silicon surface is doped by depositing a layer of phosphate glass (PSG) and annealing at 1050°C for 1 hour in a controlled argon atmosphere. A 2000 Å thermal oxide (pad oxide) is grown, which is patterned using a RIE.

The first layer to be deposited is the 0.5  $\mu\text{m}$ -thick AlN. It is patterned using a wet etch. The second layer deposited is the metal which is formed by 20 nm of chrome and 1  $\mu\text{m}$  of aluminum, and is protected during the next step subsequent Reactive Ion Etch (DRIE).

The silicon is then pattern and etched using DRIE. A protection is applied to the upper surface of the silicon layer and the silicon wafers are reversed to allow access to the substrate layer to be patterned from below. This pattern is etched using a DRIE with an oxide mask which is patterned by a RIE.

By means of wet oxide etching, the buried oxide layer is removed in the regions defined by the TRENCH mask. The protective material on the front side is removed in a dry etching process.

Table 1.5 PiezoMUMPS fabrication parameters  
Taken from (MEMSCAP Inc., 2014).

| Microtonic level name | GIF level name | GDS level number | Min. feature ( $\mu\text{m}$ ) | Min. space ( $\mu\text{m}$ ) | Max. feature length ( $\mu\text{m}$ )                        | Max. patterned (etched) area |
|-----------------------|----------------|------------------|--------------------------------|------------------------------|--|------------------------------|
| PADOXIDE              | POX            | 10               | 5                              | 5                            | Unlimited  | N/A                          |
| PZFILM                | PZF            | 20               | 10                             | 10                           | 5000   | N/A                          |
| PADMETAL              | PAD            | 30               | 3                              | 3                            | 5000   | N/A                          |
| SOI                   | SOI            | 40               | 2"                             | 2"                           | Unlimited for width > 6 $\mu\text{m}$<br>(See section 2.2.2) | 33 mm <sup>2</sup>           |
| SOIHOLE               | HOLE           | 41               | 3                              | 3                            | N/A  | N/A                          |
| TRENCH                | TRCH           | 50               | 200                            | 200                          | 5000   | 35 mm <sup>2</sup>           |

During the design process of the piezoelectric device, it is necessary to consider the limitations of the manufacturing process, which apply to both the number of layers and thicknesses for the silicon, metal and piezoelectric material, as well as the distances and tolerances of each layer. These characteristics and design rules are summarized in table 1.5.

### 1.3.2.7 Conclusion

The resonators as mass measurement systems depend on various factors that affect the sensitivity and operating range, however, among the main ones are the geometry and materials to be used, as well as the source of excitation and measurement to be used.

As we have seen above, geometries such as cantilevered beams, fixed beams at two points, as well as discs or plates are the most commonly used for this type of sensor, so designs should be evaluated. On the other hand, as we understand mathematical modeling, it is possible to make an estimate close to the expected behavior, but to obtain a precise analysis it is necessary to make a much more complex model, which must be corroborated with the characterization processes and make the necessary adjustment to the proposed mathematical model.

For the definition of the material to be used, we will continue with the commercial trend as well as with standardized manufacturing processes, so polysilicon is the most viable option to start with, once the model is adjusted, the possibility of using other materials can be analyzed, even so, the manufacturing complexity will be a weak point to use a material different from polysilicon.

With the definition of the geometry and its appropriate dimensions, as well as the type of material and manufacturing process, it is necessary to analyze the existing possibilities of the coatings; as previously analyzed the coating material will define the gas to be detected and the level of selectivity required.

#### **1.4 Material adsorbent coatings**

The resonance sensors for the measurement of gas concentration take advantage of the properties of some specific gas adsorbing materials which cause an increase in their mass, this increase generates a change in the dynamic parameters of the resonator that is reflected in the resonance frequency of this (Subhashini & Juliet, 2013). The parameters defining the advantages of a material as a gas adsorption medium can be divided into the following categories:

##### **1.4.1 Selectivity**

It is the quality of a material to adsorb the molecules of a gas type in a mixture of different gases, this factor is crucial to be able to use it as a *discretizer* for a specific gas, since, if said

material adsorbs different gases at the same time, it would be very difficult to know the proportion of each of the adsorbed gases in the material.

#### **1.4.2 Interaction with other gases**

It is an elementary quality that any material that will be used as a detection medium must be analyzed regardless of the type of sensor. This is because it could be a material with exceptional characteristics for detecting a type of gas, however, if the material tends to oxidize on contact with oxygen it will be immediately disabled on contact with air. This could affect the life of the sensor as well as its range of applications.

#### **1.4.3 External influences**

This parameter refers to how external influences can affect the performance of the sensor to perform its purpose, this can refer to the behavior at different temperatures, humidity levels, vibrations or any other parameter outside the sensor itself. This parameter can also define the sensor's range of applications.

#### **1.4.4 Deposition technique**

This parameter focuses on the manufacturing process, in which it is important to define the processes that a material requires to be applied as an adsorption medium, since if for example it is necessary to make a deposit at high temperature, it is necessary to analyze if the resonator will not be affected by this process. It also applies in the case where the deposit requires the application of acids that could affect the structure of the resonator.

#### **1.4.5 Reversibility**

The reversibility of a material is more focused on the long-term sensor process, where a material will tend to adsorb the gas molecules at a certain concentration, but once that concentration decreases, it will be necessary for the material to release the trapped molecules

and readjust to the current value. Another method may be that the molecules are not released, and the rate of change is measured over a period, but eventually the material will tend to become saturated and must be regenerated, this may be by increasing the temperature for a period, or it may be necessary to vacuum the material to release the captured molecules.

#### **1.4.6 Sensitivity**

One of the most important parameters is the ability to adsorb the gas molecules at very low concentrations and in the most linear way possible, this will represent how sensitive a material can be, as well as the linearity that can be obtained at least from the variation of the adsorbed mass that will be transmitted to the resonator.

Part of the sensitivity of the adsorbent material will be to be able to operate over a wide temperature range as well as a wide humidity range. The humidity levels to which this type of sensor will be subjected will cover practically the entire existing range, otherwise it will be a considerable disadvantage compared to other measuring techniques (Hajjam & Pourkamali, 2012).

#### **1.4.7 Partition coefficient**

To estimate the adsorption capacity of the materials to be considered, the partition coefficient is the quotient or ratio between the concentrations of that substance in the two phases of the mixture formed by two immiscible solvents in equilibrium. This coefficient therefore measures the differential solubility of a substance in these two solvents (D. D. Lee, 2001).

This ratio is defined by the following equation:

$$K = \frac{\text{Sol 1}}{\text{Sol 2}} \quad (1.13)$$

Where Sol 1 is the concentration of the substance in the first solvent and, similarly Sol 2 is the concentration of the same substance in the other solvent.

By means of this factor the mass added to the adsorbent material can be estimated and therefore the resonator frequency offset can be estimated, a value that will be transferred to the concentration of the target gas present in the air (Arshak et al., 2004).

#### **1.4.8 Regeneration of coatings**

The regeneration of the adsorption coatings is a parameter to be analyzed because the qualities and requirements of these can define the structure and operation of the sensor. This is because there are materials that must be subjected to high temperatures for long periods of time to release the molecules trapped in the structure of the material.

There are other materials that must be subjected to high vacuum to extract the trapped molecules; these types of materials cannot be considered due to the final application. There are also materials that require both processes to be regenerated, making them the least likely option for application.

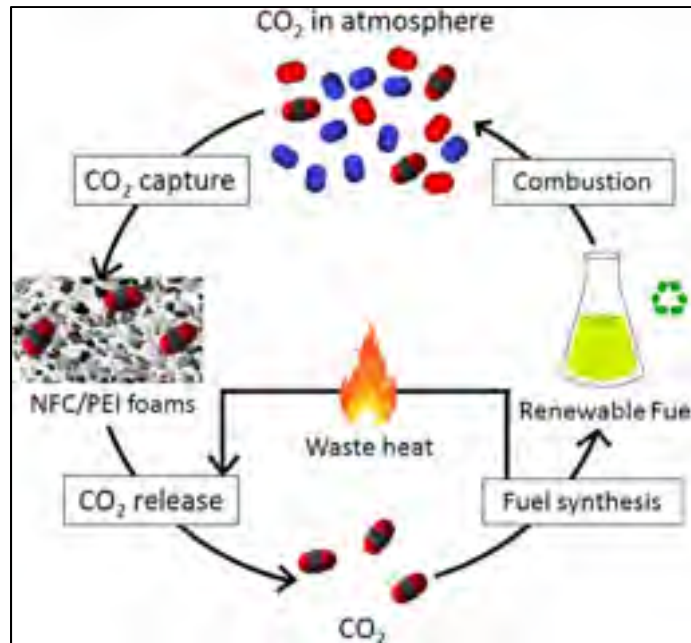


Figure 1.28 Coating regeneration diagram  
Adapted from Sehaqui et al. (2015)

Finally, there is another type of material that can be considered ideal for this type of application, since it does not require any type of regeneration, since the adsorption is only based on the difference in the concentration of the molecules, and when it decreases it will try to find its equilibrium again, releasing the trapped molecules. However, this type of material can suffer from delays in the measurements, which can be from a few minutes to hours or even days, for which it will be necessary to analyze this parameter carefully (Sehaqui et al., 2015).

The following table shows the most commonly documented materials to be used as CO<sub>2</sub> absorption coatings. In this table it is possible to find the above-mentioned analysis factors that have been rated based on the information from the reported tests.

As can be seen in the table below, one of the most reported materials is Polyethyleneimine (PEI), which is very promising due to its properties and simplicity to make the deposit, on the other hand, carbon-based materials also show excellent qualities, so it should be considered as a possibility.

Table 1.6 Most common adsorbent coating for gas sensors

| <b>Material</b>  | <b>Selectivity</b> | <b>Humidity Affect</b> | <b>CO<sub>2</sub> sensibility</b> | <b>Recovery</b> |
|--|--------------------|------------------------|-----------------------------------|-----------------|
| Polyethyleneoxide (PEO)  | N.R                | High                   | High                              | N.R             |
| Tetrahydroxyethylenediamine THEED                                    | Good               | Medium                 | High                              | High            |
| Polyethylenevinylacetate (PEVA)                                      | Very bad           | High                   | N.R                               | N.R             |
| Polyethyleneimine (PEI) and reduced graphene oxide (RGO)             | Good               | High                   | High                              | Good            |
| Monoethanolamine (MEA)   | Good               | High                   | High                              | Good            |
| Polyvinylalcohol (PVA)   | N.R                | High                   | Medium                            | N.R             |
| Activated Carbon   | Bad                | High                   | High                              | Medium          |
| Amino-functionalized silicate  | Medium             | High                   | High                              | Good            |
| Polystyrene  | Medium             | Medium                 | Medium                            | Medium          |
| Polyallylamine   | N.R                | High                   | High                              | Medium          |
| Multiwall carbon nanotube (MWNT) silicon dioxide (SiO <sub>2</sub> ) | Medium             | High                   | High                              | High            |
| Polyethyleneimine (PEI)  | High               | High                   | Medium                            | High            |
| PEI/Starch thin film   | High               | High                   | High                              | High            |

## 1.5 Conclusion

As we have been able to conclude throughout this analysis, MEMS resonators have been positioned as an option with great advantages for the measurement of gas concentration, however, they have not managed to position themselves in the market due to the challenges that need to be solved, both to improve material selectivity, reduce recovery time and improve stability in moisture and temperature variations.

It is advisable to continue with the manufacturing standard of the materials to be used for practical purposes, this being the polysilicon. The advantages of replacing this with any other option can be analyzed later on, but it will be necessary to perform a cost-benefit analysis of this replacement, both in the efficiency of the sensor, as well as in the economic investment, in time of development and applicable market, to be able to conclude if this type of update is profitable.

As for the geometry of the resonator, it has been demonstrated that suspended structures have great advantages, both in sensitivity and stability and relatively simple manufacture, so it is necessary to perform the modeling to define the parameters of the resonator based on the requirements of the sensor.

The excitation source has been analyzed and it was determined that, for this type of application, the greatest stability and reliability is sought, but with the lowest energy consumption, therefore, the piezoelectric and electrostatic systems are the best option; among the electrostatic systems that present higher qualities than the piezoelectric ones, mainly for the manufacturing process.

In the same way, the measurement of the feedback signal to the resonator control can be done by means of the same electrostatic actuator, or the same piezoelectric actuator, however, as analyzed, displacement sensitive resistors can be used, but would require the application of at least one Wheatstone bridge; so again, the best option is to use the same actuator as a sensor for the supply signal.

Finally, for the selection of the material to be adsorbed that will cause the increase in mass and therefore the delay in the natural frequency of the resonator, it is necessary to carry out a more in-depth analysis of the results provided by each of the materials and to conclude the most suitable to be used in the measurement of the CO<sub>2</sub> concentration following the MEMS resonator process.



## CHAPTER 2

### COMPARISON BETWEEN LINEAR AND BRANCHED POLYETHYLENIMINE AND REDUCED GRAPHENE OXIDE COATINGS AS A CAPTURE LAYER FOR MICRO RESONANT CO<sub>2</sub> GAS CONCENTRATION SENSORS

Alberto Prud'homme<sup>a</sup> and Frederic Nabki<sup>a</sup>

<sup>a</sup> Department of Electrical Engineering, École de Technologie Supérieure  
1100 Notre-Dame West, Montréal, Quebec, Canada H3C 1K3

Paper published in *MDPI Sensors special issue "Nanomechanical Sensors"*, March 2020

#### **Abstract:**

The comparison between potential coatings for the measurement of CO<sub>2</sub> concentration through the frequency shift in micro-resonators is presented. The polymers evaluated are Linear Polyethylenimine, Branched Polyethylenimine and reduced Graphene oxide (rGO) by microwave reduction with Polyethylenimine. The characterization of the coatings was made by using 6 MHz gold-plated quartz crystals, and a proof-of-concept sensor is shown with a diaphragm electrostatic MEMS resonator. The methods of producing the solutions of the polymers deposited onto the quartz crystals are presented. A CO<sub>2</sub> concentration range from 0.05% to 1% was dissolved in air and humidity level were controlled and evaluated. Linear Polyethylenimine showed superior performance with a reaction time obtained for stabilization after the concentration increase of 345 s, while the time for recovery was of 126 s, with a maximum frequency deviation of 33.6 Hz for an in-air CO<sub>2</sub> concentration of 0.1%.

**Keywords:** Polyethylenimine; Micro-resonator; CO<sub>2</sub> Sensor; Gas Sensor; Humidity Sensor; Reduced Graphene Oxide; Coatings; Mass Sensor.

## 2.1 Introduction

The measurement and capture of greenhouse gases such as CO<sub>2</sub> have been a subject of research in recent decades due to their significant impact on the environment and to quality of life concerns. In combustion vehicles, industrial processes, biochemical processes etc, the measurement of CO<sub>2</sub> concentration has become a critical factor in increasing process efficiency and reduce the environmental impact (Espinal, Poster, Wong-Ng, Allen, & Green, 2013; Mahyuddin & Awbi, 2012). Moreover, CO<sub>2</sub> concentrations in human-occupied environments is an important metric that can significantly impact air quality.

The constant need to monitor the concentration of gases such as CO<sub>2</sub> in open spaces or areas of common use among people, has encouraged the development of economical, reduced and low energy consumption measurement sensors. This has led to the market for gas sensors having a market valued in more that USD 2 billion since 2018 with a Compound Annual Growth Rate Calculator (CAGR) of 7.8% to reach in 2025. The sensors with the greatest expansion potential are Oxygen (O), Carbon Dioxide (CO<sub>2</sub>), and Nitrogen Oxide (NOX)("Gas Sensor Market Size, Share & Trends Analysis Report By Product (CO<sub>2</sub>, NO<sub>x</sub>, CO, O<sub>2</sub> Sensors), By Technology (Semiconductor, Infrared), By End Use (Building Automation & Domestic Appliance, Industrial), And Segment Forecasts, 2019 - 2025," 2019).

It is currently possible to perform CO<sub>2</sub> measurement with great precision and in a matter of seconds by means of commercial sensors with various measurement principles, which can be optical, resistive or capacitive, amongst others (Fernández-Ramos et al., 2020; Ghosh, Zhang, Shi, & Zhang, 2019; Hsu, Fang, Hsiao, & Chan, 2020; Y. Lin & Fan, 2020; Serban et al., 2009; R. Wang, Zhang, Guan, Chen, & Zhang, 2019). These sensors have the disadvantage of being bulky and relatively expensive. Consequently, alternative CO<sub>2</sub> sensing solutions have been investigated in recent years (Fang, Chetwynd, Covington, Toh, & Gardner, 2002; Mo et al., 2001; Nazemi et al., 2019).

The research on sensor miniaturization through microfabrication has shown that it is possible to obtain integrated measurement systems much smaller than commercial sensors today. In the case of CO<sub>2</sub> sensors, the optical sensors with the most used due to their reduced time to perform the measurement, accuracy and durability, however, these sensors can occupy areas of up to 10cm<sup>2</sup>, while a MEMS sensor of CO<sub>2</sub> with similar capacities can occupy less than 10% of the area with a minimum costs (Aving, 2013).

Microelectromechanical systems (MEMS) resonators (or micro-resonators) used as mass sensors for measuring gas concentration have evolved significantly in recent years as a result of their sensitivity, low manufacturing cost and reduced footprint. This positions micro-resonator-based CO<sub>2</sub> sensors as a potentially improved sensing technology (Fu & Xu, 2018; Hajjaj, Jaber, Alcheikh, & Younis, 2019). However, such sensors have sensitivity to external factors such as temperature, humidity and pressure, which has limited the range of applications thus far (Jaber, Ilyas, Shekhah, Eddaoudi, & Younis, 2018; Nguyen, Ngo, Le, & Li, 2019).

To use micro-resonators as CO<sub>2</sub> concentration sensors, it is necessary to add a surface coating, which has the function of capturing the gas molecules. This increases the mass of the micro-resonator, which in turn causes a reduction in the resonance frequency that can be monitored. This shift is proportional to the partition coefficient of the coating and the CO<sub>2</sub> molecules (Fanget et al., 2011; Penza, Aversa, Cassano, Wlodarski, & Kalantar-Zadeh, 2007).

The performance of the gas sensors depends on their selectivity, reaction and recovery times, and durability. These characteristics depend specifically on the capture coating, the gas selectivity being the most critical and complex of the parameters (Smulko Janusz, 2015).

When addressing the capture of CO<sub>2</sub>, a material capable of capturing the greatest number of molecules is favored. These molecules are then trapped within the coating to prevent them from being released into the environment. One aims to find a coating that captures the CO<sub>2</sub> molecules proportionally to the concentration in the environment, and that subsequently releases them when decreasing the environmental concentration. This based on the coating's

coefficient of partition (L.-B. Sun, Kang, Shi, Jiang, & Liu, 2015). In this fashion, it is possible to increase and decrease the mass added to the resonator in a manner proportional to the environmental CO<sub>2</sub> concentration, which shifts the resonance frequency within the operating range of the sensor (Bouchaala, Nayfeh, & Younis, 2017). Ideally, a linear frequency shift in response to the concentration variation is desirable.

Multiple materials have been analyzed to be used for such coatings. Amongst these materials are the adsorbent coatings based on amines, which have been extensively studied, and which exhibit advantages such as their linearity in the adsorption of CO<sub>2</sub>, their regeneration under ambient temperatures and pressures, their high selectivity and their low sensitivity to humidity (F. Liu, Fu, & Chen, 2019; Ünveren, Monkul, Sarıođlan, Karademir, & Alper, 2017).

An example of this type of polymer is Polyethylenimine (PEI). Lineal and Branched PEI are polymers that have demonstrated a CO<sub>2</sub> adsorption capacity of between 2 to 5 mmol/g. Their ability to adsorb and recover at atmospheric temperature and pressure has been demonstrated under laboratory conditions (Irani, Jacobson, Gasem, & Fan, 2018; F. Liu et al., 2019; Sehaqui et al., 2015). The selectivity of PEI as adsorbent of CO<sub>2</sub> molecules has been extensively investigated, showing that their reaction with gases such as nitrogen is considered negligible, being an important advantage considering that air consists of more than 70% nitrogen (Ben Hamouda & Roudesli, 2008; B. Sun, Xie, Jiang, & Li, 2011; Xian, Wu, Wu, Wang, & Xiao, 2015). The main research works on PEI as a CO<sub>2</sub> adsorbent seek to characterize its maximum adsorption and recovery properties.

Reduced Graphene Oxide (rGO) has also been studied as a CO<sub>2</sub> adsorbent, because of its large capture area allowing to store up to 8.10 mmol/g of CO<sub>2</sub> at 273K at low pressure (Bhanja, Das, Patra, & Bhaumik, 2016). Due to their properties, CO<sub>2</sub> molecules tend to get trapped in the rGO and can be released through pressure reduction, temperature increase or chemical processes. The combination of rGO with polymers such as PEI can increase the volume of adsorbed gas and allow its release by reducing the concentration of CO<sub>2</sub> in the environment.

Such combinations could increase the efficiency of sensors based on the adsorption and recovery of gas molecules in relation to the partition coefficient.

Accordingly, this work aims to compare the performance of both branched and linear PEI sensing materials targeted for use in CO<sub>2</sub> concentration sensors by micro-resonators operated in air. Additionally, the performance of PEI is evaluated in combination with rGO, obtained by microwave reduction of graphene oxide (Kim, Xin, Cho, Pang, & Chae, 2015).

The paper is structured as follows: the preparation of the coatings as well as the deposition techniques on the quartz crystals are detailed in Section 2. Subsequently, the methodology and instrumentation used to carry out the characterization processes are defined in Section 2.1. This is followed by Section 2.2 in which the manufacturing process of the micro-resonator device and its operating parameters are presented. Section 3 presents the results of the characterization of the quartz crystals and the micro-resonator device, including the adsorption and recovery time and frequency shift at different levels of CO<sub>2</sub> concentration, as well as the frequency shift in the presence of different levels of humidity. Section 4 discusses the results and compares them with other reported works. Finally, conclusions are presented.

## **2.2 Materials and Methods**

The characterization of the CO<sub>2</sub> adsorbing coatings aims to compare their adsorption capabilities, but also evaluate their suitability of being used as the surface coating that will be deposited onto the micro-resonators in order to implement resonant CO<sub>2</sub> sensors.

The CO<sub>2</sub> concentration range analyzed was 0.05% to 1% dissolved in air, at a steady temperature that remained between 23 and 25 °C. Additionally, the coatings were characterized under different humidity levels ranging from 15 to 75 %RH with a constant CO<sub>2</sub> concentration of 500 ppm.

For the initial characterization, quartz thickness monitor crystals of 6 MHz and 14 mm in diameter were used due to their high Q-factor of more than 15,000 at atmospheric pressure (Kato et al., 2017) and their stability to temperature variations. Branched and linear PEI coatings were analysed, and the one that yielded the best results was used to integrate with rGO to characterize its impact on adsorption performance.

Once the best performing coating was identified, a transducer proof-of-concept was implemented. This was done by using an electrostatic micro-resonator coated with the adsorbing material. The coated micro-resonator was exposed to varying CO<sub>2</sub> concentrations and the resulting resonant frequency shifts of the structure were monitored.

### 2.2.1 Coating Preparation

Branched PEI and Linear PEI are shown in Figure 2.1. The Branched PEI has an average Mw of ~25,000 by LS, an average Mn of ~10,000, and it was acquired through Sigma-Aldrich. The Linear PEI has an average Mn of ~10,000, PDI ≤1.3, and was also acquired through Sigma-Aldrich.

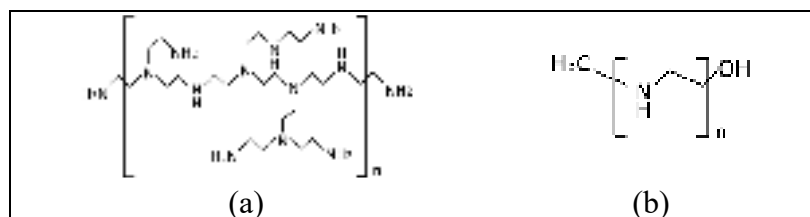


Figure 2.1 (a) Branched Polyethylenimine Molecule, and (b) Lineal Polyethylenimine Molecule

Due to the high viscosity of the branched PEI and the granulated state of the Linear PEI, a specific preparation process was necessary to obtain solutions suited to the deposition of a thin film on the quartz crystals. Similar processes used for the preparation of the solutions have been previously published in other works (B. Sun et al., 2011; Vieira & Pastore, 2014). The solution of branched PEI was prepared in these steps:

1. Dissolution of 10 ml of Branched PEI in 10 ml of distilled water at 40°C.
2. Sonification of the mixture for 2 hr at 40 °C.
3. Maintain the solution in a water bath at > 40°C (before deposition onto the quart crystal).

The crystal used for the characterization was a gold-plated quartz of 14 mm diameter and a center frequency of 5.950 MHz from Inficon. The deposition onto the crystal was done using a spin coater as shown in Figure 2a using the following sequence:

1. 500 rpm for 5 seconds while a drop of branched PEI solution is deposited.
2. 2500 rpm for 15 seconds to remove the solution in excess.
3. 5000 rpm for 30 seconds.

The deposited crystal with the branched PEI was maintained for 24 hours in controlled ambient conditions and a maximum of 500 ppm of CO<sub>2</sub>.

In the case of the Lineal PEI, the dissolution requires a minimum temperature of 50°C, so the solution was prepared at 55°C, and during the entirety of the process, the temperature was maintained at that level. The procedure is listed below:

1. Dissolution of 0.25 gr of Lineal PEI in 10 ml of water at 55°C.
2. Sonification of the mixture for 1 hr at 55°C, verifying the level of water periodically.
3. Leave the solution at room temperature (25°C +/- 1°C) for 24 hrs, at this temperature the solution will turn into a white hard paste.

The deposition was done using the same spin coater, but the crystal should be at a temperature of at least 40°C in order to reduce the solidification of the solution when in contact with the crystal. This ensures that the deposited layer is regular and suited to the application. Accordingly, the deposition of the linear PEI was done following these steps:

1. Heat the crystal with a Peltier cell with the hot side in contact with the crystal to increase the temperature to  $\sim 50^{\circ}\text{C}$ , and then remove the Peltier cell and turn on the spin coater as rapidly as possible.
2. 1800 rpm for 10 seconds while a drop of Linear PEI solution at  $55^{\circ}\text{C}$  is deposited.
3. 2500 rpm for 45 seconds.
4. The deposited crystal with the linear PEI was maintained for 24 hours in controlled ambient conditions at a maximum of 500 ppm of  $\text{CO}_2$ .

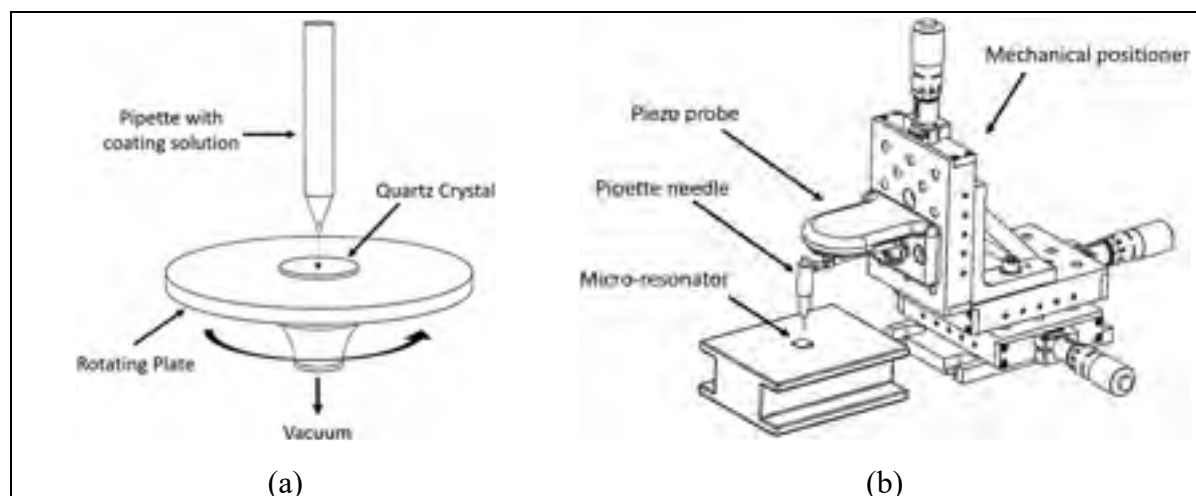


Figure 2.2 Coating deposition technique, (a) Spin coater for the Quartz Crystal used for initial coating tests, (b) Micro-drop deposition by piezo probe used for the micro-resonator

Once the crystals with both coatings were characterized, the coating with the best performance was selected considering the characteristics mentioned above. Subsequently, a third coating was produced using rGO, which was obtained by microwave reduction. This sought to increase the available area of adsorption and achieve a greater capture of  $\text{CO}_2$  molecules, resulting in increased sensitivity (Basu & Bhattacharyya, 2012; Yoon et al., 2011). As will be detailed in section 3, characterization data indicates that the Linear PEI performs better than the Branched PEI for  $\text{CO}_2$  sensing.

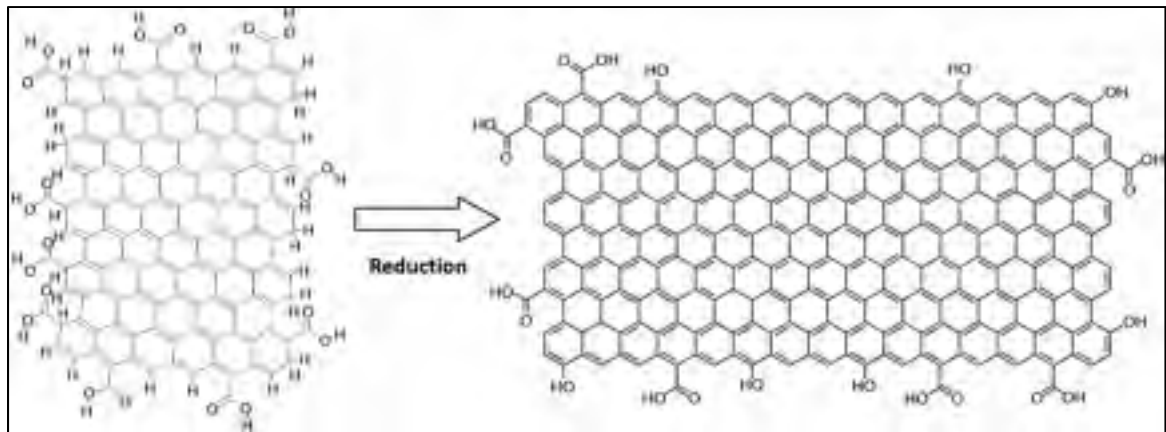


Figure 2.3 Reduced Graphene Oxide by Microwave reduction

Figure 2.3 shows the transformation of the graphene oxide (GO) treated by microwave radiation generating a considerable amount of heat followed by the reduction and then exfoliation of the GO generating the rGO.

The third coating that includes Linear PEI and rGO was produced using methods that influenced this work (W. Chen, Yan, & Bangal, 2010; Pei & Cheng, 2012). The process is described below:

1. Sonification of 0.5ml of Linear PEI solution with 20 ml of distilled water for 10 min at 50°C verifying the level of water periodically.
2. Sonification of 0.5 g of graphene oxide within the solution for 1 hr at 50°C verifying the level of water periodically.
3. Filter the solution with graphene.
4. 3 microwave reduction cycles of 7 seconds each at a 600 W power with 20 seconds between each cycle.
5. Sonification of the reduced graphene oxide with the original Linear PEI solution in a volumetric proportion of 1:1 for 3 hrs at 55°C verifying the level of water periodically.
6. Leave the solution at room temperature (25°C +/- 1°C) for 24 hrs, at this temperature the solution will turn a dark gray paste.

For the deposition of this solution, the same process used for the deposition of the Linear PEI coating was followed, however, it was important to verify that there were no agglutinated residues of rGO on the surface of the quartz.

Figure 2.4 shows the SEM micrographs of the quartz crystal's surface for the three coatings investigated. The uniformity between PEI coatings deposited are similar, which is a critical factor to be able to make an equitable comparison and to maintain the high Q factor of the crystals. In the case of the coating of rGO + PEI, the deposition of the rGO is evident and the uniformity it is equivalent to the other coatings.

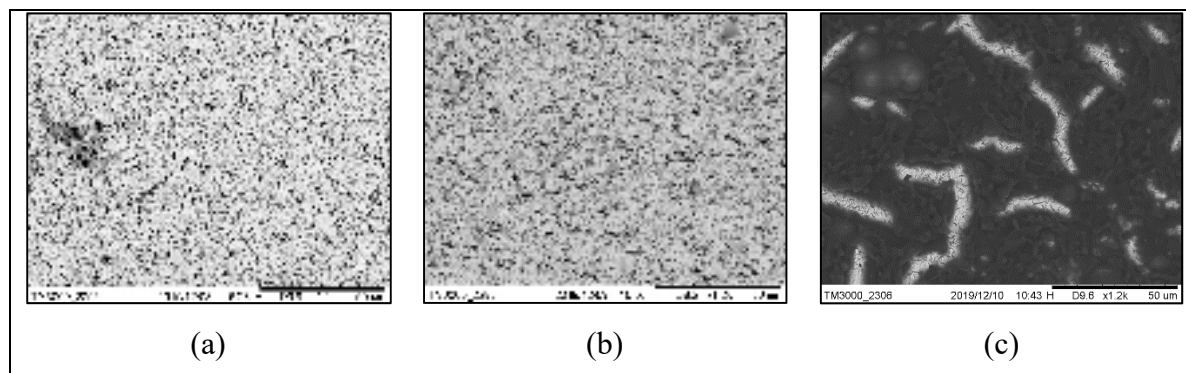


Figure 2.4 SEM image of the quartz crystal coated with the (a) Branched PEI layer, (b) Linear PEI layer and (c) rGO with Linear PEI layer

In Figure 2.5 the IR Absorption spectroscopy of the coating materials was carried-out in order to verify the integrity of the materials. For the coating formed by rGO + PEI, the presence of the Linear PEI with the influence of the rGO is observed. The coatings of Linear and Branched PEI exhibited a typical response for these kind of polymers (R. Zhao et al., 2017). Notably, the characteristic peaks of the PEI can be seen at  $2799\text{ cm}^{-1}$  caused by mode  $\text{CH}_2\text{-SS}$ , at  $3279\text{ cm}^{-1}$  caused by mode  $\text{NH}$ , at  $1644\text{ cm}^{-1}$  and  $1599\text{ cm}^{-1}$  caused by  $\text{C}=\text{N}$  and  $\text{N}-\text{H}$  (Lott, King, Hill, & Scatena, 2014; X. Wang et al., 2009; R. Zhao et al., 2017). For the reduced graphene oxide, peaks are observed at  $1730\text{ cm}^{-1}$  caused by  $\text{C}=\text{O}$ , at  $1414\text{ cm}^{-1}$  caused by the carboxy  $\text{C}-\text{O}$  and at  $1622\text{ cm}^{-1}$  caused by aromatic  $\text{CC}$  (W. Chen et al., 2010).

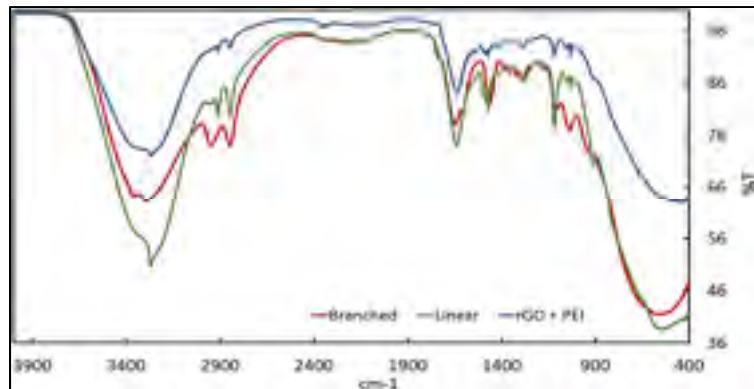


Figure 2.5 IR absorption spectroscopy result for the three deposited coatings on the quartz crystals

## 2.2.2 Test Setup

For the control of the pressure, temperature, humidity and CO<sub>2</sub> concentration conditions, an environmental test chamber was used, as shown in Figure 2.6. The S-parameter S<sub>21</sub> measurements performed for the characterization of the crystals with the coatings were done using a Vector Network Analyzer (VNA) Keysight-E5061B. This was done to determine their resonant behavior in the presence of CO<sub>2</sub> and humidity. In the case of the electrostatic micro-resonator, because the low Q-factor and the electrostatic actuation, a VNA could not be used. As such, the measurements were made using a Polytec OFV-534 vibrometer in closed loop with an OFV-2570 controller.

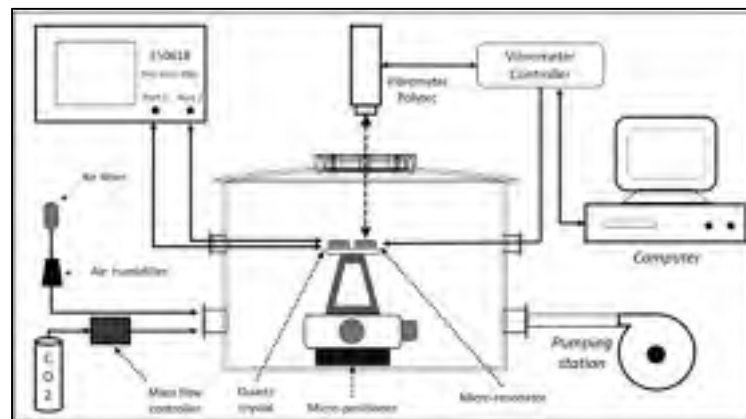


Figure 2.6 Diagram of the characterization setup

The CO<sub>2</sub> introduction and concentration level control were made with a constant low flow of air to maintain the atmospheric pressure and obtain a smooth increasing and decreasing CO<sub>2</sub> concentration in the chamber through the pumping station. The air introduced to the chamber comes from the laboratory where the temperature and humidity are automatically controlled, in a range of +/- 1 %RH and +/- 0.5 °C. Even so, during the tests the humidity, temperature and CO<sub>2</sub> levels in the laboratory were constantly supervised to avoid unexpected changes that could affect the tests. Due to the susceptibility of the coatings to these parameters, any variation would be detected immediately so the test would be eliminated and repeated. The full setup was designed to be able to develop a complete characterization in almost a fully automated process. The VNA and Vibrometer were integrated with a MATLAB platform that registered and controlled the process, while the micro-positioner was used for the alignment of the MEMS resonator with the vibrometer laser.

The characterization equipment is shown in Figure 2.7a. The fully integrated setup allows the characterization of various types of sensors. In Figure 2.7b, a close-up of the vibrometer with the micro-resonator seed through the viewport of the chamber is shown. This allows to characterize the low Q-factor micro-resonators at different pressures, temperatures and humidity, while electrostatically actuating them.

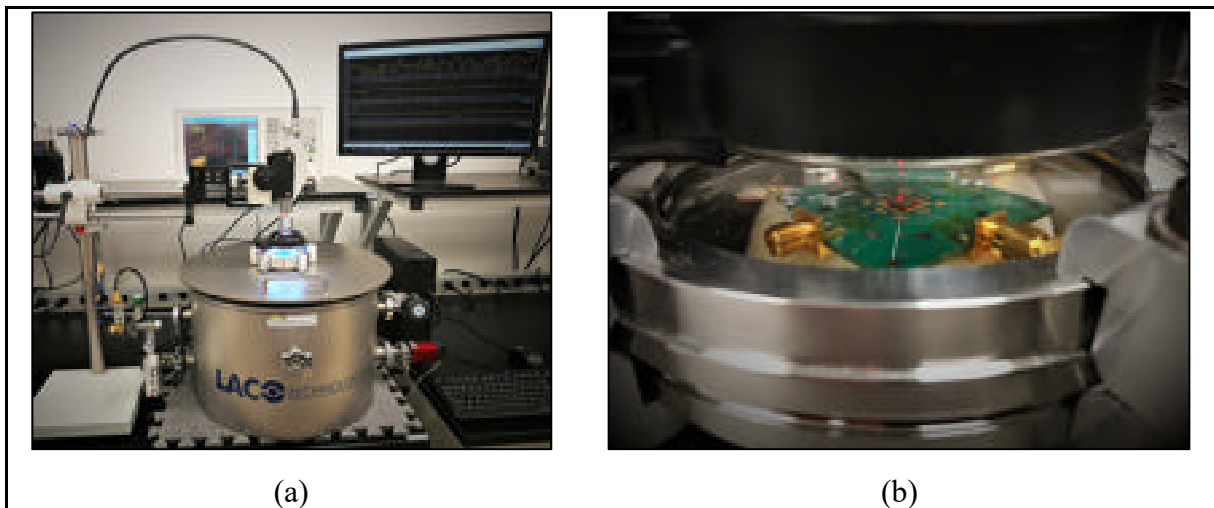


Figure 2.7 (a) Setup for the quartz crystals and the resonator characterization, (b) Close-up of the micro-resonator during the characterization with the laser from the vibrometer visible

### 2.2.3 Micro-resonator Characteristics

The micro-resonator that was used was a diaphragm structure to increase its mechanical stability and provide enough deposition area for the coating, although the Q-factor was reduced as a result of this geometry. The resonator device, with cross-section shown in Figure 2.8, was manufactured using the MEMSCAP PolyMUMPS commercial fabrication process. A polysilicon layer (Poly2) was used as the structural layer of the diaphragm and it was anchored at its sides. An underlying polysilicon layer (Poly1) allowed for the electrostatic driving of the resonator. An oxide layer (Oxide2) between both polysilicon layers was used as a sacrificial layer which was chemically removed to release the structure. The achieved gap between the diaphragm and the underlying driving electrode was of  $0.75\ \mu\text{m}$ . Such a small gap allowed for a reduced driving voltage requirement. The  $\text{CO}_2$  absorbing coating was deposited above the diaphragm post-fabrication by processing the dies received from the foundry. This was done using a micro-needle that was carrying at its tip a small drop of the coating Figure 2.2b. With micro-positioners the needle was placed at the center of the micro-resonator, slowly descending until the polymer touched the surface of the resonator. After removing the needle, the deposited size of the coating drop is estimated to be of around  $40\ \mu\text{m}$  in diameter.

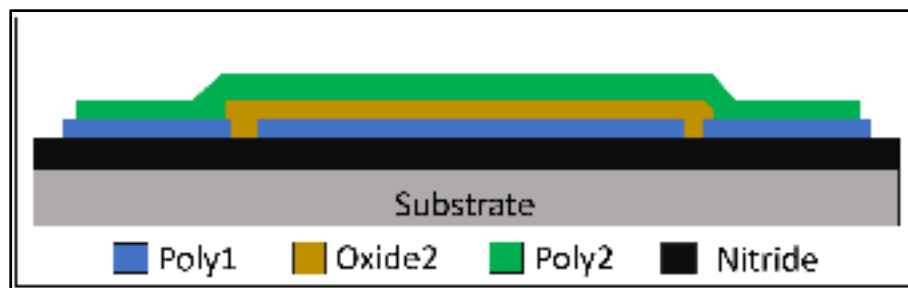


Figure 2.8 Cross-section of the micro-resonator with oxide as sacrificial layer

Figure 2.9 shows the 3D view of the imaged micro-resonator and its mode-shape simulation carried out using COMSOL. The resonator is a diaphragm with external opening to reduce the damping caused by the air flow between the plates and the increase of the amplitude of resonance. The diameter of the resonator is  $200\ \mu\text{m}$  and it is  $1.5\ \mu\text{m}$  thick.

The Eigenfrequency finite element method (FEM) mode shape simulation of the resonator estimated a resonance frequency of the first mode at 1.16 MHz. The measured resonant frequency of the fabricated resonator obtained by using the vibrometer was of 1.15 MHz, matching well with the simulations. The measured Q-factor was of 8 at atmospheric pressure and of 300 at a 1 mTorr ambient pressure. Once the micro-resonator was characterized, the Linear PEI coating was deposited following the process previously mentioned. The measured resonant frequency of the micro-resonator with the coating was of 1.139 MHz. The decrease of resonant frequency is due to the mass loading of the coating on the resonant structure.



Figure 2.9 (a) 3D view of the real micro-resonator obtained by the Olympus LEXT OLS4000 Confocal microscope, (b) Eigenfrequency FEM COMSOL simulation

### 2.3 Results

The characterization of the coatings deposited in the quartz crystals focused on three main factors, the maximum frequency shift before stabilizing in the presence of a higher concentration of CO<sub>2</sub> in a range of 0.05 to 1%, the stabilization time and the recovery time needed to return to the starting point. If during the recovery the resonant frequency did not reach the initial value, the maximum time was considered to be that required to stabilize the recovery response. In that case, the final frequency value achieved was considered as hysteresis. The impact of air humidity in a range of 15 to 75 %RH at a CO<sub>2</sub> concentration of 500 ppm was also analyzed.

The measurements were made at three different CO<sub>2</sub> concentrations of 0.1%, 0.5% and 1% to analyze the linearity of the frequency deviation. Comparisons were made between the different coatings at the same concentrations in order to compare the maximum deviation frequency, adsorption time and recovery time.

During this test the CO<sub>2</sub> was introduced until the desired concentration was reached in the chamber, during this process the coatings began to adsorb the CO<sub>2</sub> molecules, and this was reflected in the deviation of the oscillation frequency of the quartz crystal. Throughout the test, the pumping equipment maintained a constant flow of air output, so that the CO<sub>2</sub> had to be continuously introduced to maintain the concentration. This allowed the CO<sub>2</sub> concentration to be decreased naturally by closing the CO<sub>2</sub> valve without any alteration in the pressure or abrupt changes in the atmosphere inside the chamber.

### **2.3.1 Linear and Branched Polyethylenimine Coatings Characterization**

The first characterization was made with the coatings formed by Linear and Branched PEI, to define which one exhibited better performance, and to later use it to make the solution with the rGO.

Once the frequency deviation stabilized, the introduction of gas was stopped in order to decrease the concentration of CO<sub>2</sub> inside the chamber to the external value of 500 ppm. Once the quartz crystal returned to its initial frequency, the CO<sub>2</sub> was introduced again to the next concentration value.

The test results are shown below. Within each graph, the CO<sub>2</sub> concentration level inside the test chamber is indicated in colored lines, the 0.1% in red, 0.5% in blue and 1.0% in green. The frequency deviation of the crystal is shown with the black line. As can be seen, the CO<sub>2</sub> concentration level in the chamber is increased rapidly until reaching the level determined for the test. Once the adsorption phase by the coating is finished, the CO<sub>2</sub> level is rapidly decreased to analyze the recovery time of the coating that is in characterization. Each coating is analyzed

individually to facilitate the interpretation of the information provided by each test, then a comparison of the three coatings is made in detail.

In Figure 2.10, the reaction of both coatings complies with the adsorption theory and a deviation of the frequency is seen in response to the introduction of CO<sub>2</sub>. However, the frequency shift amount and recovery time is different for each material. In all cases, the frequency shift obtained using the Linear PEI coated crystal generated between 15% and 30% greater deviation than the Branched PEI coating. An identical time scale has been used in both plots to compare the adsorption time between the coatings. The recovery time was between 2 to 3 times faster for the crystal coated by Linear PEI.

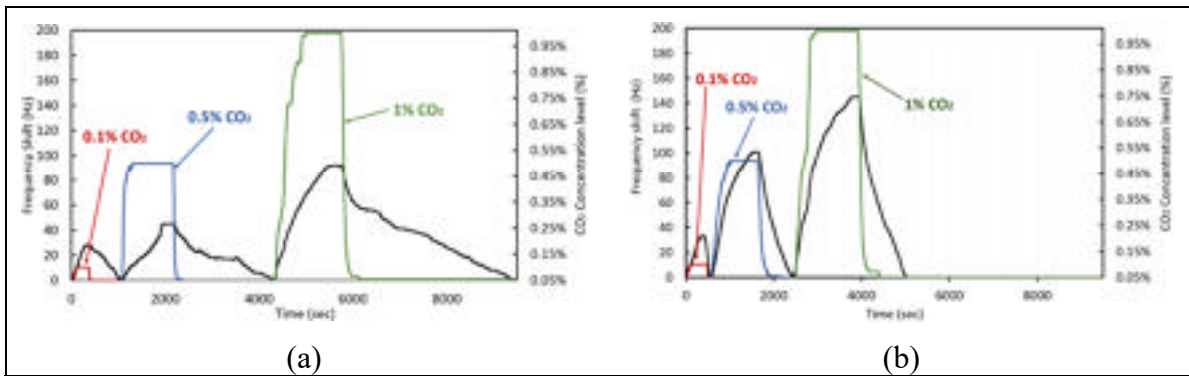


Figure 2.10 Quartz crystal frequency shift in response to different CO<sub>2</sub> concentration cycles for (a) Branched PEI coated crystal, and (b) Linear PEI coated crystal

In Figure 2.11, the frequency shift in response to humidity changes is plotted for both the Branched and Linear PEI coated crystals. The CO<sub>2</sub> concentration in these cases is constant at 500 ppm. In both cases, the frequency deviation can be considered as linear in the range shown, however, the deviation is much greater in the case of the Branched PEI coated crystal, showing more than a 60% increased shift compared to the Linear PEI coated crystal. The measurement was carried-out for both increasing (adsorption) and decreasing (recovery) humidity levels and both coatings exhibited hysteresis.

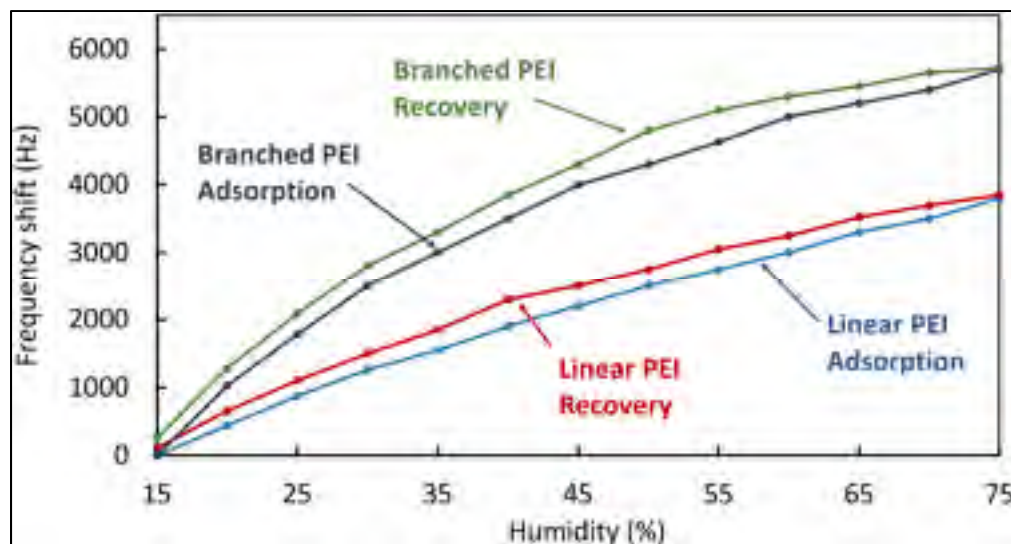


Figure 2.11 Branched PEI and Linear PEI coated crystals

The results above indicate that the Linear PEI coating has better performance in comparison to the Branched PEI. This is the case in terms of the frequency shift amount (sensitivity), reaction time and susceptibility to ambient humidity. Therefore, the Linear PEI solution was chosen to be integrated with the reduced graphene oxide as the third coating for investigation.

### 2.3.2 Linear Polyethylenimine with reduced Graphene Oxide Coating Characterization

Through the methodology discussed in section 2, the Linear PEI with rGO was deposited onto a quartz crystal to characterize its performance. Figure 2.12 shows the characterization results of the coated crystal. As expected, the coating formed by Linear PEI and rGO showed the same adsorption tendency, however, during the recovery process, the coating does not allow the adsorbed molecules to be released readily. Indeed, the desorption was limited to about 15 % when dropping the CO<sub>2</sub> concentration, and very little recovery was observed at the higher 1% CO<sub>2</sub> concentration.

This phenomenon occurs due to the combination of the rGO with the polymer-based amines, which has shown excellent properties of capturing CO<sub>2</sub>. Accordingly, external processes are required for recovery, either by increasing temperature and/or decreasing the atmospheric

pressure in order to force degassing (Song et al., 2017; Y. Zhao, Ding, & Zhong, 2012). Accordingly, forced degassing was carried-out here in order to reset the coating between CO<sub>2</sub> concentration cycles. It was necessary to place the coated quartz crystal at a 10 mTorr vacuum for 30 minutes and subsequently for 2 hours in ambient conditions at no more than 500 ppm CO<sub>2</sub> concentration in order to reset the coating. The linear PEI with rOG coated crystal exhibits a frequency deviation in response to humidity variations that is similar to that of the quartz crystal coated with branched PEI.

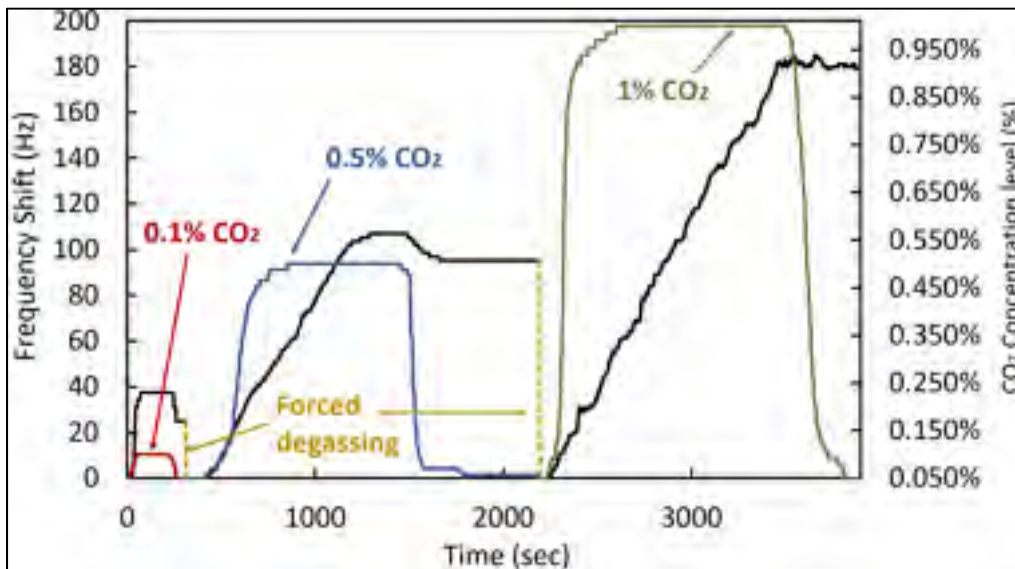


Figure 2.12 Frequency shift of the quartz crystal with LPEI+rGO

Note that the CO<sub>2</sub> capture behavior of the PEI with rOG may be suitable for sensors that aim to detect whether a CO<sub>2</sub> concentration occurs in an environment over time and retain this information. Such a sensor may be read periodically in order to determine if a high enough CO<sub>2</sub> concentration was reached or not at some point in time. Because this type of application is not part of objective of this work, no quantitative study retention time or loss level tests were carried out for prolonged periods and these should be further investigated to confirm the applicability of PEI with rOG in such applications. However, by considering others published works on coatings based on amines with graphene or carbon nanotubes, and where it is concluded that it is necessary to expose the coating to a vacuum and/or a high temperature

process for recovery, it is possible that the coating in this work would yield long-term CO<sub>2</sub> retention and be suitable to the aforementioned application (Cai et al., 2015; Niu, Yang, Zhang, Wang, & Tang, 2016).

### 2.3.3 Performance Comparison between the Coatings

The performance comparison of all coated quartz crystals under the same CO<sub>2</sub> concentration was carried out in order to analyze the total frequency deviation and reaction times of each. The results at different concentrations are shown in Figure 2.13.

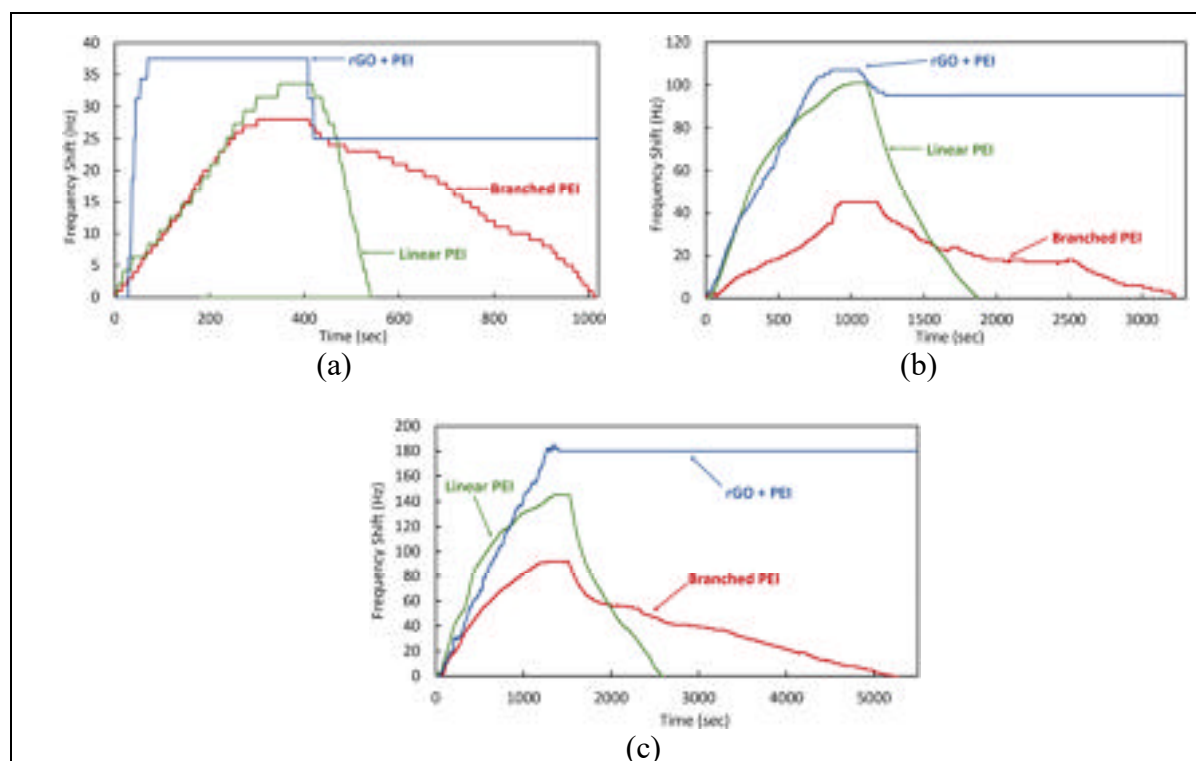


Figure 2.13 Response of the three different coatings at CO<sub>2</sub> concentrations of (a) 0.1%, (b) 0.5%, and (c) 1%

The performance of the coatings when compared by levels of CO<sub>2</sub> concentration show the same tendency to adsorb the gas molecules, however, the frequency shift rate showed a disproportional increase between Branched PEI, Linear PEI and Linear PEI + rGO due to CO<sub>2</sub> concentration. This is outlined in Table 2.1.

Table 2.1 Frequency shift of each coating at different concentration of CO<sub>2</sub>

|                            | <b>Branched PEI</b> | <b>Linear PEI</b> | <b>LPEI + rGO</b> |
|----------------------------|---------------------|-------------------|-------------------|
| <b>0.1% CO<sub>2</sub></b> | 27                  | 33.6              | 37.5              |
| <b>0.5% CO<sub>2</sub></b> | 45                  | 101               | 107               |
| <b>1.0% CO<sub>2</sub></b> | 92                  | 145               | 185               |

The difference in the frequency deviation of each coating can be observed, which shows that Linear PEI with + rGO has the greatest adsorption capacity, an advantage of the inclusion of rGO. This frequency shift is followed by that of the Linear PEI. Table 2.2 shows the linearized value of the frequency deviation per unit of ppm of CO<sub>2</sub>, outlining the sensitivity of each coating. The PEI+rGO exhibits a 25% greater adsorption capacity than the Linear PEI coating, which is 45% more adsorbent than the Branched PEI coating.

Table 2.2 Linearized coefficient of the frequency shift by ppm of CO<sub>2</sub>

| <b>Branched PEI</b> | <b>Linear PEI</b> | <b>Linear PEI + rGO</b> |
|---------------------|-------------------|-------------------------|
| 0.011 Hz/ppm        | 0.016 Hz/ppm      | 0.020 Hz/ppm            |

The frequency shift in response to the CO<sub>2</sub> concentration is shown in Figure 2.14. The ideal response for this type of sensor would be linear for any level of CO<sub>2</sub> concentration, however, the PEI has a saturation limit of up to 2 to 3 mmol/g for the Branched and Linear PEI. Accordingly, concentrations ranging from 0 to 0.2% yield a linear response. However, at higher concentration values, the proportion of adsorption capacity is progressively reduced until it reaches its saturation point (Doan et al., 2014; H. Zhang, Goeppert, Prakash, & Olah, 2015). In the case of the rGO with Linear PEI, a higher adsorption capacity of 8.10 mmol/g of CO<sub>2</sub> at 273K and low pressure has been reported (Bhanja et al., 2016; L. Liu, Zou, Yang, Luo, & Xu, 2018). Due to this, the results obtained show a higher adsorption ratio from 0.05 to 0.15%, followed by a progressive reduction in the frequency deviation.

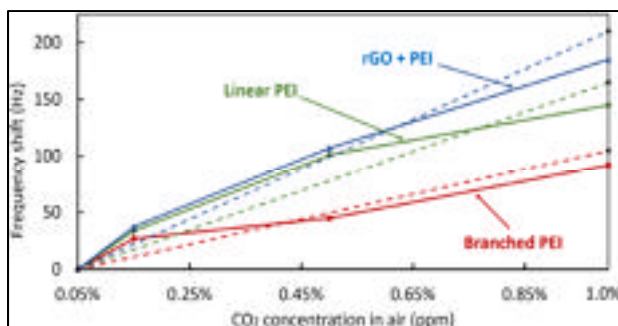


Figure 2.14 Frequency shift of each coating from 0.05% to 1% of CO<sub>2</sub>

The adsorption time for each coating was also characterized and is plotted Figure 2.15a. The adsorption was defined as the time for the frequency shift to go from 0% to 90% of its steady state value. The adsorption time of the coatings maintains a linear increase up to 0.5% of CO<sub>2</sub> concentration, subsequently the adsorption time it is reduced but still maintaining the same proportion among all the coatings evaluated. The adsorption times for each coating are summarized in Table 2.3.

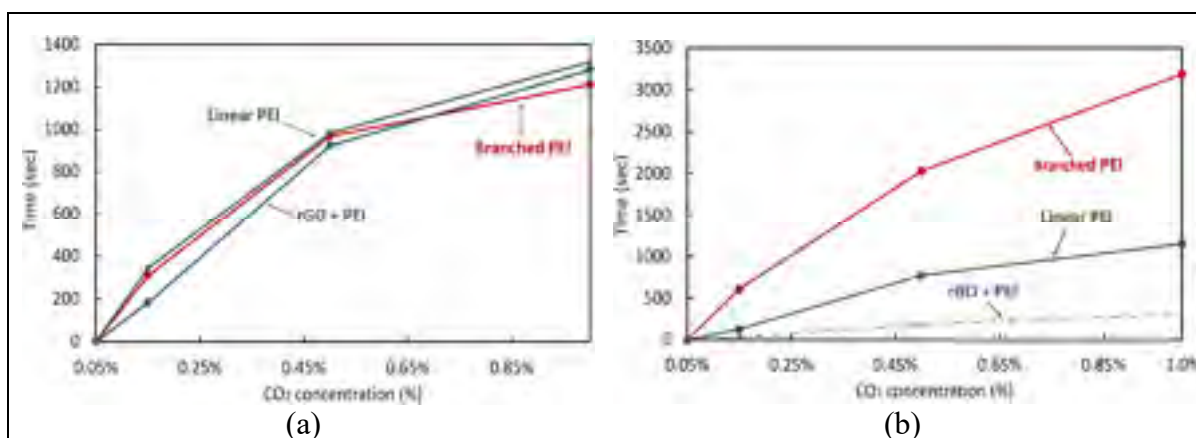


Figure 2.15 (a) Adsorption time for each coating at different CO<sub>2</sub> concentrations, (b) Recovery time for each coating at different CO<sub>2</sub> level

Table 2.3 Adsorption time for each coating

|                            | <b>Branched PEI</b> | <b>Linear PEI</b> | <b>rGO + PEI</b> |
|----------------------------|---------------------|-------------------|------------------|
| <b>0.1% CO<sub>2</sub></b> | 309 sec             | 345 sec           | 150 sec          |
| <b>0.5% CO<sub>2</sub></b> | 969 sec             | 984 sec           | 924 sec          |
| <b>1.0% CO<sub>2</sub></b> | 1210 sec            | 1317 sec          | 1281 sec         |

The Branched and Linear PEI exhibit similar adsorption times over the range of concentrations measured. In the case of the rGO + PEI, the adsorption time for low concentrations is shorter than that observed with the other coatings because of the high absorbance capacity of the rGO (Bhanja et al., 2016). For all coatings, after the CO<sub>2</sub> concentration is sufficiently increased, the slope of the adsorption time begins to decrease, this is attributed to the reduction of the adsorption capacity of the coating at higher concentrations. The recovery times of each coating was also characterized and is plotted in Figure 2.15b and summarized in Table 2.4. The recovery time for the PEI with rGO coating was not characterized in the same fashion because of the coating's capture of CO<sub>2</sub> precluding from a return of the resonant frequency to its initial condition without forced degassing. The recovery time of the coating formed by Branched PEI is more than 3 to 5 times longer than that of Linear PEI, which is an important characteristic to consider for sensing applications.

Table 2.4 Recovery time for each coating

|                            | <b>Branched PEI</b> | <b>Linear PEI</b> | <b>Linear PEI + rGO</b> |
|----------------------------|---------------------|-------------------|-------------------------|
| <b>0.1% CO<sub>2</sub></b> | 609 sec             | 126 sec           | n/a                     |
| <b>0.5% CO<sub>2</sub></b> | 2031 sec            | 771 sec           | n/a                     |
| <b>1.0% CO<sub>2</sub></b> | 3187 sec            | 1152 sec          | n/a                     |

Figure 2.16 shows the frequency shift of the quartz crystals in response to different levels of humidity. The behavior of the Branched PEI and Linear PEI is linear, while the PEI with rGO shows a reduced adsorption as the humidity level increases. Overall Linear PEI shows lower sensitivity to humidity variations.

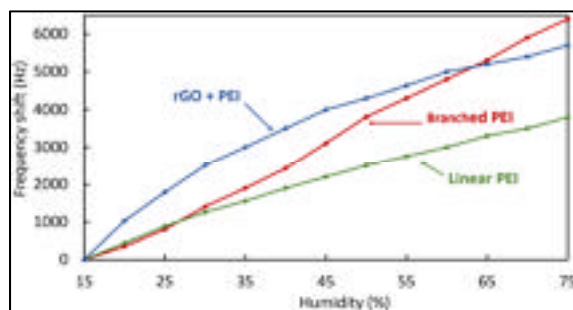


Figure 2.16 Frequency shift at different range of air humidity from 15 to 75 %RH

Once the results obtained from the tests of characterization of the coatings are analyzed, it can be concluded that the formed by Linear PEI presents qualities and superior performance for the type of application for which it has been proposed. Therefore this will be the coating to be used in the MEMS resonator to perform the proof of concept.

### 2.3.4 Micro-resonator CO<sub>2</sub> sensor Proof-of-concept

Following the above methodology, the electrostatic diaphragm micro-resonator described in section 2.3 was coated with the Linear PEI solution, which exhibited the overall better behavior for a proof-of-concept. The micro-resonator was first characterized to determine its behavior before and after a CO<sub>2</sub> concentration variation. The adsorption and recovery frequency shift response of the micro-resonator to a 0.8% CO<sub>2</sub> concentration increase is shown in Figure 2.17. The nominal resonant frequency of the micro-resonator is of 1.139 MHz.

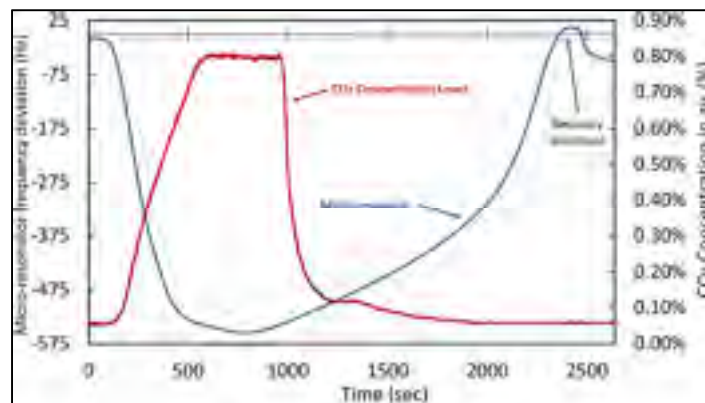


Figure 2.17 Response of the coated micro-resonator to a 0.8% CO<sub>2</sub> concentration variation

The coated micro-resonator shows a behavior that is similar to that obtained by the quartz crystal. However, the low Q-factor decreases the accuracy with which measurements can be made. Even so, a deviation shift of 0.0675 Hz/ppm was attained which compares favourably to the quartz crystal-based sensors. Another important factor to mention is the overshoot that appears in the last phase of the recovery, where the value of the frequency exceeds the original value by approximately 35 Hz before stabilising a few minutes later.

The observed overshoot is attributed to the kinetics of the gas molecules adsorption in Linear PEI because generally the CO<sub>2</sub> is adsorbed on the surface of the material and then diffuses into the bulk of the absorbent. This causes the stabilization process to not always be progressive resulting in overshoots (Al-Marri, Kuti, Khraisheh, Kumar, & Khader, 2017; Andreoli, Cullum, & Barron, 2015). Moreover, in high concentrations (>20%) and for long periods, the capacity of the adsorbent to release the molecules is reduced and hysteresis is generated.

The micro-resonator was also characterized by performing a cycling of different CO<sub>2</sub> concentrations in order to determine its stability throughout each concentration period. For this, CO<sub>2</sub> was introduced to obtain a 1% concentration for a period of 15 minutes, followed by 2.5% for an equal period of 15 minutes, and 5% for a period of 20 minutes. Subsequently the concentration was reduced to 1.5% for a period of 50 minutes and finally 0.05% for 30 minutes. Note that the initial CO<sub>2</sub> concentration before the test was of 0.05%. The resulting response is shown in the Figure 2.18.

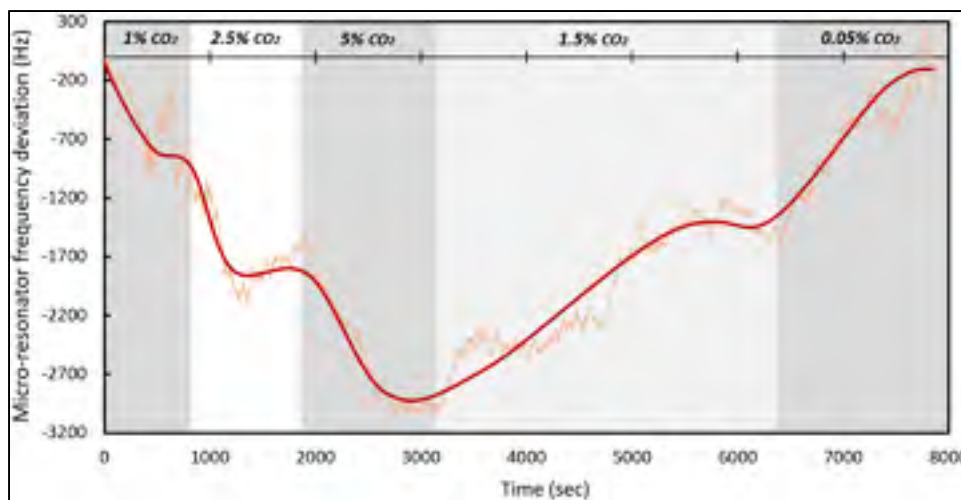


Figure 2.18 Behavior of the micro-resonator over time at different concentrations of CO<sub>2</sub>

During this test the resonator was able to maintain the upward and downward trend adequately, both in reaction time and in frequency deviation. Again, the overshoot can be seen at each stabilization point. On this occasion, the final hysteresis was approximately 55 Hz. Table 2.5 lists the frequency shift and ppm/Hz variation achieved over each phase. An absolute value

ppm/Hz average of all the cycles was also calculated to be of 0.0646 Hz/ppm. This is consistent with the 0.0675Hz/ppm value observed in the prior single concentration test reported above.

Table 2.5 Frequency shift of the micro-resonator at different CO<sub>2</sub> concentrations

| Concentration period | Frequency shift (Hz) from the last level | Hz/ppm |
|----------------------|--|--------|
| 1%                   | 750                                      | 0.075  |
| 2.5%                 | 1050                                     | 0.07   |
| 5%                   | 1200                                     | 0.048  |
| 1.5%                 | -1600                                    | -0.045 |
| 0.05%                | -1350                                    | -0.085 |
|                      | <i>Average (Hz/ppm)</i>                  | 0.0646 |

## 2.4 Discussion

The results obtained have shown the possibility of using PEI as a coating layer for CO<sub>2</sub> sensors. Linear PEI shows superior performance mainly during the recovery phase over (H. Zhang et al., 2015). Table 2.6 compares the performance of the coatings evaluated in this work to other previously published works that consider adsorbing coatings for CO<sub>2</sub> concentration sensors as well.

The performance obtained by the Linear PEI is similar than that reported using acrylonitrile–styrene copolymer (AS3), where the recovery time for the Linear PEI coating is slower by 1.85 minutes. The results obtained from the coating formed by linear PEI with rGO showed results not initially anticipated, however, it opens the opportunity to develop in depth the study of the capabilities of such a coating as a CO<sub>2</sub> gas sensor for industrial and/or environmental applications. It can also be studied as an adsorbent coating for sensors where it is desired to retain the highest concentration value recorded during a given time period. The linear PEI with rGO recovery process must be further studied, as it would be possible to add an integrated heater to the micro-resonator structure in order to reset the sensor. This could allow to benefit from the higher adsorption capabilities of that coating while mitigating its CO<sub>2</sub> capture limitation.

Table 2.6 Comparison of the studied CO<sub>2</sub> adsorbing coatings with other published works

|   | <b>Sensing Material</b>               | <b>Sensor Response (ppm)</b> | <b>Test Device</b>          | <b>Adsorption Time (min)</b> | <b>Recovery Time (min)</b> |
|---|---------------------------------------|------------------------------|-----------------------------|------------------------------|----------------------------|
| This work                                     | Linear PEI                            | -16.8                        | 6 MHz gold quartz xtal      | 16.4                         | 12.85                      |
|   | Branched PEI                          | -7.5                         | 6 MHz gold quartz xtal      | 16.15                        | 33.85                      |
|   | rGO + Linear PEI                      | -17.8                        | 6 MHz gold quartz xtal      | 15.4                         | n/a                        |
|   | Linear PEI                            | -474                         | 1.13 MHz diaphragm          | 13.5                         | 20.4                       |
| B. Sun et al. (2011)                          | PEI                                   | -3.33                        | 7 MHz AT-quartz xtal        | 11.7                         | 20.7                       |
| B. Sun et al. (2011)                          | PEI + Starch                          | -11.66                       | 7 MHz AT-quartz xtal        | 18.9                         | 21.6                       |
| Muraoka, Kiyohara, Oue, et Higashimoto (2014) | acrylonitrile–styrene copolymer (AS2) | -7.5                         | 10 MHz cut quartz xtal      | 6                            | 11                         |
| Muraoka et al. (2014)                         | acrylonitrile–styrene copolymer (AS3) | -20                          | 10 MHz AT-cut quartz xtal   | 7                            | 11                         |
| Gomes, Duarte, et Oliveira (1995)             | 1,2-diaminoethane                     | -25                          | 9 MHz AT-cut quartz crystal | N/A                          | N/A                        |
| Ong et Grimes (2001)                          | Carbon nanotubes (MWNTs)              | -1800                        | Coated plates               | 1.1                          | 1.3                        |
| Andò et al. (2015)                            | Graphene with PEDOT/PSS               | 2050                         | Coated plates               | 2                            | N/A                        |
| Boudaden, Klumpp, Endres, et Eisele (2019)    | Branched PEI with Silica              | -105e3                       | Coated plates               | 5                            | 8                          |

\*\* The PEI type was not indicated, however considering the properties and the solution preparation process it is assumed that branched PEI was used.

Interestingly, the increased sensor response of the diaphragm micro-resonator sensor proof-of-concept presented in comparison to the linear PEI coated quartz (i.e., -474 ppm vs -16.8 ppm) illustrates the advantage of miniaturizing the resonant structure of the sensor.

During the development of this work, the ambient temperature was maintained in a controlled manner at  $25 \pm 1$  °C and the ambient humidity was maintained between 20 and 35 %RH. It can be relevant to perform a similar study with more tightly controlled conditions as ambient conditions may influence the coatings performance.

Ultimately, the sensitivity to humidity of all of the coatings will require the use of calibration alongside a humidity sensing device that is not sensitive to CO<sub>2</sub> in order to implement a reliable sensing device.

The micro-resonator used in this study could demonstrate the sensing operation and the miniaturization capabilities of such a device, however, as the Q-factor was relatively too low, the device makes it difficult to obtain high-precision measurements without significant averaging. Accordingly, a higher-Q micro-resonator structure should be considered.

As previously commented, CO<sub>2</sub> concentration measurement has multiple applications with different requirements in either the capacity of the measuring range and the reaction time. Among some applications such as the exhaust gases measurement from a combustion engine, the reaction time must be as short as possible, for which mainly the optical IR sensors are used whose reaction time can be as low as between 5 to 30 ms, while a resistive sensor for the same application can take up to 30 seconds, in both cases with sensors capable of measure until 90% of CO<sub>2</sub> (Clifford et al., 2008; Sutela, Collings, & Hands, 1999). Applications that do not require such short reaction times like the CO<sub>2</sub> measurement in the environment which can range from a few seconds to minutes, with measuring ranges of less than 10% (Singh, Howe, & Malarvili, 2018).

The results obtained in this work determine that the PEI base coatings for measuring the CO<sub>2</sub> concentration, due to the reaction time, mainly in the recovery stage, limit the applications for atmospheric type sensors, whether for indoor or open areas. The detection of the increase in CO<sub>2</sub> in an accelerated form such as a fire or laboratories safety sensor can be another application where this coating is used, since the recovery phase is not critical factor.

## 2.5 Conclusion

The purpose of this work was to study different CO<sub>2</sub> adsorbing coatings and to assess whether a micro-resonator CO<sub>2</sub> gas sensor could be implemented. Linear or Branched PEI were considered as the adsorbent coating. Additionally, a linear PEI with rOG coating was also studied.

Results showed congruence with previously published studies and has opened the possibility of deepening its application in micro-resonators. Linear Polyethylenimine coating has stood out for its capture and recovery properties, as well as its reduced hysteresis and reduced sensitivity to humidity. Linear PEI with rOG has shown interesting adsorption capabilities but captures the CO<sub>2</sub> molecule which requires an active reset mechanism, making this coating ill-suited for some application. However, the coating can be further investigated to integrate a reset mechanism within the sensor.

This work also presented a proof-of-concept micro-resonator-based CO<sub>2</sub> gas sensor operating with a Linear PEI coating. The sensor represents a highly integrated solution which could be batch fabricated, as the underlying resonant structure is fabricated using a commercial MEMS fabrication process. This work thus represents an initial effort towards achieving a highly integrated low-cost CO<sub>2</sub> sensor structure and future work could focus on integrating electronics to the structure in order to obtain a full-featured sensor device.

**Author Contributions:** A.P did all the experimental work, data acquisition, and analysis. F.N contributed expertise, direction, materials, and experimental tools.

**Funding:** The authors wish to thank the Natural Science and Engineering Research Council (NSERC) of Canada for its financial support of this work.

**Acknowledgments:** The author would like to thank CMC Microsystems for providing the layout design tools and enabling chip fabrication.



## CHAPTER 3

### AN 8 MW FULLY INTEGRATED REGENERATIVE RESONANT MEMS CO<sub>2</sub> SENSOR USING LINEAR POLYETHYLENIMINE AS A CAPTURE LAYER

Alberto Prud'homme<sup>a</sup> and Frederic Nabki<sup>a</sup>

<sup>a</sup>Department of Electrical Engineering, École de Technologie Supérieure  
1100 Notre-Dame West, Montréal, Quebec, Canada H3C 1K3

Paper submitted to *IEEE Sensors*, April 2020

#### **Abstract:**

A fully integrated regenerative CO<sub>2</sub> MEMS sensor using a micro-resonator coated with Linear Polyethylenimine as an adsorbent layer is presented. The pyramidal cantilever micro-resonator used has a resonant frequency of 315.24 kHz with a Q factor of 1125 at atmospheric pressure. The micro-resonator was integrated with a sustaining amplifier that consumes 8 mW. The MEMS sensor sensitivity was characterized in a CO<sub>2</sub> concentration range from 1200 to 10500 ppm, showing a frequency shift of -12 Hz at 1200 ppm with a slope of 3.50 mHz / ppm over the characterized range. The adsorption and recovery times are characterized to be as low as 170 seconds and 280 seconds, respectively. The impacts of pressure, temperature and humidity on the sensor were also characterized. The behavior of the MEMS sensor is compared to that of an optical CO<sub>2</sub> sensor.

**Keywords:** MEMS resonator, CO<sub>2</sub> sensor, Polyethylenimine, Mass sensor, Regenerative sensor, CO<sub>2</sub> adsorbent.

### 3.1 Introduction

Greenhouse gases like CO<sub>2</sub> have become one of the most important problems of our time. This has prompted the development of new measurement techniques that are efficient, robust, accurate and that require less power consumption in order to help increase the efficiency of industrial processes, combustion engines, biochemical processes, etc. In addition, CO<sub>2</sub> concentrations in human-occupied environments are an important metric that can significantly affect air quality, and are increasingly monitored (Espinal et al., 2013; Mahyuddin & Awbi, 2012).

The measurement of CO<sub>2</sub> concentration is complex, especially when the gas to be measured is in a mixture of other gases. In air, CO<sub>2</sub> (>0.03%) is present with nitrogen (78%), oxygen (20%), noble gases (~1%) and water. In this mixture, reaching the level of selectivity necessary to obtain the actual CO<sub>2</sub> concentration is challenging.

There are various methods for CO<sub>2</sub> concentration measurement. Resistive, capacitive and IR optical sensors have a good accuracy and reliability for general applications (Aleixandre & Gerboles, 2012; Brunet, Garcia, Pauly, Varenne, & Lauron, 2008; Fernández-Ramos et al., 2020; R. Wang et al., 2019). The main disadvantages of these techniques are the dimensions of the transducers and the power consumed during their operation. In some cases such as resistive and capacitive sensors, the lifetime of the sensor may be limited, while the optical sensors offer a longer lifetime (Fang et al., 2002; Hanafi et al., 2019; Ji, Zeng, & Li, 2019; Smulko Janusz, 2015).

Microelectromechanical systems (MEMS) that leverage microfabrication processes have in the few last years allowed the appearance of new sensors based on the resonance of microstructures that have a resonant frequency determined mainly by their geometry and manufacturing material. These MEMS resonators, or micro-resonators, are designed to exhibit a resonant frequency shift in response to a mass change of a thin gas-adsorbent layer that is deposited onto the micro-resonator (Fang et al., 2011; Hajjaj et al., 2019; Nazemi et al.,

2019). This layer adsorbs gas molecules, which results in a mass increase and causes a resonant frequency shift that is proportional to the gas concentration.

Micro-resonators of different geometries, dimensions and materials have been reported; in some cases capable of measuring masses in the range of picograms (Bouchaala et al., 2017; Fu & Xu, 2018; Li, Zhou, He, Liu, & Wang, 2017). The selectivity and dynamic performance that these sensors achieve is determined by the adsorbent coating used. Coating properties of interest are the selectivity of the target gas, the ability to adsorb the greatest possible volume of gas molecules and the regeneration by the release of the gas molecules when gas concentrations drop without the need of any external process restoring the frequency of the micro-resonator to its initial value. Multiple materials such as carbon nanotubes, amine-based polymers, acrylonitrile-styrene, diaminoethane, among many others have been proposed (Penza et al., 2007; Serban et al., 2009; C.-H. Yu et al., 2012).

In our previous work (Prud'homme & Nabki, 2020), Linear Polyethylenimine (LPEI) and Branched Polyethylenimine (BPEI) adsorbent coatings were compared for use in micro-resonators for CO<sub>2</sub> gas sensors. This work showed that LPEI presented better performance. Consequently, this work aims to develop and characterize a fully integrated regenerative CO<sub>2</sub> MEMS sensor based on a micro-resonator and LPEI adsorbent coating. The regenerative property of the sensor allows it to recover its original state after being exposed to a CO<sub>2</sub> concentration without any external process being required, simplifying the sensor control and reducing its power consumption. The influence of temperature, humidity and pressure on the performance of the sensor is also studied. The capabilities of a commercial optical CO<sub>2</sub> sensor are compared with the proposed MEMS CO<sub>2</sub> sensor.

The paper is structured as follows: the fabrication and characterization of the micro-resonator are detailed in Section II.A. Subsequently, the deposition process of the LPEI coating is introduced in section II.B. Section II.C overviews the test methodology and section II.D presents the sustaining amplifier topology design and characterization. Section III outlines the

measurements results of the MEMS CO<sub>2</sub> sensor. Section IV discusses the results and compares them with other reported works. Finally, a conclusion is presented.

## **3.2 System Integration**

The MEMS CO<sub>2</sub> sensor is composed of three main elements. The first is the micro-resonator whose resonant frequency is a function of its mechanical properties, the mass of the microstructure being of interest for this application. The excitation transducer may be formed by a layer of piezoelectric material, parallel plates for electrostatic excitation or resistive elements for thermal excitation (R. Abdolvand et al., 2016; Ali & Prasad, 2020; C. Zhao et al., 2016). In this work, a piezoelectric aluminum nitride film is used as a method of excitation. This simplifies biasing of the micro-resonator and presents a relatively low motional resistance for the sustaining amplifier (Ali & Prasad, 2020).

The second element is the sustaining amplifier whose function is to provide the micro-resonator with the excitation necessary to keep it operating as close as possible to its resonant frequency in an electronic oscillator loop. Finally, the last element is the adsorbent coating to capture the CO<sub>2</sub> molecules and thus increase the mass of the micro-resonator proportionally to the concentration of CO<sub>2</sub> in the air, which is reflected in a shift of the micro-resonator oscillator loop's oscillation frequency (Joshi, Kumar, Jain, Akhtar, & Singh, 2019).

### **3.2.1 MEMS micro-resonator fabrication and characterization**

The micro-resonator was manufactured using the MEMSCAP PiezoMUMPS commercial microfabrication process. The cross-section of the micro-resonator is shown in Figure 3.1. The cantilever structure is formed by a 10 μm doped single-crystal silicon conductive layer onto which a 0.5 μm piezoelectric layer of Aluminum Nitride (AlN) is deposited. For electrical connections of the top side of the AlN and for wire-bonding pads, a metal stack of 20 nm of chrome and 1 μm of aluminum is deposited. Finally, a 200 nm oxide layer insulates the metal traces and the bottom silicon layer (Inc., 2014).

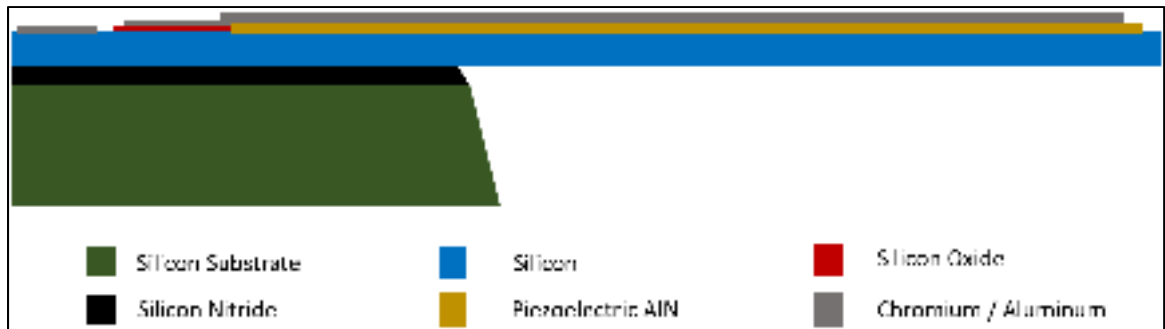


Figure 3.1 Cross-section of the MEMS resonator based on a cantilever structure.

The cantilever is 220  $\mu\text{m}$  long. Its tip is 22  $\mu\text{m}$  wide and its anchored side is 40  $\mu\text{m}$  wide. A SEM micrograph and 3D confocal microscope image of the fabricated device are shown in Figure 3.2

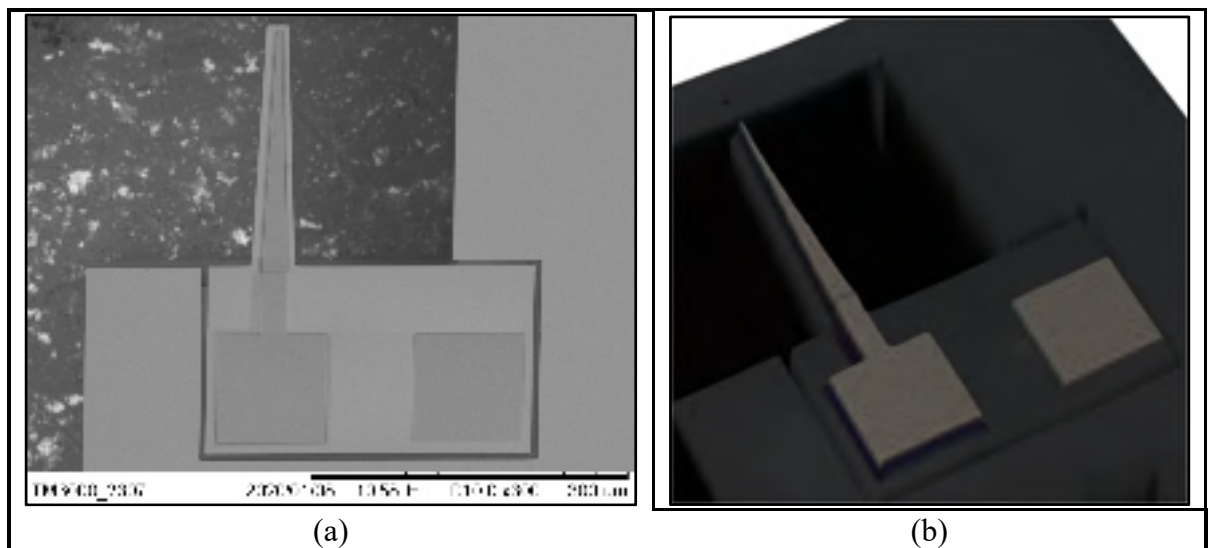


Figure 3.2 Uncoated micro-resonator (a) SEM micrograph, and (b) 3D view obtained by confocal microscope.

Finite element methods (FEM) eigenfrequency simulation of the micro-resonator was performed using COMSOL in order to estimate its resonant frequency. This yielded a resonant frequency of 315.60 kHz for mode 1, 628.10 kHz for mode 2 and 963.40 kHz for mode 3. The mode shapes of the micro-resonator and the displacement frequency response measured by doppler vibrometer are shown in Figure 3.3.

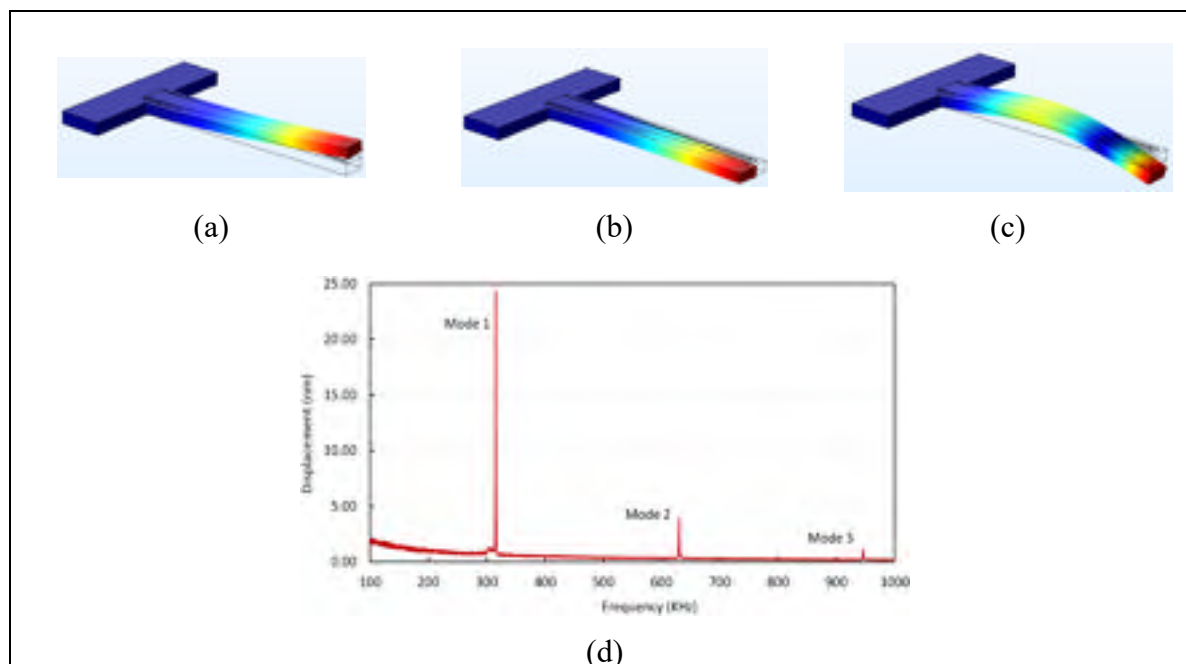


Figure 3.3 Micro-resonator resonance frequency at (a) mode 1, (b) mode 2, (c) mode 3; (d) Vibrometer resonant frequency measurement of the three modes of the micro-resonator

The results obtained by vibrometer measurements correspond well to the FEM simulations. For instance, the difference between mode 1 measured by the vibrometer and the value estimated in COMSOL was of 360 Hz, or 0.11%.

### 3.2.2 Adsorption coating deposition

In order to use the micro-resonator as a CO<sub>2</sub> sensor, it is necessary to add an adsorbent layer for the gas molecules. In our prior work (Prud'homme & Nabki, 2020), different coatings based on Polyethylenimine (PEI) were compared for this application. The best performing coating was LPEI and is used here. The LPEI has an average Mn of ~10,000, PDI ≤1.3, and was acquired through Sigma-Aldrich.

As LPEI is in a solid state at room temperature, it is necessary to increase the temperature beyond 60 °C to obtain a viscous solution for deposition. Due to the micro-resonator's dimensions, only a droplet smaller than 20 μm could be deposited. To achieve droplet placement at the center of the cantilever tip without breakage of the micro-resonator, a two-

axis piezoelectric actuator was designed and yielded high precision and repeatability. The deposition setup of the piezo-actuator on the heated probe station chuck is shown in Figure 3.4.

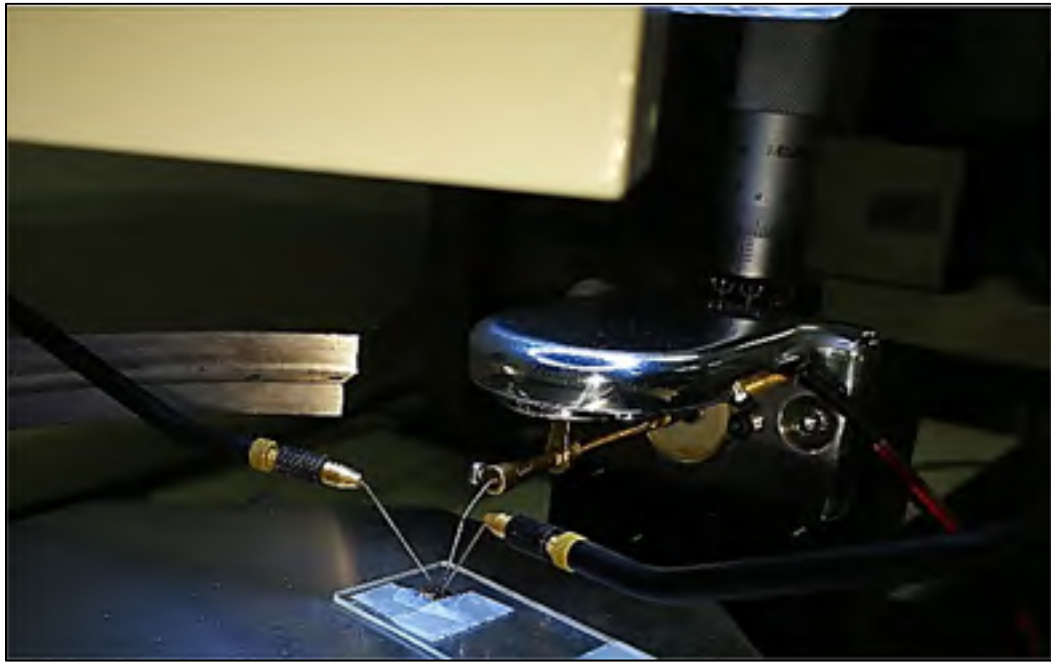


Figure 3.4 Setup used for the deposition of the LPEI coating using the two-axis piezo actuator

During the coating deposition, the die containing the micro-resonator was placed on a heated chuck at 65 °C. Once the die reached the same temperature, a small quantity of room temperature LPEI was placed in one of the empty areas of the DIE, as close as possible to the micro-resonator, and after several minutes, the solution became viscous allowing the use of a micro-needle to perform the transfer to the tip of the resonator. After deposition of the LPEI droplet onto the micro-resonator tip, the frequency shift caused by the added LPEI mass was measured, as shown in Figure 3.5.

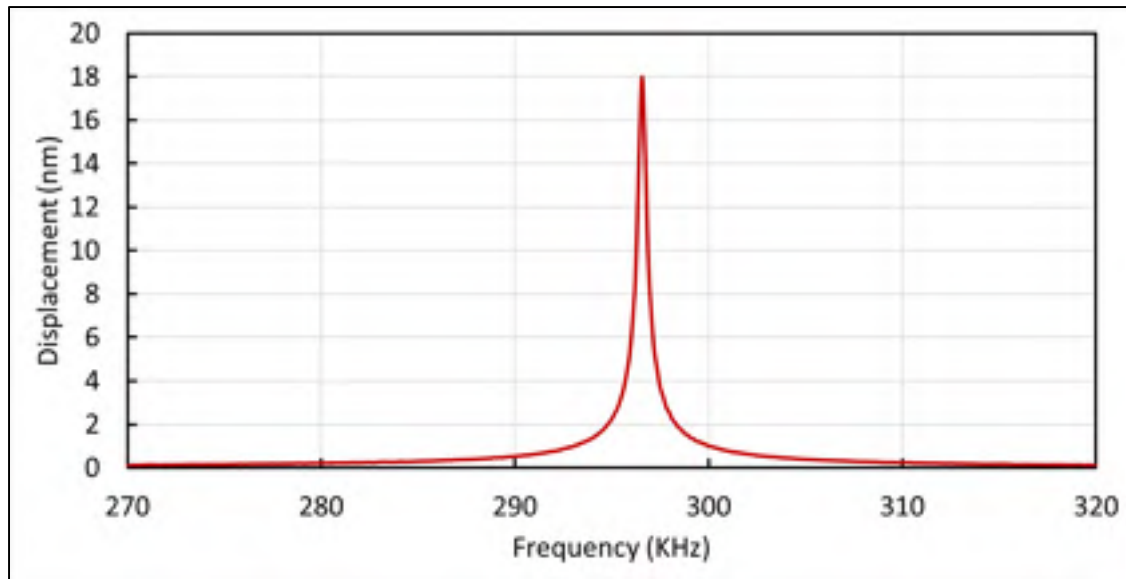


Figure 3.5 Vibrometer measurement after the LPEI coating deposited

After the deposition of the LPEI, the resonant frequency of the resonator was shifted from 315.24 kHz to 297.12 kHz with a Q factor of 706. The aggregated mass of the coating reduced the resonant frequency and displacement amplitude of the resonator as expected. Due to the additional thermoelastic damping caused by the LPEI adsorbent coating, the recorded Q-factor decrease is expected. Assuming no significant change in the resonator's spring constant due to the LPEI, as it is applied at the tip of the cantilever, a 12.6% mass increase of the resonator can be estimated from the resonant frequency shift. To more precisely estimate the mass of the deposited LPEI, the FEM model of the micro-resonator in COMSOL was used, analyzing the resonant frequency deviation as a function of the aggregate mass. The center of mass of the micro-drop of the coating was simulated to be 10  $\mu\text{m}$  away from end of the micro-resonator tip. The added mass was swept from 0 ng to 8 ng, yielding a shifted resonant frequency matching measurements for a 5.9 ng added mass.

### 3.2.3 CO<sub>2</sub> sensor characterization setup

The characterization process for CO<sub>2</sub> sensors requires that the pressure, temperature, humidity and CO<sub>2</sub> concentration conditions be controlled. For this purpose, an environmental chamber was used, with a frequency counter and signal analyzer (i.e., an oscilloscope Tektronix

MDO4054-3). The characterization setup is shown Figure 3.6a and the characterization equipment is shown in Figure 3.6b.

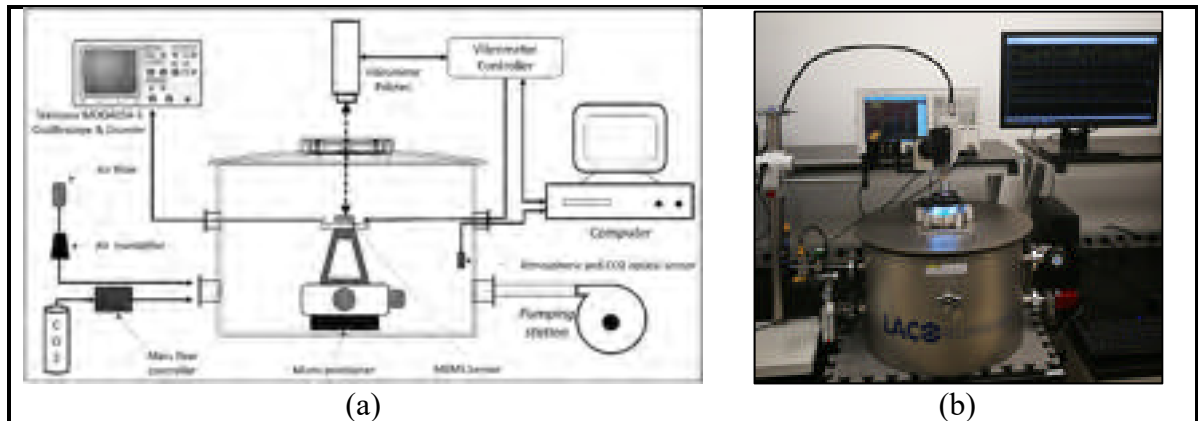


Figure 3.6 (a) Diagram of the characterization setup,  
(b) Setup for the CO<sub>2</sub> gas sensor characterization

The CO<sub>2</sub> introduction and concentration level control were made with a constant low flow of air to maintain the atmospheric pressure and obtain a smooth increasing and decreasing CO<sub>2</sub> concentration in the chamber through the pumping station. The setup was designed to be automated. An atmospheric and optical CO<sub>2</sub> sensor CM-40831 from GasLab was used to compare the conditions in the chamber with the MEMS CO<sub>2</sub> sensor. The oscilloscope and the optical sensor were integrated within a Matlab / Simulink platform that registered and controlled the test process, while the micro-positioner was used for the alignment of the micro-resonator with the vibrometer laser to monitor its motion.

### 3.2.4 MEMS CO<sub>2</sub> integration

The MEMS CO<sub>2</sub> sensor was implemented with a four-stage sustaining amplifier in closed-loop with the micro-resonator. This allows for an oscillation of the circuit at the micro-resonator's resonant frequency. The Texas Instruments OPA4684 operational amplifier was selected due to its low noise level, sufficient bandwidth and high gain. One OPA4684 device has the four necessary amplifiers, which reduces the signal noise, improves the power consumption and reduces the sensor's footprint.

The block diagram of the MEMS CO<sub>2</sub> sensor is shown in Figure 3.7.

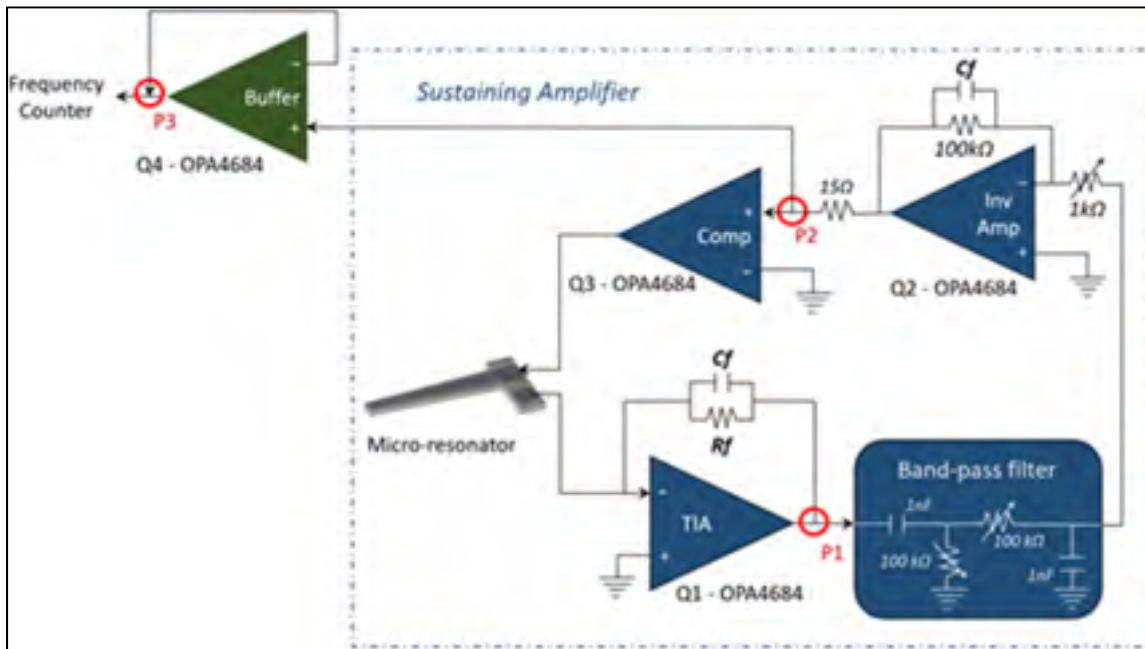


Figure 3.7 MEMS CO<sub>2</sub> sensor block diagram

The first stage is a transimpedance amplifier (TIA) Q1 achieved with a resistive feedback topology. A 0.5 pF parallel capacitor  $C_f$  was used to increase the stability of the amplifier in closed-loop (Mekky, Cicek, & El-Gamal, 2013; Salvia, Lajevardi, Hekmat, & Murmann, 2009). The gain of the TIA was set to  $-100\text{ k}\Omega$ . The second stage is a passive band-pass filter consisting of 1 nF capacitors and 100 k $\Omega$  variable resistors that will allow the sustaining amplifier bandwidth to be adjusted in a range from 2 kHz to more than 10 MHz, which will block the frequencies of the higher modes of the micro-resonator in order to preclude spurious oscillation that could occur at other resonant modes. The third stage is an amplifier Q2 in inverting configuration to provide the additional 180° phase shift required for oscillation. Amplifier Q3 acts as a comparator to increase loop gain sufficiently to achieve oscillation (H. CHEN, ZHONG, & MENG, 2017; Wasisto, Zhang, Merzsch, Waag, & Peiner, 2014). Finally, an amplifier Q4 is drives the oscilloscope that acts as a frequency counter

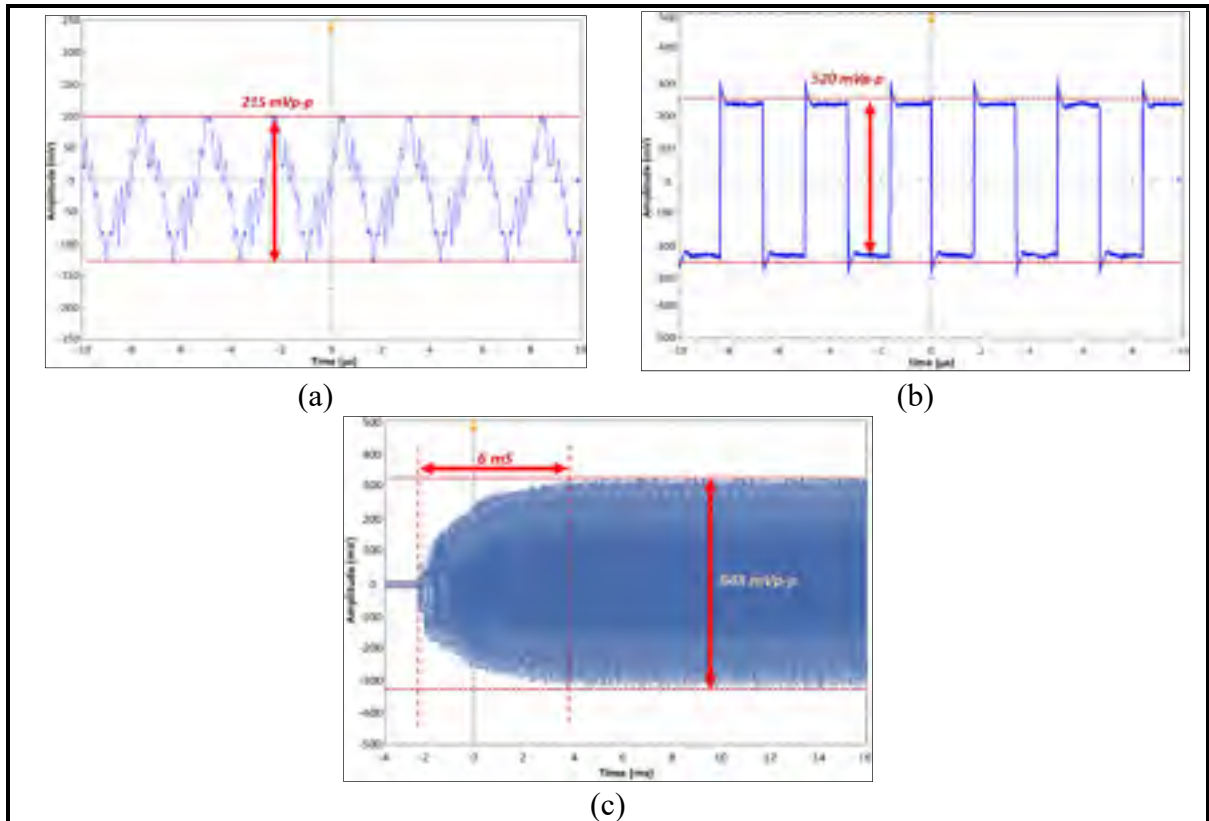


Figure 3.8 Measured CO<sub>2</sub> MEMS sensor signal waveforms at the different points labelled in Fig. 3.7 steady-state at (a) P1 and (b) P2, and (c) startup transient of the resonator at P3.

Measurements of the signals in the sustaining amplifier were taken with the oscilloscope and are shown in Figure 3.8. The signal after the TIA amplifier contains the resonator modes as expected, then the bandpass filter rejects the out-of-band frequencies while the inverting amplifier and the comparator adapt the signal to provide the drive for the micro-resonator.

In Figure 8c the resonator transient toward stabilization is shown after power up, taking 6 ms. The steady buffered output amplitude is of 648 mVpp, with a frequency of 299.08 kHz in ambient conditions. The micro-resonator excitation has a duty cycle of 51.2 %. The sustaining amplifier operates with a power supply of  $\pm 1.2$  V and has a power consumption of 8 mW.

The fully integrated sensor PCB is shown in Figure 3.9, and was integrated on a single-sided PCB with SMD components. The shortest electrical path between the resonator and the TIA were ensured to reduce the influence of noise and parasitics.

Two gold pellets were welded to the PCB to allow the micro-resonator die to be directly wire-bonded with the PCB. Precision potentiometers allowed for the adjustment of the filter and the inverting amplifier gain.

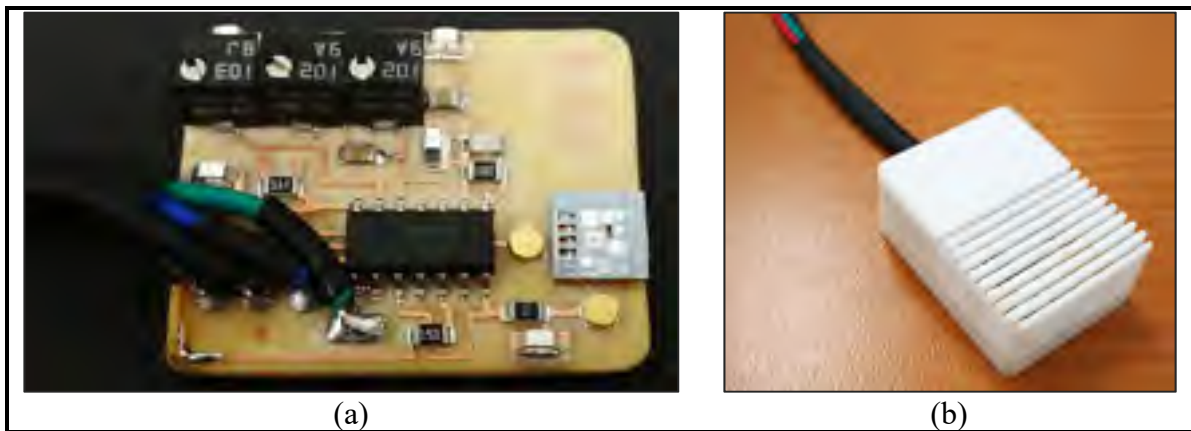


Figure 3.9 Fully integrated sensor, (b) Sensor integrated with protector casing

Figure 3.9b, the sensor is shown with a 3D printed case that allowed free flow of air while protecting the sensor.

### 3.3 Measurement Results

The MEMS CO<sub>2</sub> sensor was subjected to various tests to benchmark its sensing capabilities, and its behavior to temperature, humidity and atmospheric pressure variations. Due to the application for which this system was designed, it is essential to know its stability over a long period of time, therefore, a stability test was carried out over a 24 hours period.

### 3.3.1 Response to CO<sub>2</sub> concentrations

The CO<sub>2</sub> characterization has as objective the frequency deviation quantification of the MEMS sensor as a consequence of the variation of the CO<sub>2</sub> concentration, the time it takes to reach stability after the concentration changes and the capability of the sensor to recover the original frequency at the initial CO<sub>2</sub> concentration. The reaction and stabilization times are compared with the optical sensor mentioned in the previous section and a brief comparative analysis was performed. All tests were performed at atmospheric pressure, temperature of  $21 \pm 1$  °C and humidity level of  $25 \pm 5$  %RH. The CO<sub>2</sub> concentration levels evaluated were 1200, 4000, 6500 and 10500 ppm, with an initial ambient concentration of 500 ppm. The results of the developed tests are shown in the Figure 3.10.

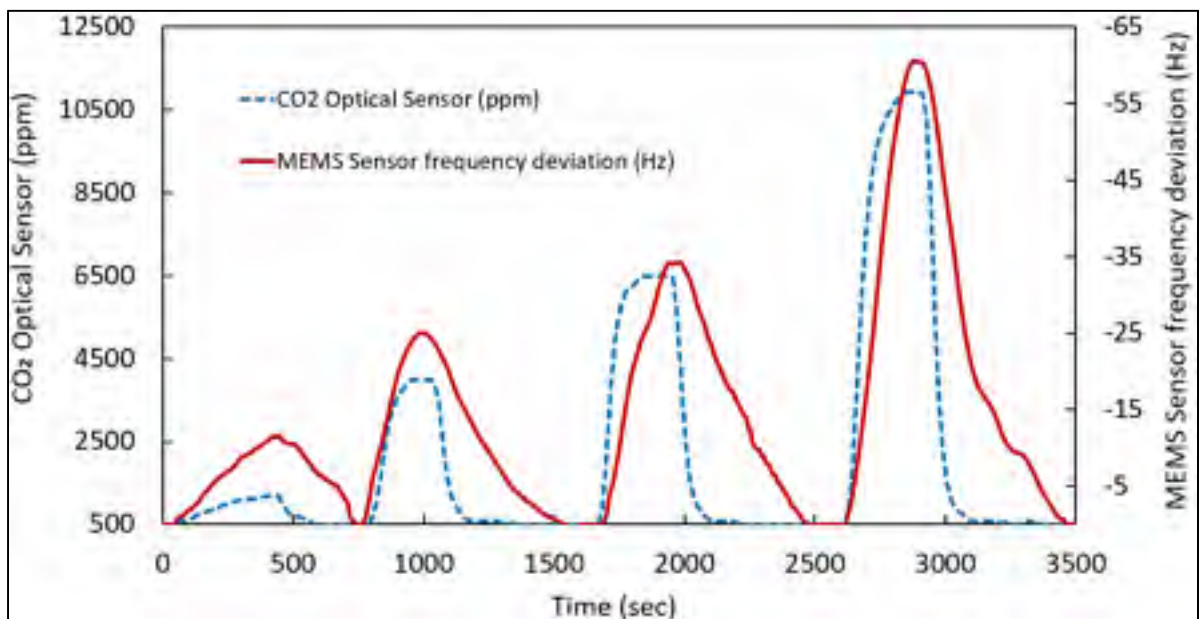


Figure 3.10 MEMS and optical sensor response to different CO<sub>2</sub> concentrations

The deviation of the frequency in Hz of the CO<sub>2</sub> MEMS sensor is shown on the left y-axis, where the values' order has been inverted to make the reaction comparison between both sensors in a simplified manner. The optical sensor is shown on the right y-axis in CO<sub>2</sub> ppm.

Figure 3.10 shows the reaction of the MEMS sensor to various CO<sub>2</sub> concentrations, where as expected the frequency deviation increases with increasing concentration. As the CO<sub>2</sub> concentration decreases, the resonance frequency tends to return to its original value without showing any hysteresis within the evaluated range.

The comparison between the MEMS and the optical sensor allows to evaluate the CO<sub>2</sub> concentration range where the performance of both is competitive. The adsorption and recovery were defined as the time for the frequency shift to go from 0% to 90% of its steady state value.

Figure 3.10 shows that the adsorption time after which the CO<sub>2</sub> concentration was set to 1200 ppm is similar for both sensors, with the MEMS sensor being 25 seconds slower. The recovery was 190 seconds longer for the MEMS sensor. For a CO<sub>2</sub> concentration of 4000 ppm, the difference between the MEMS and the optical sensor tends to be similar to the 1200 ppm test. The main difference between both tests is the recovery times, where the optical sensor is between 2 to 3 times faster than the MEMS sensor when recovering from a 1200 or 4000 ppm CO<sub>2</sub> concentration. For CO<sub>2</sub> concentrations of 6500 and 10500 ppm, the optical sensor presents a faster adsorption performance than the MEMS sensor with adsorption times between 1.5 to 3 times shorter, as well as recovery times that are 2 to 4 times faster.

The LPEI coating deposited onto the micro-resonator of the MEMS sensor was shown to have the ability to adsorb the CO<sub>2</sub> molecules and release them proportionally to the concentration in the air, and the adsorption and recovery time have been shown to be linearly related to the CO<sub>2</sub> concentration at less than 6500 ppm (Prud'homme & Nabki, 2020). For higher CO<sub>2</sub> concentration levels however, the time increase with concentration is not linear and starts to flatten because of the decrease in adsorption capacity of the LPEI when approaching its saturation point (Al-Marri et al., 2017; Andreoli et al., 2015). The adsorption and recovery times for each concentration are summarized in Figure 3.11.

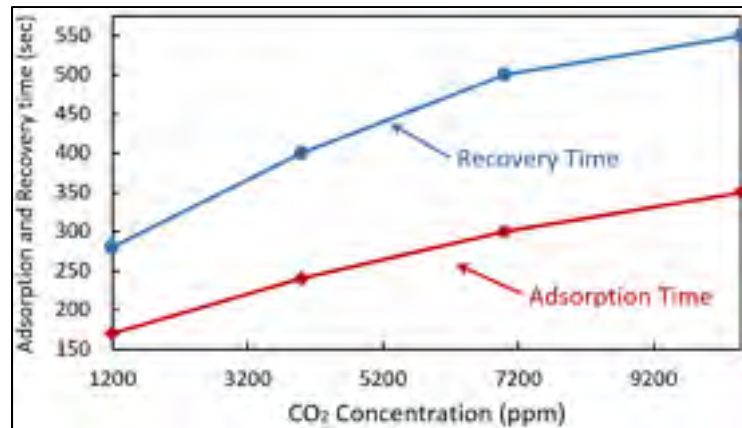


Figure 3.11 Adsorption and Recovery times based in the CO<sub>2</sub> concentration

The results of the tests performed have shown that the adsorption time from 500 to 1200 ppm requires 170 seconds and an additional 19.3 ms / ppm of CO<sub>2</sub> over the evaluated range. The recovery time from 1200 to 500 ppm requires 280 seconds and an additional 29 ms / ppm of CO<sub>2</sub> over the evaluated range. Note that it would be possible to characterize the sensor in a piecewise linear curve with a different slope from 7200 ppm to 10500 ppm. The linearization shows that the MEMS sensor recovery requires ~50% more time than the absorption process within the CO<sub>2</sub> range between 1200 and 10500 ppm.

The frequency deviation of the MEMS sensor based on the CO<sub>2</sub> concentration in the air is a critical factor to be evaluated, since it will allow to know its sensitivity and its linearity in the characterization range. The frequency deviation of the MEMS CO<sub>2</sub> sensor for each concentration are summarized in Figure 3.12.

The MEMS sensor response to the presence of different CO<sub>2</sub> concentration levels, shows a slight tendency to reduce the slope gradually depending on the concentration increase. This behavior is congruent with previously published works on the interaction of LPEI and CO<sub>2</sub> (Al-Marri et al., 2017; Gomes et al., 1995; S. Lin & Theato, 2013; B. Sun et al., 2011; C.-H. Yu et al., 2012), where it has been determined that the adsorption of CO<sub>2</sub> with LPEI in the concentration range less than 2000 ppm it behaves linearly and subsequently the slope decreases until it reaches its saturation point (Al-Marri et al., 2017; Andreoli et al., 2015).

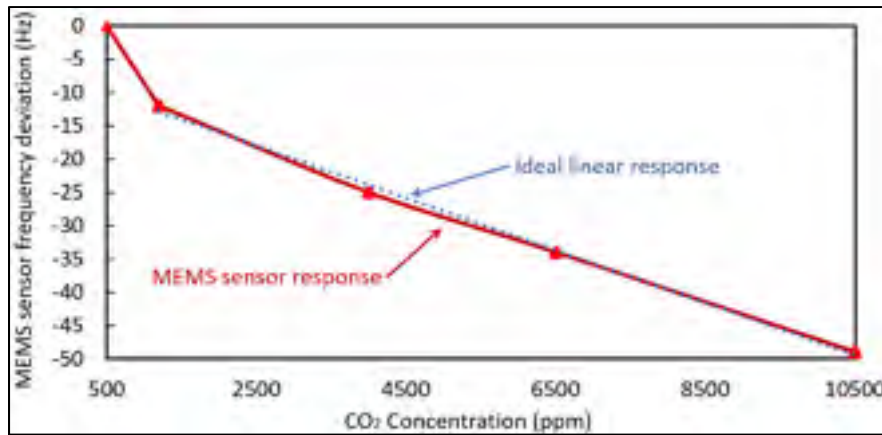


Figure 3.12 MEMS sensor frequency deviation by CO<sub>2</sub> concentration

Although the sensor behavior is not completely linear, the variation between the ideal linear response and the results obtained can be neglected in the evaluated range. The linearization of the frequency deviation allows to define that in a range from 1200 ppm with a deviation of -12 Hz, for each additional CO<sub>2</sub> ppm the sensor frequency will deviate -0.0035 Hz within the maximum characterized concentration of 10500 ppm.

Although the sensor behavior is not completely linear, the variation between the ideal linear response and the results obtained is not significant in the 1200 to 10500 ppm range. The linearization of the frequency shift shows a sensitivity of 3.50 mHz / ppm of CO<sub>2</sub> over this range, starting at -12 Hz at 1200 ppm. Note that between 500 and 1200 ppm, the slope increases to 17 mHz / ppm due to the LPEI behavior at low concentrations, as previously discussed.

Another important factor is the coating degradation after each adsorption and recovery cycle, which would reduce the accuracy and repeatability of the sensor. In this work, multiple measurements were made at different concentrations, humidity and temperature levels, and no degradation was detected within the concentration range in which the characterization tests were performed. The LPEI allowed for more than 30 cycles without having an impact on repeatability of the sensor. This has been confirmed by other works in which more than 150 adsorption and recovery cycles were carried-out without experiencing coating degradation (Muraoka et al., 2014; B. Sun et al., 2011; H. Zhang et al., 2015).

### 3.3.2 Impact of ambient conditions

Micro-resonators have shown great sensitivity as mass detectors, however they are affected by external parameters, such as humidity, temperature and pressure. For instance, the LPEI coating that was deposited onto the micro-resonator has a high sensitivity to humidity (Prud'homme & Nabki, 2020). Determining the impact that these ambient conditions have on the sensor is crucial to be able to compensate and calibrate. The characterization of the MEMS sensor behavior to humidity was done by introducing humidified air in the chamber in a range from 15 to 85 %RH. In the case of the temperature, the characterized range was from 15 to 40 °C, due to chamber limitations. The resulting frequency deviations of the MEMS CO<sub>2</sub> sensor because humidity and temperature are plotted in Figure 3.13.

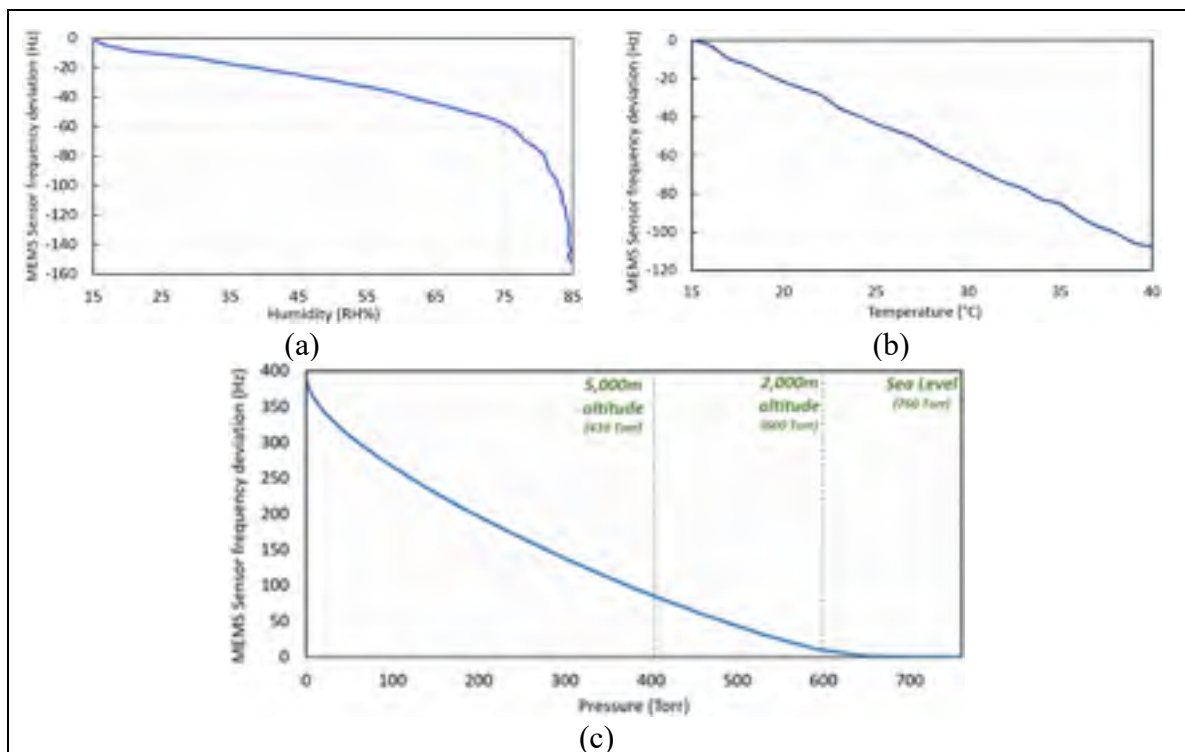


Figure 3.13 Response of the MEMS sensor to variations in (a) humidity, (b) temperature and (c) atmospheric pressure.

Figure 3.13a shows how that humidity leads to a deviation in the frequency of the MEMS sensor of up to -155 Hz at 85 %RH. It can be considered that in the range of 15 to 75 %RH,

the sensor has a linear behavior having a slope of  $-1.00 \text{ Hz} / \%RH$ , and subsequently both the saturation of the coating, as well as the condensation on the micro-resonator, cause the variation to be larger. The impact of the temperature on the MEMS sensor is shown in can be seen in Figure 3.13b , where it is considered that in the range of 15 to 40 °C the frequency deviation is linear with a slope of  $4.28 \text{ Hz} / ^\circ\text{C}$ .

The atmospheric pressure also affects the micro-resonator due to the change in its mechanical damping coefficient caused by the surrounding air. The frequency deviation of the MEMS CO<sub>2</sub> sensor due to atmospheric pressure variations is shown in Figure 3.13c, where the atmospheric pressure was reduced to 3 mTorr inside the vacuum chamber to observe the MEMS sensor response. The frequency deviation is well correlated to the pressure reduction. It is expected that this sensor would operate in typical atmospheric pressure such that the corresponding linear dependency around 650 Torr can be taken as a reference, which has a slope of  $0.025 \text{ Hz} / \text{Torr}$ . From 650 to 200 Torr, the sensor exhibits a linearized slope of  $0.68 \text{ Hz} / \text{Torr}$ .

According to the previous results, the impact of humidity, temperature and pressure should be taken into account in order to compensate the sensor response, as is done in many sensors that use reference devices, for instance (Mumyakmaz, Özmen, Ebeoğlu, Taşaltın, & Gürol, 2010; Padilla et al., 2010).

### **3.3.3 Long term stability**

A 24 hours stability test was carried-out where the temperature, humidity and pressure were monitored, as well as the output frequency of the sensor. The CO<sub>2</sub> concentration was kept constant at 500 ppm; however, the temperature and humidity could not be controlled, which caused sensor fluctuations during the test period. The frequency deviation of the MEMS CO<sub>2</sub> sensor in the long term is showed in Figure 3.14.

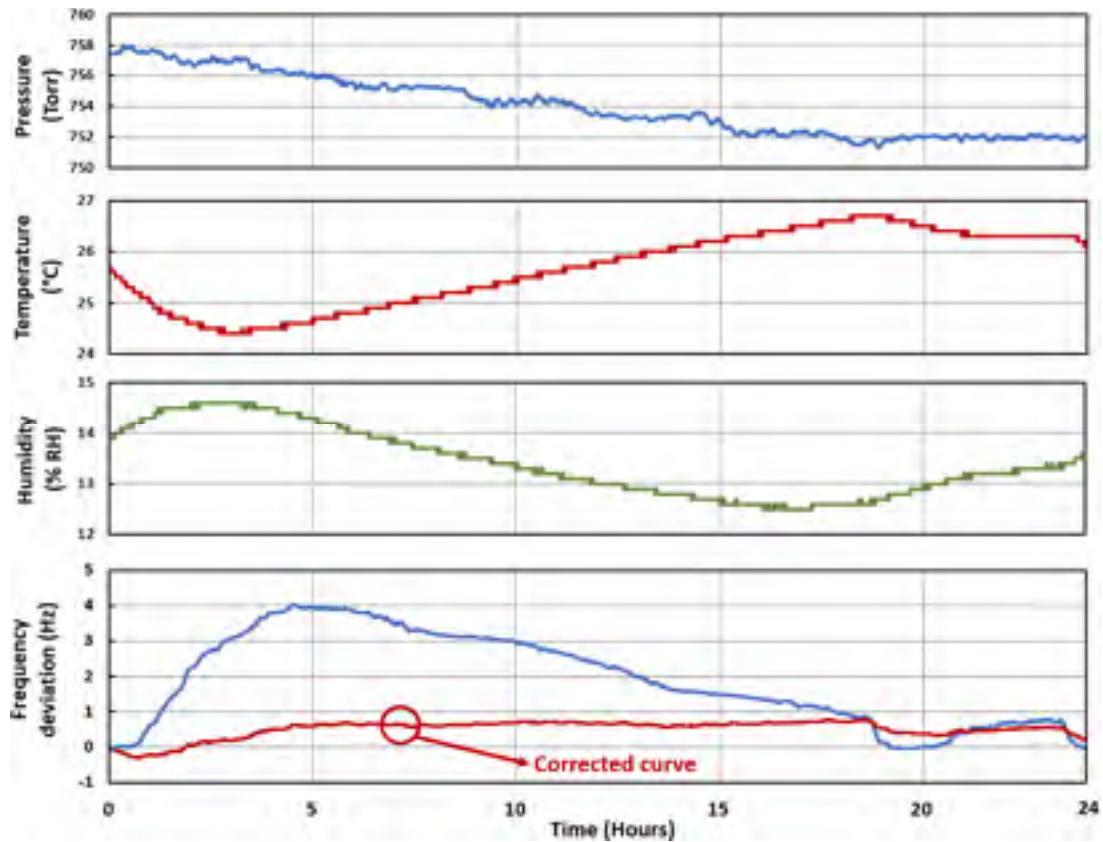


Figure 3.14 Long term test of the CO<sub>2</sub> MEMS sensor

During the 24 hours period, the device exhibited a 4 Hz deviation (733 ppm of CO<sub>2</sub>, linearly approximating using Figure 3.14). Figure 3.14 also shows the humidity, pressure and temperature variations during the entire period of the test. The MEMS sensor deviation was generated due to the change in temperature in a range of  $\pm 1.31$  °C,  $\pm 1.15$  %RH and  $\pm 3.50$  Torr. The combination of these three parameters resulted in the MEMS device shifting its frequency corroborating the results obtained previously. In addition, a corrected curve is included in Figure 3.14. In order to correct the sensor reading by using the linearization factors of temperature, pressure and humidity the following equation was applied.

$$Freq_{res} = K(\Delta Temp * F_T + \Delta Hum * F_H + \Delta Pres * F_P) + Freq_{(res - 1)} \quad (3.1)$$

where the variables  $F_x$  correspond to the linearization factors,  $K$  is a scale factor that will compensate for the variation in air damping due to the interaction of temperature, humidity

and pressure, and  $F_{\text{freq}}$  is the corrected MEMS sensor frequency. In this case the sensor response is much more stable, staying within  $\pm 0.5$  Hz ( $\pm 29$  ppm of CO<sub>2</sub>), indicating the possibility of compensating for temperature, pressure and humidity effects if these quantities are monitored as well.

### 3.4 Discussion

In this work, the proposed CO<sub>2</sub> MEMS sensor relies on the mass variation of the LPEI adsorbent coating to changes in CO<sub>2</sub> concentration. The use of LPEI to capture the CO<sub>2</sub> molecules has a relatively fast response time. It is also able to release the CO<sub>2</sub> molecules without the need for an external process (e.g., heating) creating a reversible CO<sub>2</sub> sensor. Table 3.1 compares the performance of the fabricated MEMS CO<sub>2</sub> sensor to other previously published works that use a micro-resonator-based sensing mechanism. The proposed sensor compares favorably in response time and sensitivity and operates at a low frequency which relaxes the requirements on the sustaining amplifier electronics, reducing power consumption.

As discussed above, humidity, temperature and atmospheric pressure have an important influence on the MEMS CO<sub>2</sub> sensor, so it is necessary to perform compensation of the CO<sub>2</sub> measurement by using temperature, humidity and pressure data.

As future work, the integration of a heating element on the micro-resonator should be considered in order to maintain a fixed elevated temperature (e.g., 80°C). This will speed up the capture and release of adsorbed gas molecule, at the cost of added power consumption, and will reduce the influence of the ambient temperature on the sensor. It will be interesting to carry out a study on the influence of pressure and humidity on the micro-resonator when it is maintained at elevated temperatures, including the viability of the more viscous LPEI at such temperatures.

Table 3.1 Comparison of the studied CO<sub>2</sub> MEMS sensor with other published works

|                                   | <b>Adsorption material</b>             | <b>Resonant device</b> | <b>Frequency deviation (ppm)</b> | <b>Adsorption time</b> | <b>Recovery time</b> |
|-----------------------------------|--|------------------------|----------------------------------|------------------------|----------------------|
| This work                         | LPEI                                   | 297.1 KHz Cantilever   | 175 ppm                          | 5.83 min               | 9.1 min              |
| Muraoka et al. (2014)             | acrylonitrile–styrene copolymer (AS-1) | 10 MHz QCM             | 3 ppm                            | 8 min                  | 8 min                |
| Muraoka et al. (2014)             | acrylonitrile–styrene copolymer (AS-2) | 10 MHz QCM             | 5.8 ppm                          | 5 min                  | 10 min               |
| B. Sun et al. (2011)              | Branched PEI                           | 8 MHz QCM              | 2.5 ppm                          | 11.7 min               | 20.7 min             |
| (B. Sun et al., 2011)             | Branched PEI + Starch                  | 8 MHz QCM              | 8.75 ppm                         | 18.9 min               | 21.6 min             |
| Gomes et al. (1995)               | 1,2-diaminoethane                      | 9 MHz QCM              | 16.6 ppm                         | n.a                    | n.a                  |
| Chapter 2                         | LPEI                                   | 6 MHz QCM              | 16.83 ppm                        | 16.4 min               | 12.85 min            |
| Chapter 2                         | Branched PEI                           | 6 MHz QCM              | 7.5 ppm                          | 16.15 min              | 33.85 min            |
| H. Yu, Xu, Xia, Lee, et Li (2012) | NH <sub>2</sub> -group-functionalized  | 75 KHz Cantilever      | 160 ppm                          | 3.3 min                | 5 min                |

As mentioned in the introduction, the objective of this work is the integration of a MEMS sensor for the measurement of CO<sub>2</sub> concentration. MEMS gas sensors have been widely studied, however, the works published previously have the objective of studying the individual elements that make up these complete systems, so the point of comparison of the performance of this work with another fully integrated resonant system for CO<sub>2</sub> published previously has been limited.

The performance obtained by the MEMS sensor follows the trend of other previously published works, mainly those that use cantilevers as a resonant element. Various CO<sub>2</sub> adsorbing materials have been published. Among them, Guanidine (CH<sub>5</sub>N<sub>3</sub>) has shown to perform better than LPEI in terms of CO<sub>2</sub> capture, however, work in (H. J. Lee, Park, Kupnik, & Khuri-Yakub, 2012) has demonstrated the necessity to carry out a heating process for prolonged periods to regenerate that material and many others. In the case of LPEI, it has been shown that it does not require an external regeneration process, simplifying sensor operation and control. Work in n (H. Zhang et al., 2015) points out that at an increased temperature to 85 °C, the LPEI adsorption time required will be decreased by up to 70%. It is also possible to reduce recovery time by more than 85 % if the LPEI is heated to 85 °C. While heating is not necessary for the proposed sensor to remain stable and recover from CO<sub>2</sub> exposure, it can be used to enhance its response time, as suggested by (H. Zhang et al., 2015).

Finally, in this work, multiple adsorption and recovery cycles with the MEMS sensor were performed without any significant degradation being seen in the LPEI. Other works have also corroborated this finding for hundreds of adsorption and recovery cycles. However, the behavior of the coating in cycles of much greater CO<sub>2</sub> concentration (i.e., >20%), despite not being in the range of interest of this work, could be verified in order to quantify the limitations of this type of sensor.

### **3.5 Conclusions**

This work presented a compact low-power (i.e., 8 mW) regenerative micro-resonator-based CO<sub>2</sub> sensor. An LPEI coating was deposited onto the micro-resonator after fabrication and allowed for the measurement of CO<sub>2</sub> concentration in the air by monitoring of the frequency shifts caused by mass variations. The sensor included an integrated sustaining amplifier with sensitivity and response times that compare favorably to other published works leveraging similar sensing principles. This is due in part to the coating used and integration of the coating, micro-resonator and electronics.

This work also presented a brief comparison between the MEMS sensor manufactured and an optical CO<sub>2</sub> sensor. It could be concluded that for concentrations below 4000 ppm, the performance of the proposed sensor compares well, while the faster recovery time of the optical sensor was observed. However, considering that the variations of CO<sub>2</sub> in the air are often not abrupt, it can be considered that the proposed sensor can be suited to many applications nonetheless, while having the potential of being batch fabricated at lower cost and having lower power consumption and smaller footprint.

**Author Contributions:** A.P did all the experimental work, data acquisition, and analysis. F.N contributed expertise, direction, materials, and experimental tools.

**Funding:** The authors wish to thank the Natural Science and Engineering Research Council (NSERC) of Canada for its financial support of this work.

**Acknowledgments:** The author would like to thank CMC Microsystems for providing the layout design tools and enabling chip fabrication.

## CONCLUSION AND DISCUSSION

Measuring concentration of gases in air has been a subject of research both academically and industrially due to its wide range of applications. To achieve CO<sub>2</sub> gas sensing, this thesis applied the principle of resonance in silicon micro-structures and the shift of the natural resonance in proportion of the addition of mass in the resonator.

CO<sub>2</sub> concentration ranges from 500 ppm to 10,500 ppm were studied. To be able to obtain a reliable measurement, different capture coating materials were evaluated, Linear Polyethylenimine, Branched Polyethylenimine, graphene and PEI/GO thin film.

The application of the coating over the resonator surface represented a challenge because the size of the structures can reach 20 μm. Different techniques were evaluated. An actuator with micro-needle was devised for the deposition of the micro-drop on the micro-resonator surface.

For the performance evaluation of the micro-resonator geometries, a first MEMS chip was designed using electrostatic resonators and a second chip was designed using piezoelectric resonators.

The gas sensor was implemented by the integration of a coated micro-resonator with a sustaining amplifier, and the resulting sensor was characterized and compared to a commercial CO<sub>2</sub> sensor.

### **Novelty aspect and importance of the project**

The microfabrication process used to the development of this gas sensor opens new opportunities for the development of highly integrated microsensors, with lower energy consumption, required volume, and fabrication costs than the actual technology of optical and reactive sensors.

The resulting sensor is a proof-of-concept that can be, in time, adapted to become a commercial system. The development of this sensor is focused on the measurement of CO<sub>2</sub> due to the security and stability of this gas, but the same system could be used to monitor different gases by replacing the type of adsorbent coating. It could also potentially be used to measure molecules in liquids.

Additionally, the sensor was used to measure other parameters such as temperature, humidity, and pressure. The results obtained showed that the same system can be used to measure multiple variables with high precision and a minimum reaction time.

### **Potential applications**

The microsensors for mass measurement used for gas concentration have applications in the industrial sector for process gas sensors. In meteorological systems the measurement of humidity, CO<sub>2</sub> and oxygen levels are applications where the developed sensor offers alternatives to current systems.

In the biomedical sector, the measurement of glucose and the detection of molecules in saliva or blood are potential applications that have been demonstrated in other works carried out with the same technology. In hospitals it can be applied to detect the presence of infectious agents that commonly become sources of mass contamination.

The reaction time and sensitivity offered by these types of sensors allow them to be used in military applications that require the identification of pollutants or toxic agents in the air, where additionally energy consumption is a critical factor to be considered.

### **Future Work**

The CO<sub>2</sub> MEMS sensor developed in this work consists of three main elements, the micro-resonator, the sustaining amplifier, and the CO<sub>2</sub> adsorption coating. In this work, it was

demonstrated that it is possible to integrate and achieve a working sensor , however, it is possible to improve the sensor further.

The micro-resonator has the potential to be improved to obtain a higher Q-factor and better stability to temperature changes, either by modifying the design of its anchors, dimensions and other more complex geometries, as well as considering the use of other excitation and measurement elements.

The sustaining amplifier should be redesigned to improve stability, reduce power consumption and increase the Q-factor of the resonator and the closed-loop system frequency fidelity. The integration of the micro-resonator with the support amplifier on one chip will reduce the energy required to operate, the footprint of the system, manufacturing costs and increase the quality and stability of the system. An additional element to be added to the control system is a means of compensating for external factors such as temperature, humidity and pressure. An example of compensation was made in this work, however, an integrated method with digital calibration based on reference temperature and humidity sensors in the sensing subsystem could be implemented.

One of the most important elements that have defined the gas selectivity in these sensors is the coating, which has shown good performance, but also its susceptibility to changes in the humidity level. There are other coatings that have shown good performance in CO<sub>2</sub> capture, such as Guanidine (CH<sub>5</sub>N<sub>3</sub>) and other types of polymer amines that should be evaluated to define if there is a more selective coating for this application.

Finally, after optimizing each element that makes up the MEMS CO<sub>2</sub> sensor, a high performance, low energy consumption, low cost system can be obtained that can be competitive with the commercial sensors currently on the market.

## **Conclusion**

The purpose of this work was to verify the viability of using a MEMS sensor for CO<sub>2</sub> based on micro-resonators and was confirmed that through the integration of a sustaining amplifier a highly integrated system could be obtained. It was also verified that the LPEI coatings in micro-resonators can be used to measure the concentration of CO<sub>2</sub> in the air by mass addition.

This work also presented a brief comparison between the MEMS sensors manufactured with a CO<sub>2</sub> optical sensor, concluding that for concentrations below 4000 ppm the performance of both sensors for the adsorption phase are competitive, while for the abrupt recovery phase the optical sensor has better performance, however, considering that the variations of CO<sub>2</sub> in the air are normally not abrupt, it can be considered that for concentrations less than 4000 ppm both sensors are competitive.

Finally, it has been shown that a micro-resonator mass sensor can be used to accurately measure temperature, humidity, pressure and any particle that can adhere to the surface of the resonator generating its frequency deviation. The power required for this type of sensors is significantly less than that for commercial sensors, which makes MEMS gas sensors a great option to replace them, however, it is necessary to perform a full integration to compensate for the influence of external variables in order to have a reliable sensor.



## BIBLIOGRAPHY

- Abdolvand, R., Bahreyni, B., Lee, J. E.-Y., & Nabki, F. (2016). Micromachined Resonators: A Review. *Micromachines*, 7(9), 160.
- Abdolvand, R., Bahreyni, B., Lee, J. E. Y., & Nabki, F. (2016). Micromachined resonators: A review. *Micromachines*, 7(9). doi: 10.3390/mi7090160.
- Akbari, E., Buntat, Z., Ahmad, M., Enzevae, A., Yusof, R., Iqbal, S. M. Z., . . . Karimi, H. (2014). *Analytical Calculation of Sensing Parameters on Carbon Nanotube Based Gas Sensors* (Vol. 14). doi: 10.3390/s140305502.
- Al-Marri, M. J., Kutti, Y. O., Khraisheh, M., Kumar, A., & Khader, M. M. (2017). Kinetics of CO<sub>2</sub> Adsorption/Desorption of Polyethyleneimine-Mesoporous Silica. *Chemical Engineering & Technology*, 40(10), 1802-1809. doi: 10.1002/ceat.201600452.
- Alexandre, M., & Gerboles, M. (2012). Review of small commercial sensors for indicative monitoring of ambient gas. *Chem. Eng. Trans*, 30.
- Ali, W. R., & Prasad, M. (2020). Piezoelectric MEMS based acoustic sensors: A review. *Sensors and Actuators, A: Physical*, 301. doi: 10.1016/j.sna.2019.111756.
- Andò, B., Baglio, S., Di Pasquale, G., Pollicino, A., D'Agata, S., Gugliuzzo, C., . . . Re, G. (2015). An Inkjet Printed CO<sub>2</sub> Gas Sensor. *Procedia Engineering*, 120, 628-631. doi: <https://doi.org/10.1016/j.proeng.2015.08.755>.
- Andreoli, E., Cullum, L., & Barron, A. R. (2015). Carbon Dioxide Absorption by Polyethylenimine-Functionalized Nanocarbons: A Kinetic Study. *Industrial & Engineering Chemistry Research*, 54(3), 878-889. doi: 10.1021/ie504277s.
- Arshak, K. (2004). A review of gas sensors employed in electronic nose applications. *Sensor Review*, 24(2), 181-198. doi: 10.1108/02602280410525977.
- Arshak, K., Moore, E., Lyons, G. M., Harris, J., & Clifford, S. (2004). A review of gas sensors employed in electronic nose applications. *Sensor Review*, 24(2), 181-198. doi: 10.1108/02602280410525977.
- Aving. (2013). TCC ELT, 19 New CO<sub>2</sub> Sensors which Last up to 10 Years. 2020(20/02/2020). doi: <http://us.aving.net/news/view.php?articleId=718053>.
- Basu, S., & Bhattacharyya, P. (2012). Recent developments on graphene and graphene oxide based solid state gas sensors. *Sensors and Actuators B: Chemical*, 173, 1-21. doi: <https://doi.org/10.1016/j.snb.2012.07.092>.

- Ben Hamouda, S., & Roudesli, S. (2008). Transport properties of PVA/PEI/PEG composite membranes: sorption and permeation characterizations. *Central European Journal of Chemistry*, 6(4), 634-640. doi: 10.2478/s11532-008-0053-0.
- Bhanja, P., Das, S. K., Patra, A. K., & Bhaumik, A. (2016). Functionalized graphene oxide as an efficient adsorbent for CO<sub>2</sub> capture and support for heterogeneous catalysis. *RSC Advances*, 6(76), 72055-72068. doi: 10.1039/C6RA13590K.
- Binions, R., & Naik, A. J. T. (2013). Metal oxide semiconductor gas sensors in environmental monitoring. Dans R. Jaaniso & O. K. Tan (Éds.), *Semiconductor Gas Sensors* (pp. 433-466). Woodhead Publishing. doi: <https://doi.org/10.1533/9780857098665.4.433>.
- Bogue, R. (2015). Detecting gases with light: a review of optical gas sensor technologies. *Sensor Review*, 35(2), 133-140. doi: 10.1108/SR-09-2014-696.
- Bouchaala, A., Nayfeh, A. H., & Younis, M. I. (2017). Analytical study of the frequency shifts of micro and nano clamped-clamped beam resonators due to an added mass. *Meccanica*, 52(1), 333-348. doi: 10.1007/s11012-016-0412-4.
- Boudaden, J., Klumpp, A., Endres, H.-E., & Eisele, I. (2019). Towards Low Cost and Low Temperature Capacitive CO<sub>2</sub> Sensors Based on Amine Functionalized Silica Nanoparticles. *Nanomaterials*, 9(8), 1097.
- Brunet, J., Garcia, V. P., Pauly, A., Varenne, C., & Lauron, B. (2008). An optimised gas sensor microsystem for accurate and real-time measurement of nitrogen dioxide at ppb level. *Sensors and Actuators B: Chemical*, 134(2), 632-639. doi: <https://doi.org/10.1016/j.snb.2008.06.010>.
- Cai, H., Bao, F., Gao, J., Chen, T., Wang, S., & Ma, R. (2015). Preparation and characterization of novel carbon dioxide adsorbents based on polyethylenimine-modified Halloysite nanotubes. *Environmental Technology*, 36(10), 1273-1280. doi: 10.1080/09593330.2014.984772.
- CHEN, H., ZHONG, Y., & MENG, Z. (2017). A Practical Pll-Based Drive Circuit with Ultra-Low-Noise Tia for Mems Gyroscope. *仪器仪表学报 (英文版)*, (3), 2.
- Chen, W., Yan, L., & Bangal, P. R. (2010). Preparation of graphene by the rapid and mild thermal reduction of graphene oxide induced by microwaves. *Carbon*, 48(4), 1146-1152. doi: <https://doi.org/10.1016/j.carbon.2009.11.037>.
- Clifford, J., Mulrooney, J., Dooly, G., Fitzpatrick, C., Lewis, E., Merlone-Borla, E., & Flavia, G. (2008). On board measurement of carbon dioxide exhaust car emissions using a mid-infrared optical based fibre. Dans *SENSORS, 2008 IEEE* (pp. 914-918). doi: 10.1109/ICSENS.2008.4716590.

- Dey, A. (2018). Semiconductor metal oxide gas sensors: A review. *Materials Science and Engineering: B*, 229, 206-217. doi: <https://doi.org/10.1016/j.mseb.2017.12.036>.
- Doan, T. C. D., Baggerman, J., Ramaneti, R., Tong, H. D., Marcelis, A. T. M., & van Rijn, C. J. M. (2014). Carbon dioxide detection with polyethylenimine blended with polyelectrolytes. *Sensors and Actuators B: Chemical*, 201, 452-459. doi: <https://doi.org/10.1016/j.snb.2014.05.023>.
- EPA. (2017). Sources of Greenhouse Gas Emissions. 2020(20-02-2020). doi: <https://www.epa.gov/ghgemissions/sources-greenhouse-gas-emissions>.
- Espinal, L., Poster, D. L., Wong-Ng, W., Allen, A. J., & Green, M. L. (2013). Measurement, Standards, and Data Needs for CO<sub>2</sub> Capture Materials: A Critical Review. *Environmental Science & Technology*, 47(21), 11960-11975. doi: 10.1021/es402622q.
- ESRL, E. S. R. L. (2020). Global Monthly Mean CO<sub>2</sub>. *NORA*. doi: <https://www.esrl.noaa.gov/gmd/ccgg/trends/global.html#global>.
- Fang, Q., Chetwynd, D. G., Covington, J. A., Toh, C. S., & Gardner, J. W. (2002). Micro-gas-sensor with conducting polymers. *Sensors and Actuators B: Chemical*, 84(1), 66-71. doi: [https://doi.org/10.1016/S0925-4005\(01\)01076-0](https://doi.org/10.1016/S0925-4005(01)01076-0).
- Fanget, S., Hentz, S., Puget, P., Arcamone, J., Matheron, M., Colinet, E., . . . Roukes, M. L. (2011). Gas sensors based on gravimetric detection—A review. *Sensors and Actuators B: Chemical*, 160(1), 804-821. doi: <https://doi.org/10.1016/j.snb.2011.08.066>.
- Fernández-Ramos, M. D., Moreno-Puche, F., Escobedo, P., García-López, P. A., Capitán-Vallvey, L. F., & Martínez-Olmos, A. (2020). Optical portable instrument for the determination of CO<sub>2</sub> in indoor environments. *Talanta*, 208. doi: 10.1016/j.talanta.2019.120387.
- Fowler, A. G., Bulut Coskun, M., & Reza Moheimani, S. O. (2017). Q control of a microfabricated piezoelectric cantilever with on-chip feedthrough cancellation. Dans *1st Annual IEEE Conference on Control Technology and Applications, CCTA 2017* (Vol. 2017-January, pp. 123-128). Institute of Electrical and Electronics Engineers Inc. doi: 10.1109/CCTA.2017.8062451.
- Fu, X., & Xu, L. (2018). A Micro-Resonant Gas Sensor with Nanometer Clearance between the Pole Plates. *Sensors*, 18(2), 362.
- Gargiulo, N., Pepe, F., & Caputo, D. (2014). *CO<sub>2</sub> Adsorption by Functionalized Nanoporous Materials: A Review* (Vol. 14). doi: 10.1166/jnn.2014.8893.

- Gas Sensor Market Size, Share & Trends Analysis Report By Product (CO<sub>2</sub>, NO<sub>x</sub>, CO, O<sub>2</sub> Sensors), By Technology (Semiconductor, Infrared), By End Use (Building Automation & Domestic Appliance, Industrial), And Segment Forecasts, 2019 - 2025. (2019).
- Ghosh, A., Zhang, C., Shi, S., & Zhang, H. (2019). High temperature CO<sub>2</sub> sensing and its cross-sensitivity towards H<sub>2</sub> and CO gas using calcium doped ZnO thin film coated langasite SAW sensor. *Sensors and Actuators, B: Chemical*, 301. doi: 10.1016/j.snb.2019.126958.
- Gomes, M. T., Duarte, A. C., & Oliveira, J. P. (1995). Detection of CO<sub>2</sub> using a quartz crystal microbalance. *Sensors and Actuators B: Chemical*, 26(1), 191-194. doi: [https://doi.org/10.1016/0925-4005\(94\)01584-5](https://doi.org/10.1016/0925-4005(94)01584-5).
- Hajjaj, A. Z., Jaber, N., Alcheikh, N., & Younis, M. I. (2019). A Sensitive Resonant Gas Sensor Based on Multimode Excitation of a Buckled Beam. Dans *2019 20th International Conference on Solid-State Sensors, Actuators and Microsystems & Eurosensors XXXIII (TRANSDUCERS & EUROSENSORS XXXIII)* (pp. 769-772). doi: 10.1109/TRANSDUCERS.2019.8808228.
- Hajjam, A., & Pourkamali, S. (2012). Fabrication and Characterization of MEMS-Based Resonant Organic Gas Sensors. *IEEE Sensors Journal*, 12(6), 1958-1964. doi: 10.1109/JSEN.2011.2181360.
- Han, J., Huang, R., Zhang, P., Cheng, B., Dong, L., & Han, D. (2018). A Novel Film Thermal Converter Based on an Electrothermally Excited/Piezoresistively Detected Microbridge Resonator. *IEEE Transactions on Instrumentation and Measurement*. doi: 10.1109/TIM.2018.2831388.
- Hanafi, R., Mayasari, R. D., Masmui, Agustanhakri, Raharjo, J., & Nuryadi, R. (2019). Electrochemical sensor for environmental monitoring system: A review. Dans F. Bakri, F. C. Wibowo, I. Sugihartono, E. Budi, W. Indrasari, Umiatin & T. B. Prayitno (Éds.), *8th National Physics Seminar 2019* (Vol. 2169). American Institute of Physics Inc. doi: 10.1063/1.5132657.
- Hsu, K. C., Fang, T. H., Hsiao, Y. J., & Chan, C. A. (2020). Highly response CO<sub>2</sub> gas sensor based on Au-La<sub>2</sub>O<sub>3</sub> doped SnO<sub>2</sub> nanofibers. *Materials Letters*, 261. doi: 10.1016/j.matlet.2019.127144.
- Inc., M. (2014). PiezoMUMPs™ Design Handbook. Dans MEMSCAP (Éd.), *PiezoMUMPs™ Design Handbook*.
- Irani, M., Jacobson, A. T., Gasem, K. A. M., & Fan, M. (2018). Facilely synthesized porous polymer as support of poly(ethyleneimine) for effective CO<sub>2</sub> capture. *Energy*, 157, 1-9. doi: <https://doi.org/10.1016/j.energy.2018.05.141>.

- Jaber, N., Ilyas, S., Shekhah, O., Eddaoudi, M., & Younis, M. I. (2018). Multimode MEMS Resonator for Simultaneous Sensing of Vapor Concentration and Temperature. *IEEE Sensors Journal*, 18(24), 10145-10153. doi: 10.1109/JSEN.2018.2872926.
- Ji, H., Zeng, W., & Li, Y. (2019). Gas sensing mechanisms of metal oxide semiconductors: A focus review. *Nanoscale*, 11(47), 22664-22684. doi: 10.1039/c9nr07699a.
- Jimenez, G., Riu, J., & Rius, X. (2007). Gas sensors based on nanostructured materials. *Analyst*, 132(11), 1083-1099. doi: 10.1039/B704562J.
- Joshi, P., Kumar, S., Jain, V. K., Akhtar, J., & Singh, J. (2019). Distributed MEMS mass-sensor based on piezoelectric resonant micro-cantilevers. *Journal of Microelectromechanical Systems*, 28(3), 382-389. doi: 10.1109/JMEMS.2019.2908879.
- Kato, F., Noguchi, H., Kodaka, Y., Chiku, N., Shibata, H., Abe, F., & Ogi, H. (2017). Multi-channel wireless quartz crystal microbalance biosensor fabricated with poly(dimethylsiloxane). Dans *2017 19th International Conference on Solid-State Sensors, Actuators and Microsystems (TRANSDUCERS)* (pp. 1664-1667). doi: 10.1109/TRANSDUCERS.2017.7994384.
- Kim, N., Xin, G., Cho, S. M., Pang, C., & Chae, H. (2015). Microwave-reduced graphene oxide for efficient and stable hole extraction layers of polymer solar cells. *Current Applied Physics*, 15(9), 953-957. doi: 10.1016/j.cap.2015.05.011.
- Konno, M., Ikehara, T., Murakami, S., Maeda, R., Kimura, M., Fukawa, T., & Mihara, T. (2011). Novel MEMS oscillator using in-plane disk resonator with sensing platform and its mass sensing characteristics. Dans *2011 16th International Solid-State Sensors, Actuators and Microsystems Conference, TRANSDUCERS'11* (pp. 518-521). doi: 10.1109/TRANSDUCERS.2011.5969670.
- Kumar, A., Kim, H., & Hancke, G. P. (2013). Environmental Monitoring Systems: A Review. *IEEE Sensors Journal*, 13(4), 1329-1339. doi: 10.1109/JSEN.2012.2233469.
- Layton, T. M. A. R. A. (2010). *Introductory MEMS - Fabrication and Applications*. Springer.
- Lee, D. D. (2001). Environmental gas sensors. *IEEE Sensors Journal*, 1(3), 214-224. doi: 10.1109/JSEN.2001.954834.
- Lee, H. J., Park, K. K., Kupnik, M., & Khuri-Yakub, B. T. (2012). Functionalization layers for CO<sub>2</sub> sensing using capacitive micromachined ultrasonic transducers. *Sensors and Actuators B: Chemical*, 174, 87-93. doi: <https://doi.org/10.1016/j.snb.2012.08.025>.

- Li, X., Zhou, D., He, J., Liu, X., & Wang, D. F. (2017). Mode-localized cantilever array for picogram order mass sensing. Dans *12th IEEE International Conference on Nano/Micro Engineered and Molecular Systems, NEMS 2017* (pp. 587-590). Institute of Electrical and Electronics Engineers Inc. doi: 10.1109/NEMS.2017.8017091.
- Lin, S., & Theato, P. (2013). CO<sub>2</sub>-responsive polymers. *Macromolecular Rapid Communications*, *34*(14), 1118-1133. doi: 10.1002/marc.201300288.
- Lin, Y., & Fan, Z. (2020). Compositing strategies to enhance the performance of chemiresistive CO<sub>2</sub> gas sensors. *Materials Science in Semiconductor Processing*, *107*. doi: 10.1016/j.mssp.2019.104820.
- Liu, F., Fu, W., & Chen, S. (2019). Synthesis, characterization and CO<sub>2</sub> adsorption performance of a thermosensitive solid amine adsorbent. *Journal of CO<sub>2</sub> Utilization*, *31*, 98-105. doi: <https://doi.org/10.1016/j.jcou.2019.02.019>.
- Liu, L., Zou, G., Yang, B., Luo, X., & Xu, S. (2018). Amine-Functionalized Mesoporous Silica @ Reduced Graphene Sandwichlike Structure Composites for CO<sub>2</sub> Adsorption. *ACS Applied Nano Materials*, *1*(9), 4695-4702. doi: 10.1021/acsanm.8b00943.
- Liu, X., Cheng, S., Liu, H., Hu, S., Zhang, D., & Ning, H. (2012). A Survey on Gas Sensing Technology. *Sensors*, *12*(7), 9635.
- Lott, G. A., King, M. D., Hill, M. W., & Scatena, L. F. (2014). Effects of Relative Humidity on the Surface and Bulk Structures of Linear Polyethylenimine Thin Films. *The Journal of Physical Chemistry C*, *118*(31), 17686-17698. doi: 10.1021/jp504321r.
- Lv, Y., Xu, P., Yu, H., Xu, J., & Li, X. (2018). Ni-MOF-74 as sensing material for resonant-gravimetric detection of ppb-level CO. *Sensors and Actuators B: Chemical*, *262*, 562-569. doi: <https://doi.org/10.1016/j.snb.2018.02.058>.
- Mahajan, F. K. a. R. (2006). MEMS Introduction and Fundamentals. *Taylor & Francis Group, LLC*.
- Mahdavi, M., Mehdizadeh, E., & Pourkamali, S. (2018). Piezoelectric MEMS resonant dew point meters. *Sensors and Actuators, A: Physical*, *276*, 52-61. doi: 10.1016/j.sna.2018.04.024.
- Mahyuddin, N., & Awbi, H. (2012). A Review of CO<sub>2</sub> Measurement Procedures in Ventilation Research. *International Journal of Ventilation*, *10*(4), 353-370. doi: 10.1080/14733315.2012.11683961.

- Mekky, R. H., Cicek, P., & El-Gamal, M. N. (2013). Ultra low-power low-noise transimpedance amplifier for MEMS-based reference oscillators. Dans *2013 IEEE 20th International Conference on Electronics, Circuits, and Systems (ICECS)* (pp. 345-348). doi: 10.1109/ICECS.2013.6815425.
- MEMSCAP Inc., M. (2014). PiezoMUMPs™ Design Handbook. Dans MEMSCAP (Éd.), *PiezoMUMPs™ Design Handbook*.
- MEMSCAP, M. (2011). PolyMUMPs™ Design Handbook. Dans MEMSCAP (Éd.), *PolyMUMPs™ Design Handbook*.
- MIT. (2016). Mechanical Vibrations and Waves. *MITopencourseware*.  
doi: <https://ocw.mit.edu/courses/physics/8-03sc-physics-iii-vibrations-and-waves-fall-2016/part-i-mechanical-vibrations-and-waves/>.
- Mo, Y., Okawa, Y., Tajima, M., Nakai, T., Yoshiike, N., & Natukawa, K. (2001). Micro-machined gas sensor array based on metal film micro-heater. *Sensors and Actuators B: Chemical*, 79(2), 175-181. doi: [https://doi.org/10.1016/S0925-4005\(01\)00871-1](https://doi.org/10.1016/S0925-4005(01)00871-1).
- Mumyakmaz, B., Özmen, A., Ebeoğlu, M. A., Taşaltın, C., & Gürol, İ. (2010). A study on the development of a compensation method for humidity effect in QCM sensor responses. *Sensors and Actuators B: Chemical*, 147(1), 277-282.  
doi: <https://doi.org/10.1016/j.snb.2010.03.019>.
- Muraoka, S., Kiyohara, Y., Oue, H., & Higashimoto, S. (2014). A CO<sub>2</sub> Sensor Using a Quartz Crystal Microbalance Coated with a Sensitive Membrane. *Electronics and Communications in Japan*, 97(2), 60-66. doi: 10.1002/ecj.11601.
- Muro, H. (2013). History and Recent Progress of MEMS Physical Sensors. *Advances in Science and Technology*, 81, 1-8. doi: 10.4028/[www.scientific.net/AST.81.1](http://www.scientific.net/AST.81.1).
- Nazemi, H., Joseph, A., Park, J., & Emadi, A. (2019). Advanced Micro- and Nano-Gas Sensor Technology: A Review. *Sensors*, 19(6), 1285.
- Nguyen, C. C., Ngo, V. K. T., Le, H. Q., & Li, W. L. (2019). Influences of relative humidity on the quality factors of MEMS cantilever resonators in gas rarefaction. *Microsystem Technologies*, 25(7), 2767-2782. doi: 10.1007/s00542-018-4239-x.
- Niu, M., Yang, H., Zhang, X., Wang, Y., & Tang, A. (2016). Amine-Impregnated Mesoporous Silica Nanotube as an Emerging Nanocomposite for CO<sub>2</sub> Capture. *ACS Applied Materials & Interfaces*, 8(27), 17312-17320. doi: 10.1021/acsami.6b05044.
- Ong, K. G., & Grimes, C. A. (2001). A Carbon Nanotube-based Sensor for CO<sub>2</sub> Monitoring. *Sensors*, 1(6), 193-205.

- Padilla, M., Perera, A., Montoliu, I., Chaudry, A., Persaud, K., & Marco, S. (2010). Drift compensation of gas sensor array data by Orthogonal Signal Correction. *Chemometrics and Intelligent Laboratory Systems*, 100(1), 28-35.  
doi: <https://doi.org/10.1016/j.chemolab.2009.10.002>.
- Pashapur, M. p., Pesteii, S. M., Rezazadeh, G., & kouravand, s. (2009). Thermo-Mechanical Behavior of a Bilayer Microbeam Subjected to Nonlinear Electrostatic Pressure. *J Sens Transducers*, 103, 161-170.
- Pei, S., & Cheng, H.-M. (2012). The reduction of graphene oxide. *Carbon*, 50(9), 3210-3228.  
doi: <https://doi.org/10.1016/j.carbon.2011.11.010>.
- Penza, M., Aversa, P., Cassano, G., Wlodarski, W., & Kalantar-Zadeh, K. (2007). Layered SAW gas sensor with single-walled carbon nanotube-based nanocomposite coating. *Sensors and Actuators B: Chemical*, 127(1), 168-178.  
doi: <https://doi.org/10.1016/j.snb.2007.07.028>.
- Prud'homme, A., & Nabki, F. (2020). *Comparison Between Linear and Branched Polyethylenimine (PEI) and Reduced Graphene Oxide Coatings as a Capture Layer for Micro Resonant CO<sub>2</sub> Gas Concentration Sensors*. Department of Electrical Engineering, École de Technologie Supérieure.
- Romani, A., Sangiorgi, E., Tartagni, M., & Paganelli, R. (2011). Joint Modeling of Piezoelectric Transducers and Power Conversion Circuits for Energy Harvesting Applications. *Sensors Journal, IEEE*, 13, 36-39. doi: 10.1109/ICSENS.2011.6127223.
- Salvia, J., Lajevardi, P., Hekmat, M., & Murmann, B. (2009). A 56M $\Omega$  CMOS TIA for MEMS applications. Dans *2009 IEEE Custom Integrated Circuits Conference* (pp. 199-202).  
doi: 10.1109/CICC.2009.5280878.
- Satish, U., Mendell, M. J., Shekhar, K., Hotchi, T., Sullivan, D., Streufert, S., & Fisk, W. J. (2012). Is CO<sub>2</sub> an Indoor Pollutant? Direct Effects of Low-to-Moderate CO<sub>2</sub> Concentrations on Human Decision-Making Performance. *Environmental Health Perspectives*, 120(12), 1671-1677.  
doi: doi:10.1289/ehp.1104789.
- Sehaqui, H., Gálvez, M. E., Becatinni, V., cheng Ng, Y., Steinfeld, A., Zimmermann, T., & Tingaut, P. (2015). Fast and Reversible Direct CO<sub>2</sub> Capture from Air onto All-Polymer Nanofibrillated Cellulose—Polyethylenimine Foams. *Environmental Science & Technology*, 49(5), 3167-3174. doi: 10.1021/es504396v.
- Serban, B., Kumar, A. S., Costea, S., Mihaila, M., Buiu, O., Brezeanu, M., . . . Cobianu, C. (2009). Polymer-amino carbon nanotube nanocomposites for surface acoustic wave CO<sub>2</sub> detection. *Romanian Journal of Information science and technology*, 12(3), 376-384.

- Singh, O. P., Howe, T. A., & Malarvili, M. B. (2018). Real-time human respiration carbon dioxide measurement device for cardiorespiratory assessment. *Journal of Breath Research*, 12(2), 026003. doi: 10.1088/1752-7163/aa8dbd.
- Smith, A. L. (2007). Using Quartz Crystal Microbalance-Heat Conduction Calorimetry to Monitor the Drying and Curing of an Alkyd Spray Enamel. Dans *New Developments in Coatings Technology* (Vol. 962, pp. 261-277). American Chemical Society. doi: doi:10.1021/bk-2007-0962.ch017 10.1021/bk-2007-0962.ch017.
- Smulko Janusz, M. (2015). New approaches for improving selectivity and sensitivity of resistive gas sensors: a review. *Sensor Review*, 35(4), 340-347. doi: 10.1108/SR-12-2014-0747.
- Song, Y., Cao, L., Yu, J., Zhang, S., Chen, S., & Jiang, Y. (2017). Amino-functionalized graphene oxide blend with monoethanolamine for efficient carbon dioxide capture. *Journal of Alloys and Compounds*, 704, 245-253. doi: <https://doi.org/10.1016/j.jallcom.2017.01.310>.
- Spinelle, L., Gerboles, M., Kok, G., Persijn, S., & Sauerwald, T. (2017). Review of Portable and Low-Cost Sensors for the Ambient Air Monitoring of Benzene and Other Volatile Organic Compounds. *Sensors (Basel, Switzerland)*, 17(7), 1520. doi: 10.3390/s17071520.
- Stephen Beeby, G. E., Michael Kraft, Neil White. (2004). MEMS Mechanical Sensors. *ARTECH HOUSE, INC.*
- Subhashini, S., & Juliet, A. V. (2012). Toxic gas sensor using resonant frequency variation in micro-cantilever. Dans *2012 IEEE Conference on Sustainable Utilization and Development in Engineering and Technology (STUDENT)* (pp. 87-91). doi: 10.1109/STUDENT.2012.6408371.
- Subhashini, S., & Juliet, A. V. (2013) CO<sub>2</sub> gas sensor using resonant frequency changes in micro-cantilever. du volume): *Vol. 131 LNEE. 4th International Conference on Networks and Communications, NetCom 2012* (pp. 75-80). Chennai.
- Sun, B., Xie, G., Jiang, Y., & Li, X. (2011). Comparative CO<sub>2</sub>-Sensing Characteristic Studies of PEI and PEI/Starch Thin Film Sensors. *Energy Procedia*, 12, 726-732. doi: <https://doi.org/10.1016/j.egypro.2011.10.098>.
- Sun, L.-B., Kang, Y.-H., Shi, Y.-Q., Jiang, Y., & Liu, X.-Q. (2015). Highly Selective Capture of the Greenhouse Gas CO<sub>2</sub> in Polymers. *ACS Sustainable Chemistry & Engineering*, 3(12), 3077-3085. doi: 10.1021/acssuschemeng.5b00544.
- Sutela, C., Collings, N., & Hands, T. (1999). *Fast Response CO<sub>2</sub> Sensor for Automotive Exhaust Gas Analysis*. doi: <https://doi.org/10.4271/1999-01-3477>.

- Ünveren, E. E., Monkul, B. Ö., Sariođlan, Ş., Karademir, N., & Alper, E. (2017). Solid amine sorbents for CO<sub>2</sub> capture by chemical adsorption: A review. *Petroleum*, 3(1), 37-50. doi: <https://doi.org/10.1016/j.petlm.2016.11.001>.
- Vasiliev, A. A., Pislakov, A. V., Sokolov, A. V., Samotaev, N. N., Soloviev, S. A., Oblov, K., . . . Legin, A. V. (2016). Non-silicon MEMS platforms for gas sensors. *Sensors and Actuators, B: Chemical*, 224, 700-713. doi: 10.1016/j.snb.2015.10.066.
- Vieira, R. B., & Pastore, H. O. (2014). Polyethylenimine-Magadiite Layered Silicate Sorbent for CO<sub>2</sub> Capture. *Environmental Science & Technology*, 48(4), 2472-2480. doi: 10.1021/es404501e.
- Wang, R., Zhang, M., Guan, Y., Chen, M., & Zhang, Y. (2019). A CO<sub>2</sub>-responsive hydrogel film for optical sensing of dissolved CO<sub>2</sub>. *Soft Matter*, 15(30), 6107-6115. doi: 10.1039/c9sm00958b.
- Wang, X., Schwartz, V., Clark, J. C., Ma, X., Overbury, S. H., Xu, X., & Song, C. (2009). Infrared Study of CO<sub>2</sub> Sorption over “Molecular Basket” Sorbent Consisting of Polyethylenimine-Modified Mesoporous Molecular Sieve. *The Journal of Physical Chemistry C*, 113(17), 7260-7268. doi: 10.1021/jp809946y.
- Wasisto, H. S., Zhang, Q., Merzsch, S., Waag, A., & Peiner, E. (2014). A phase-locked loop frequency tracking system for portable microelectromechanical piezoresistive cantilever mass sensors. *Microsystem Technologies*, 20(4), 559-569. doi: 10.1007/s00542-013-1991-9.
- Wood, G., Svilicic, B., Mastropaolo, E., & Cheung, R. (2016). *3C-Silicon Carbide Microresonators for Timing and Frequency Reference* (Vol. 7). doi: 10.3390/mi7110208.
- Xian, S., Wu, Y., Wu, J., Wang, X., & Xiao, J. (2015). Enhanced Dynamic CO<sub>2</sub> Adsorption Capacity and CO<sub>2</sub>/CH<sub>4</sub> Selectivity on Polyethylenimine-Impregnated UiO-66. *Industrial & Engineering Chemistry Research*, 54(44), 11151-11158. doi: 10.1021/acs.iecr.5b03517.
- Yoon, H. J., Jun, D. H., Yang, J. H., Zhou, Z., Yang, S. S., & Cheng, M. M.-C. (2011). Carbon dioxide gas sensor using a graphene sheet. *Sensors and Actuators B: Chemical*, 157(1), 310-313. doi: <https://doi.org/10.1016/j.snb.2011.03.035>.
- Yu, C.-H., Huang, C.-H., & Tan, C.-S. (2012). A review of CO<sub>2</sub> capture by absorption and adsorption. *Aerosol Air Qual. Res*, 12(5), 745-769.
- Yu, H., Xu, P., Xia, X., Lee, D., & Li, X. (2012). Micro-/Nanocombined Gas Sensors With Functionalized Mesoporous Thin Film Self-Assembled in Batches Onto Resonant Cantilevers. *IEEE Transactions on Industrial Electronics*, 59(12), 4881-4887.

doi: 10.1109/TIE.2011.2173094.

- Zaman, I., Mohamed Salleh, M., Ismon, M., Manshoor, B., Khalid, A., Mohd Sani, M. S., & Araby, S. (2014). Study of Passive Vibration Absorbers Attached on Beam Structure. *Applied Mechanics and Materials*, 660, 511-515.  
doi: 10.4028/[www.scientific.net/AMM.660.511](http://www.scientific.net/AMM.660.511).
- Zhang, H., Goepfert, A., Prakash, G. K. S., & Olah, G. (2015). Applicability of linear polyethylenimine supported on nano-silica for the adsorption of CO<sub>2</sub> from various sources including dry air. *RSC Advances*, 5(65), 52550-52562.  
doi: 10.1039/C5RA05428A.
- Zhang, J., Jiang, G., Cumberland, T., Xu, P., Wu, Y., Delaat, S., . . . Chen, Z. (2019). A highly sensitive breathable fuel cell gas sensor with nanocomposite solid electrolyte. *InfoMat*, 1(2), 234-241. doi: 10.1002/inf2.12017.
- Zhao, C., Montaseri, M. H., Wood, G. S., Pu, S. H., Seshia, A. A., & Kraft, M. (2016). A review on coupled MEMS resonators for sensing applications utilizing mode localization. *Sensors and Actuators, A: Physical*, 249, 93-111.  
doi: 10.1016/j.sna.2016.07.015.
- Zhao, R., Li, X., Sun, B., Li, Y., Li, Y., Yang, R., & Wang, C. (2017). Branched polyethylenimine grafted electrospun polyacrylonitrile fiber membrane: a novel and effective adsorbent for Cr(vi) remediation in wastewater. *Journal of Materials Chemistry A*, 5(3), 1133-1144. doi: 10.1039/C6TA09784G.
- Zhao, Y., Ding, H., & Zhong, Q. (2012). Preparation and characterization of aminated graphite oxide for CO<sub>2</sub> capture. *Applied Surface Science*, 258(10), 4301-4307.  
doi: <https://doi.org/10.1016/j.apsusc.2011.12.085>.
- Zribi, A., Knobloch, A., Tian, W.-C., & Goodwin, S. (2005). Micromachined resonant multiple gas sensor. *Sensors and Actuators A: Physical*, 122(1), 31-38.  
doi: <https://doi.org/10.1016/j.sna.2004.12.034>.